NUMERICAL SIMULATIONS OF SEMICONDUCTOR DEVICES BY STREAMLINE-DIFFUSION METHODS

By

Xunlei Jiang

B.Sc. (Mathematics), Fudan University, Shanghai, P.R.China, 1984

M.Sc. (Mathematics), Fudan University, Shanghai, P.R.China, 1987

A THESIS SUBMITTED IN PARTIAL FULFILLMENT OF

THE REQUIREMENTS FOR THE DEGREE OF

DOCTOR OF PHILOSOPHY

in

THE FACULTY OF GRADUATE STUDIES

INSTITUTE OF APPLIED MATHEMATICS

DEPARTMENT OF MATHEMATICS

We accept this thesis as conforming

to the required standard

. . . . . .

. . . . . .

. . . . . .

THE UNIVERSITY OF BRITISH COLUMBIA

February 1995

Abstract

Theoretical and practical aspects of the design and implementation of the streamline-diffusion (SD) method for semiconductor device models are explored systematically. Emphasis is placed on the hydrodynamic (HD) model, which is computationally more challenging than the drift-diffusion (DD) model, but provides some important physical information missing in the DD model.

We devise a non-symmetric SD method for device simulations. This numerical method is uniformly used for the HD model (including a proposed simplification (SHD)) and the DD model. An appropriate SD operator is derived for the general non-symmetric convection-diffusion system. Linear stability analysis shows that our proposed numerical method is stable if the system can be symmetrized. Stability arguments and numerical experiments also suggest that the combination of the method of lines and the semi-discrete SD method may not be appropriate for the transient problem, a fact which often has been ignored in the literature.

An efficient method, consistent with the SD method used for conservation laws, is developed for the potential equation. The method produces a more accurate electric field than the conventional Galerkin method. Moreover, it solves for the potential and electric field in a decoupled manner.

We apply our numerical method to the diode and MESFET devices. Shocks for the diode in one and two space dimensions and the electron depletion near the gate for the MESFET in two space dimensions are simulated. Model comparisons are implemented. We observe that the difference in solutions between the HD and DD models is significant. The solution discrepancy between the full HD and SHD models is almost negligible in MESFET simulation, as in many other engineering applications. However, an exceptional case is found in our experiments.

Table of Contents

List of Tables

List of Figures

Nomenclature

κ	Thermal conductivity
λ	Dielectric constant
μ_0	Electron mobility
ρ	Electron density
ρ_0	Surface electron density
ρ_D	Doping profile
ρ_i	Intrinsic electron density
τ_J, τ_W	Relaxation times
ϕ_B	Barrier height function
ϕ_m	Working function
ϕ_n	Quasi-Fermi level
χ_s	Electron affinity
ψ	Electro-static potential
ψ_{bi}	Built-in potential
Γ	Device boundary
Γ_1, Γ_2	Contact and insulating parts of Γ
Ω	Device domain
Δt	Time step
c, c^*	Sound speeds
e	Charge of an electron
h	Spacing parameter
k_b	Boltzmann constant
m	Effective mass of an electron
t	Time variable

v	Mean velocity
v_s	Saturation velocity
v_{th}	Thermionic emission velocity
x, y	Space variables
C_J, C_W	Intraband collision terms
$\mathcal{D}$	Boundary operator
D_0	Electron diffusivity
E	Electric field
E_C, E_V	Conduct and valence band edges
E_F	Fermi level
J	Electron current density
$\mathcal{L}$	Differential operator
N_C	Effective density of state
T	Electron temperature
T_0	Lattice or room temperature
$\mathcal{T}^h, \mathcal{T}_g^h$	Space-time Finite element subspaces
U	Solution of PDEs
U^h	Numerical solution of PDEs
$\mathcal{V}^h, \mathcal{V}_g^h$	Semi-discrete Finite element subspaces
V_D	Biased voltage at the drain
W	Electron energy density
W_d	Depletion width

Acknowledgement

I would like to express my deep gratitude to my supervisor Dr. Uri Ascher for his encouragement and guidance throughout the course of this work. I sincerely thank him for the fruitful suggestions and the patient proofreading so that this thesis could be completed.

Thanks also go to the members of my supervisory committee: Drs. Robert Miura, Michael Ward and Brian Wetton. Their helpful comments during this research and writing of the thesis are greatly appreciated.

Chapter 1

Introduction

1.1 Preliminary

1.1.1 Semiconductor Device Models

Numerical simulation of semiconductor devices provides an effective tool for device design in many cases of practical relevance. This is a thriving research area for scientists and engineers. Reliable numerical simulators must apply robust discretization techniques to a sufficiently accurate device model. This model should reflect important physical features needed, while redundant information is discarded.

Semiconductor device modeling started in the early fifties when the fundamental semiconductor device model, the so-called drift-diffusion (DD) model, was formulated by Van Roosbroeck [70]. This remarkable work started what today is an interdisciplinary subject that combines the efforts of physicists, electrical engineers and mathematicians. Much of the progress has been achieved in understanding the characteristics of devices and improving device design using perturbation analysis, numerical computation and solid state physics. In 1970, a sophisticated transport model was established for devices by Blotekær [6], which is usually referred to as the hydrodynamic (HD) model. This model includes the non-negligible hot carrier effect for submicron devices. As compared with the conventional DD model, much less work has been done on the HD model until recently.

The HD model consists of an incompletely parabolic system of conservation laws for

charge density[1] ρ, momentum J and energy W, and Poisson's equation for the electrostatic potential ψ. It is a highly nonlinear convection-diffusion system. The conservation laws can be derived from the Boltzmann equation by taking the first three moments with an additional heat conductivity term. The parabolic continuity equation in the DD model, however, is derived by the first moment method (see [60]).

The HD model is a cost-affordable extension of the conventional DD model. The recovery of the DD model from the HD model can be attained under assumptions of low carrier densities and small electric fields. Although the DD model constitutes a popular model for the semiconductor device simulation and is mathematically better understood than the HD model, the limitations of this model have been encountered more and more frequently with the miniaturization of devices or with the increment of the field strength. (Reduction of the active device size can be reflected by the increase of the field strength if one scales the equations of the model with suitable scaling parameters.) Alternatively, the HD model represents a reasonable model, which takes into account important physical phenomena such as velocity overshoots that are missing in the DD model [68, 57, 76].

A thorough investigation of carrier dynamics in semiconductor devices may be carried out using, for example, the Boltzmann equation for particle transport. This, however, involves a large amount of computational effort and makes application of numerical methods a formidable task. Moreover, it contains a lot of redundant information. Shur [76] demonstrated that in order to describe electron dynamics, the full solution of the Boltzmann equation is not necessary. For today's technology, the HD model (and its extensions and in many cases its simplifications) represents a reasonable compromise between the contradictory requirements of physical accuracy and computational tractability. It should be possible to develop semiconductor device analysis programs based on the HD

[1] In the semiconductor context, the notation n, not the ρ, is commonly used for the electron charge density. However we will use n for another purpose in the thesis.

model with the same generality as those based on the simpler DD model which are now routinely used in research and design environments.

Although advantages of the HD model over the DD model have been reported in the literature (cf. [76, 17]), weaknesses in the HD model also exist. For example, the commonly used model for the thermal conductivity

$$\kappa = \frac{\kappa_0 m \mu_0 T_0}{e}$$

is an empirical one. The lack of a rigorous model for the heat conductivity causes serious problems like the artificial velocity overshoot [22, 51]. Even though some intuitive remedies were proposed (see [30]), the limitations of these models are still unknown. Therefore discrepancies between solutions of the HD model and the real physical behavior are inevitable in some circumstances.

The DD model is by no means obsolete. It is valid under certain conditions and is still widely used either to simulate a variety of devices or to develop and test numerical simulation tools [11, 78]. The boundary of validity of the DD model is not entirely clear in applications. The established work on the DD model provides at least a gateway towards understanding the sophisticated HD model. As a compromise, some simplifications of the HD model (see [7, 8, 55]) were also employed and are considered good approximations to the full HD model in the engineering community. These simplifications alleviate some numerical difficulties inherited in the full HD model while still capturing the important physical phenomena missing in the DD model. However, it is questionable whether one can completely replace the full HD model by one of its simplifications and still obtain reasonably accurate physical data of interest, such as the I-V characteristics, for wide parameter ranges.

The order of complexity of the addressed models is: the DD model $\rightarrow$ the simplification of the HD model $\rightarrow$ the full HD model. Their associated ranges of applicability

have yet to be determined. Comparisons of the ability of these models to reproduce desirable properties are needed. It is especially interesting to investigate how "close" the simplification of the HD model approximates the full HD model, and in what situations their difference appears.

1.1.2 Numerical Tools

Numerical simulation of semiconductor devices is one of the challenging tasks in the area of scientific computation. Difficulties associated with solving the semiconductor device equations were discussed by many researchers (see e.g., [1, 3, 58, 60, 22, 29, 51]). The primary sources of difficulties are:

- Some of the coefficient functions and unknowns appearing in the device equations vary by several orders of magnitude so that their variations cannot be accurately resolved on a mesh of practical size by classical discretizations.

- These are singular perturbation problems with possible boundary and interior junction layers.

- Extremely large condition numbers are often encountered for the linearized discrete problem. Possible instability of nonlinear iterations may result [3].

- The conservation laws in the HD model possess hyperbolic modes. It is known that they can develop discontinuities or shocks (cf. Gardner *et al.* [29]). Numerical techniques in handling the transonic electron flow problems are more difficult to devise than for the subsonic case.

- The time-dependent problems are stiff and give differential-algebraic systems of index 1 or 2 (see [1]).

Efforts towards designing reliable numerical methods were made in the last two decades to overcome one or more of the difficulties addressed above. In particular, the successful Scharfetter-Gummel (SG) discretization [71] (in its original form based on the physically motivated approach to the one-dimensional diode, or in the modified and extended form) has been used up to now for the DD model. Comparatively, very slow progress has been made in developing reliable numerical tools for the HD model. Some efficient methods, such as the so-called essential non-oscillatory (ENO) method, were applied to solve the HD model, but they are one-dimensional in nature. Though applications to multi-dimensional problems are possible (see [51]), they lack theoretical backing. Attempts at designing reliable numerical methods for the multi-dimensional HD models were even less successful than for the one-dimensional ones. Previous work, including attempts to extend the SG discretization, either was not robust enough to resolve shock discontinuities or poorly smeared the shock fronts [69, 78].

The shock-capturing capability is an important concern in this thesis. Even without shocks, other sharp layers, such as junction layers, still cause difficulty. The classical methods, such as the central difference and Galerkin methods, are not good candidates. They often generate spurious oscillations near sharp layers. Upwinding schemes (which are designed according to the influence of the flow direction and strength) are therefore required, not only for the HD model but for the DD model as well (see [78, 11]). On the other hand, the requirement for higher resolution of sharp profiles demands a special kind of upwinding method. Simple minded upwinding methods, such as the artificial viscosity method, are not suitable.

The streamline-diffusion (SD) finite element method, introduced by Hughes and Brooks [34], provides a tool to achieve the goal. It is also called the streamline/upwinding Petrov-Galerkin (SUPG) method. The essence of the SD method is a Petrov modification of the test functions in the standard finite element subspace along the streamline

direction. An upwinding effect is then introduced, therefore spurious oscillations can be suppressed in the presence of discontinuities or sharp changes of solutions. The advantages of the SD method are:

- The algorithm does not need particular adjustments in the case when shocks are present as compared with other shock-capturing methods, so it is a general purpose method suitable for both hyperbolic and parabolic problems. A suitable amount of artificial diffusion (mainly along the streamline direction) is "turned on" when the problem considered is convection-dominated, and is "turned off" when the problem is diffusion-dominated.

- Local dissipation (or smearing) does not strongly degrade the sharpness of shocks or interior layers as compared with conventional upwinding schemes.

- It is especially suitable for handling multi-dimensional cases. The layers need not align with grid lines.

- It has theoretical backing (see e.g., [51, 46, 50] and a series of papers by Hughes *et al.* [38, 42, 40, 41, 36, 39, 37, 35, 75, 77]).

- It is a reasonable extension of the SG discretization (see [78]). Mathematically, both of them are methods of exponential fitting. The mechanism makes it possible for us to solve both the HD and DD models in the same framework, whereas in previous work, researchers more often than not tended to treat them separately.

1.2 Brief History Review I: Numerical Simulations

The emphasis towards numerical simulation techniques for semiconductor devices began in the early sixties. The breakthrough was made by Scharfetter and Gummel [71] in 1970.

They proposed a nonstandard discretization based on a physical approach to the one-dimensional silicon diode. In spite of its success, the mechanism was not well understood mathematically until 1980 when Doolan *et al.* [20] explained it. The mathematical formulation of the SG discretization was termed exponential fitting. It has since been generalized to two- and three-dimensional DD problems. Bank *et al.* [4] extended the SG method to two-dimensional problems by using the control volume method on rectangular meshes and by using the finite element method on triangular meshes. Polak *et al.* [65] further generalized the SG method to allow the use of quadrilateral meshes. Similar types of SG versions were analyzed on tetrahedra by Bank *el al* [5] and by Sever [74]. However, the multi-dimensional SG extensions were not as successful as the original one-dimensional one. Brezzi *et al.* [11] introduced the exponential fitting idea to the two-dimensional DD model using mixed and hybrid finite element methods. Nice properties of the methods and satisfactory numerical results were presented. However, the mixed or hybrid finite element subspaces should satisfy the so-called Brezzi-Babuška condition (see [10]). Different settings of nodal points (staggered grids) have to be used for different solution components. This usually brings some inconvenience. Moreover, their work was done just for the continuity equation, not for the whole system. For the time-dependent problem, an implicit time discretization scheme is recommended. Based on this idea, various time evolutionary schemes for the DD model in two and three dimensions were evaluated by Wu [81]. The linkage of the SD method to the SG method is attributed to the work of Sharma and Carey [78]. They showed that the original form of the SG method coincides with the SD method for the one-dimensional DD model. Therefore, the SD method provides a reasonable extension of the SG method for multi-dimensional problems.

Recent literature pertaining to the numerical solution of the HD models includes the studies of Rudan and Odeh [69] and Odeh *et al.* [62]. The SG discretization was

extended to the case of HD models. But these efforts, to some extent, were confined to only cover the case of subsonic transport, i.e., solutions were not expected to experience shock discontinuities.

The hyperbolic nature of the HD model may cause shocks for the transonic flow. The investigation of this phenomenon has become an interesting topic and has attracted much attention recently. For model studies of the one-dimensional ρ^+-ρ-ρ^+ ballistic diode, mathematical analysis by means of viscosity approximations was considered by Gamba [24, 25]. She claimed there was the possibility of boundary layer formation. Ascher *et al.* [2] presented an analysis of transonic shocks for a current driven problem in the isentropic case. A phase plane analysis gave a full explanation of how and when the shocks occur. A similar analysis was carried out later by Markowich and Pietra [59] in the non-isentropic case. In both cases, numerical computations illustrating the structure of the solutions were also reported.

In the simulations of the ρ^+-ρ-ρ^+ diode by the full HD model, shocks were found by Gardner [26] and Fatemi *et al.* [22] in the one-dimensional steady state and non-steady state cases, respectively. A two-dimensional simulation with shocks was done by Jiang [45] using the shock-capturing SD method.

Simulations for more realistic devices beyond the simple ρ^+-ρ-ρ^+ model comprise the early work by Cook and Frey [17] for the MESFET, and by Kreskovsky *et al.* [54] for the PBT. The recent work by Jerome and Shu [51], using the operator splitting ENO method, and Chen *et al.* [13], using the discontinuous Galerkin method for the two-dimensional MESFET, are more method oriented. Although there were no shocks observed, the shock-capturing algorithms proved to be useful when sharp layers were encountered.

In many situations, simplifications of the full HD model proved to be easy to use. One of them is to neglect the convective term in the momentum equation of the conservation laws. This was used by Lin *et al.* [55] to express the HD model in self-adjoint form

through a set of new Slotboom-like variables like those that are commonly used for the DD model. The so-called energy balance (EB) model is almost exclusively used in the engineering field in place of the full HD model (see the papers by Rahmat *et al.* [67] and Benvennuti *et al.* [7, 8]). In the full HD model, the energy W is the sum of kinetic energy and thermal energy, whereas in the EB model, W is assumed to be the thermal energy alone. Although the difference between solutions of the full HD and EB models is small in many cases, exceptional situation do happen in which the kinetic energy is no longer small.

1.3 Brief History Review II: Streamline-Diffusion Methods

The SD method was introduced for the stationary convection-dominated convection-diffusion equation by Hughes and Brooks in 1979 [34]. They proposed a Petrov modification of the classical Galerkin finite element method, which is also known as the SUPG method. This new method introduces artificial diffusion only along the streamline direction to suppress possible oscillations near discontinuities or sharp layers of the solution without causing overly large crosswind diffusion. Mathematical studies of the method were started by Johnson and Nävert [46], and continued by Nävert [61] and Johnson *et al.* [47, 50]. The work includes the extension to the time-dependent problem with the discontinuous Galerkin methodology. Primary stability, convergence and crosswind smear evaluation results were established for the model problem. The SD method gives added stability as compared with the classical Galerkin method. However, the L^2-norm error estimation for the former is a half-order lower than for the latter. That the error bound can not be improved was shown by Peterson [64], who presented an example using the discontinuous Galerkin method, a counterpart of the SD method.

From numerical experiments, a proper amount of crosswind dissipation is needed to

entirely control the oscillations near the discontinuities. A further Petrov modification of the SD method, a shock-capturing (SC) modification, was proposed by Hughes *et al.* [42]. The method is a true nonlinear one even if the problem considered is linear. It was adopted by Johnson and Szepessy [51] for solving the nonlinear Burgers equation. The explanation of such a modification was given by Johnson *et al.* [49] later. There were many efforts along this line afterwards, such as those of Codina [15] and Carmo and Galeão [12]. Now the shock-capturing SD method has become a standard formulation.

Systematic research was done by Hughes and his coworkers in the sequence of ten papers entitled *A new finite element formulation for computational fluid dynamics.* The cardinal forms of the SD operator (and its variant, the least-squares operator) and the SC operators were well established for the convection-diffusion scalar equation as well as for the case of a symmetric system. Thorough analyses of the stability, convergence and nonlinear iterative technique were carried out. Their work was directly applied to the compressible Euler and Navier-Stokes equations with success. Their contribution therefore laid a foundation for standardizing the SD method.

The advantage of the SD method utilizing the symmetric form for a PDE system was addressed in the above mentioned papers. For instance, there is guaranteed entropy stability of the symmetric SD scheme for the compressible Navier-Stokes equations [77]. However, the method depends strongly on symmetrization (that may not be known sometimes) of each individual problem. Even when a symmetrization procedure is known, the use of primitive variables to avoid added complexity is often preferred in applications. In [9] (by Le Beau *et al.*), SD methods based on both symmetric and non-symmetric forms of Euler equations were investigated and compared intensively for subsonic, transonic and supersonic flow problems. The experiment indicates that the advantage in using the symmetric formulation is invisible computationally.

It seems that analysis for the non-symmetric case may not be carried out by a straightforward extension of the symmetric one. Some of the early treatments were inappropriate (see [43]). Awareness of the importance of a choice of the SD operator was reflected in the recent literature comprising the work by Zhou [83] and Le Beau *et al.* [9] for the Euler equations, and by Jiang [45] for the HD model of the semiconductor device equations. In [45], which forms part of this thesis, a proper operator scaling is also presented, which was often ignored and yet is important. The importance of the scaling was stressed by Hughes and Mallet [40].

1.4 Objectives and Scope of the Thesis

The aim of the thesis is to investigate efficient, robust and consistent numerical methods for solving semiconductor device problems as formulated via the HD and DD models, and to explore the physical behaviors of the models through device simulations in applications.

In Chapter 2, we present semiconductor device models which we are going to consider in an decreasing order of complexity: the HD model $\rightarrow$ a proposed simplified HD (SHD) model $\rightarrow$ the mixed formulation DD (DD2) model $\rightarrow$ the conventional DD (DD1) model. Some properties of the device models useful for formulation of the non-symmetric SD method are investigated.

In Chapter 3, the non-symmetric SD method for convection-diffusion systems is designed to avoid the extra complexity of symmetric formulations of the systems involved. We derive a non-trivial SD operator for the non-symmetric system, which extends the previous work in [45]. The design includes two concerns: one is to follow the correct directions of streamlines and another is to provide suitable scaling. Both of them are important as is shown by concrete examples. The linear stability analysis presented shows that the proposed numerical method is stable if the system can be symmetrized.

This analysis, together with the support of the numerical evidence that we give, suggests that the combination of the method of lines and the SD semi-discretization may not be appropriate for time-dependent problems.

In Chapter 4, we propose a consistent Poisson solver which provides a higher-order convergence rate for the electric field $E = -\nabla\psi$ which is the only quantity needed in the conservation laws. The consistency of this Poisson solver is composed of two parts: (1) the order of accuracy of the electric field E is the same as that of solutions for the system of conservation laws when employing finite element subspaces with the same degree of polynomials; (2) it uses the same grid points as used by the SD scheme for the system, and therefore the device simulation algorithm can be more easily coded. Not much attention was previously paid regarding this consistency. This new method also provides a way to solve ψ and E in a decoupled nature as compared with its other counterparts. Error estimation and numerical tests are presented.

In Chapter 5, the ρ^+-ρ-ρ^+ diode is simulated by our numerical method. The effect of the "in-flow" boundary condition is incorporated weakly in the SD formulation for the first time in device simulations. This enhances the numerical stability. Shocks are captured at 77K for transonic flows in one and two space dimensions. In these cases, we find from our numerical evidence that the SHD model no longer approximates the full HD model very well as compared with many other cases encountered in applications.

In Chapter 6, we consider the simulation of 2-D MESFET (metal semiconductor field effect transistor) devices. Electron depletion near the gate is simulated. The leakage current of electrons is correctly reflected, although it is very small and can be neglected. The method successfully handles the case where the abrupt junctions are not aligned with grid lines. Experiments show that the performance of the method is very satisfactory and the computational results correctly reflect physical expectations.

Model comparisons are implemented. The difference in solutions between the HD and

DD models is significant in simulation of the MESFET device. However, the difference in solutions between the full HD and SHD models is negligible in this simulation.

Finally, in Chapter 7, we conclude by summarizing the work that has been done in the thesis and propose future research directions.

Chapter 2

Semiconductor Device Models

2.1 Introduction

Both the hydrodynamic (HD) and drift-diffusion (DD) models have been discussed and used in the literature of semiconductor device simulation. The HD model, however, has received additional attention in recent years with the development of VLSI technology. It is known that the HD model takes into account important physical phenomena missing in the DD model. Though the limitations of the DD model are becoming more and more obvious, studies of this model are by no means useless. Not only is the simpler DD model sufficient in many simulation cases, also many ideas which originated in the study of the DD model are often readily extendable to the study of the HD model (e.g., see the extension of the SG method by Rudan and Odeh [69] and the new Slotboom-like state variable by Lin *et al.* [55]).

In this chapter, mathematical formulations of the HD and DD models are presented. The DD model can be attained as a simplification from the HD model under certain assumptions. We consider, in Section 2.2, a hierarchical deduction from the full HD model to the simplified HD (SHD) model, to the mixed-formulation DD (DD2) model and finally to the conventional DD (DD1) model. Some properties of the formulated systems of PDEs, which are useful in the later chapters, are presented in Section 2.3. The issue of boundary conditions is discussed in Section 2.4.

All the models that we consider are for electron carrier transportation only, i.e.,

ignoring the hole carrier transportation. These models can be used to simulate devices such as the ρ^+-ρ-ρ^+ diode and the MESFET. For other devices, where the electron and hole carriers are equally important, it is possible to modify the models presented here for the electron by adding counterparts for the hole (see [55] and [54]). From the numerical point of view, we can decouple the effects of the electron and hole iteratively (but with care as discussed in [3]). Therefore, with such a procedure we essentially solve a PDE system for one carrier at each iteration.

2.2 Mathematical Equations

In this section, we review mathematical formulations for d-dimensional (d=1, 2) semiconductor device problems via the HD and DD models. We assume that the formulations have been properly scaled.

2.2.1 PDEs for HD Models

Let us consider first the HD model (or full HD model) of semiconductor device equations which can be derived from taking the first three moments of the Boltzmann equation. It expresses the conservation of charge, current and energy (see [6, 60])

HD Model:

$$\rho_t + \nabla \cdot J = 0, \tag{2.1a}$$

$$J_t + v\nabla \cdot J + J \cdot \nabla v + \nabla(\rho T) = -\tfrac{e\rho E}{m} + C_J, \tag{2.1b}$$

$$W_t + \nabla \cdot ((W + \rho T)v) = -\tfrac{eJ.E}{m} + C_W + \nabla \cdot (\kappa\rho\nabla T). \tag{2.1c}$$

Here $(\rho, J, W)^t$ is an unknown vector which represents the electron density, "(negative) current density" (which is different from the actual current density by multiplying a negative charge, but we still refer to it as a current density) and total energy density,

respectively. The conservation laws (2.1) are coupled with Poisson's equation for the electrostatic potential ψ by

$$\nabla \cdot (\lambda \nabla \psi) = \rho - \rho_D. \tag{2.2}$$

In the above equations, $E = -\nabla\psi$ stands for the electric field, v is the mean velocity and T is the scaled temperature (the usual temperature in Kelvin $T \leftarrow k_b T/m$, with k_b the Boltzmann constant). The physical parameters are: e the charge of the electron, m the effective mass of the electron, κ the thermal conductivity and λ the dielectric constant. The terms C_J and C_W, represent the rate of change of J and W respectively, due to intraband collisions. The forms of C_J and C_W are (see [26])

$$\begin{aligned} C_J &= -\frac{J}{\tau_J}, \\ C_W &= -\frac{W - \frac{3}{2}\rho T_0}{\tau_W}. \end{aligned}$$

In the above, τ_J and τ_W are relaxation times which are obtained empirically by

$$\begin{aligned} \tau_J &= \frac{m\mu_0 T_0}{eT}, \\ \tau_W &= \frac{3m\mu_0 T_0 T}{2ev_s^2(T_0 + T)} + \frac{\tau_J}{2}, \end{aligned}$$

where T_0 is the lattice temperature, μ_0 is the electron mobility and v_s is the saturation velocity. The thermal conductivity is taken as

$$\kappa = \frac{\kappa_0 m\mu_0 T_0}{e}.$$

The so called doping profile is given by ρ_D which is a function of only the space variables. Finally, to close the above system, we need the following current-velocity and energy-temperature relations

$$\begin{aligned} J &= \rho v, \\ W &= \frac{1}{2}\rho \mid v \mid^2 + \frac{3}{2}\rho T, \end{aligned}$$

which are ensured by the parabolic energy band structure.

The full HD model has highly nonlinear hyperbolic modes due to the presence of the convection term $v\nabla\cdot J + J\cdot\nabla v$ in (2.1b). This causes difficulties in the numerical treatment of this model. To remove such difficulties, a reduced HD (RHD) model (neglecting the convection term in (2.1b)) is often used [55]. It is considered to be a good approximation of the full HD model in applications. However, we propose a slightly different, still simplified (SHD) model as follows.

SHD Model:

$$\rho_t + \nabla \cdot J = 0, \tag{2.3a}$$

$$J_t + \nabla(\rho T) = -\tfrac{e\rho E}{m} + C_J, \tag{2.3b}$$

$$W_t + \nabla \cdot ((W + \rho T)v) + A_c^* = -\tfrac{eJ\cdot E}{m} + C_W + \nabla \cdot (\kappa\rho\nabla T). \tag{2.3c}$$

Here the correction term A_c^* is given by

$$A_c^* = -\frac{J}{\rho} \cdot (v\nabla \cdot J + J \cdot \nabla v).$$

The rationale for adding the correction term A_c^* will be given later in Section 2.3.

Note that shocks are supported by the HD model, but not by the SHD model. For the HD model, possible discontinuities caused by nonlinear shock waves (if there are any) are in the velocity v and electron density ρ [29].

2.2.2 PDEs for DD Models

The DD models can be derived by taking the zeroth-order moment of the Boltzmann equation. But we can obtain them by simply using the SHD model. If we further assume that $T = T_0$, (2.3) yields the following DD model with a system of two equations (DD2).

DD2 Model:

$$\rho_t + \nabla \cdot J = 0, \tag{2.4a}$$

$$J_t + T_0 \nabla \rho = -\tfrac{\epsilon \rho E}{m} + C_J. \tag{2.4b}$$

This is known to be a suitable approximation for the cases of small electric field or near thermal equilibrium [60].

If we define $D_0 = m\mu_0 T_0/\epsilon$ (Einstein relation), the diffusivity, then (2.4b) can be written as

$$\frac{m\mu_0}{\epsilon} J_t + \mu_0 \rho E + D_0 \nabla \rho = -J.$$

Ignoring the term $\frac{m\mu_0}{\epsilon} J_t$ (which is assumed to be small for ultra-small devices [60]), we are able to express the current J explicitly as

$$J = -(\mu_0 \rho E + D_0 \nabla \rho).$$

If we plug the above J into (2.4a), we obtain the conventional DD (DD1) model.

DD1 Model:

$$\rho_t - \nabla \cdot (\mu_0 \rho E + D_0 \nabla \rho) = 0. \tag{2.5}$$

The DD2 model can be viewed as a mixed formulation of the DD1 model, but (2.4) is not used as frequently as (2.5). Here we use it to test the capacity of our designed streamline-diffusion scheme for systems, which is generalized from the optimal formulation of the same scheme for scalar equations. This can be done by comparing numerical solutions of the two models in steady state where the analytical solutions of the two models are identical but numerical solutions are no longer the same.

2.3 Vector Form of HD Models

To ease our numerical formulation, we change $(\rho, J, W)^t$, the vector of primitive variables, to $(\rho, J, T)^t$, a vector of working variables. System (2.1) or (2.3) (assuming $d = 2$ for the

moment to simplify our notation) is then transformed to

$$A_0 U_t + A \cdot \nabla U + C(U) = \nabla \cdot (\mathcal{K} \nabla U), \tag{2.6}$$

where, $U = (\rho, J, T)^t$. A_0, A, C and $\mathcal{K}$ are defined below.

2.3.1 Form of the HD Model

In equation (2.6) for the HD model, the convection matrix is

$$A = \begin{pmatrix} A_1^t \\ A_2^t \end{pmatrix} \tag{2.7}$$

with

$$A_1 = \begin{pmatrix} 0 & 1 & 0 & 0 \\ T - \frac{J_1^2}{\rho^2} & \frac{2J_1}{\rho} & 0 & \rho \\ -\frac{J_1 J_2}{\rho^2} & \frac{J_2}{\rho} & \frac{J_1}{\rho} & 0 \\ -\frac{J_1 T}{\rho} & T & 0 & \frac{3}{2} J_1 \end{pmatrix}, \quad A_2 = \begin{pmatrix} 0 & 0 & 1 & 0 \\ -\frac{J_1 J_2}{\rho^2} & \frac{J_2}{\rho} & \frac{J_1}{\rho} & 0 \\ T - \frac{J_2^2}{\rho^2} & 0 & \frac{2J_2}{\rho} & \rho \\ -\frac{J_2 T}{\rho} & 0 & T & \frac{3}{2} J_2 \end{pmatrix}. \tag{2.8}$$

The mass matrix

$$A_0 = diag(1, 1, 1, \frac{3}{2}\rho) \tag{2.9}$$

is symmetric positive definite. The force term is

$$C = \begin{pmatrix} 0 \\ \frac{e}{m}\rho E_1 + \frac{J_1}{\tau_J} \\ \frac{e}{m}\rho E_2 + \frac{J_2}{\tau_J} \\ -\frac{|J|^2}{\rho \tau_J} + \frac{\frac{3}{2}\rho(T - T_0) + \frac{J^2}{2\rho}}{\tau_W} \end{pmatrix} \tag{2.10}$$

and the diffusion matrix

$$\mathcal{K} = diag(K, K) \tag{2.11}$$

with the symmetric positive semi-definite matrix

$$K = diag(0, 0, 0, \kappa\rho), \tag{2.12}$$

Since A_1 and A_2 are not symmetric, we will say that the system (2.6) is non-symmetric.

2.3.2 Form of the SHD Model

The matrices A_1 and A_2 in equation (2.6) corresponding to the SHD model are

$$A_1 = \begin{pmatrix} 0 & 1 & 0 & 0 \\ T & 0 & 0 & \rho \\ 0 & 0 & 0 & 0 \\ -\frac{J_1 T}{\rho} & T & 0 & \frac{3}{2}J_1 \end{pmatrix}, \quad A_2 = \begin{pmatrix} 0 & 0 & 1 & 0 \\ 0 & 0 & 0 & 0 \\ T & 0 & 0 & \rho \\ -\frac{J_2 T}{\rho} & 0 & T & \frac{3}{2}J_2 \end{pmatrix}. \tag{2.13}$$

We have added the correction term A_c^* in (2.3c). To see why such a term is added, we look into the details of the transformation from (2.1) to (2.6) by changing the variables. It is obvious from the energy-temperature relation that

$$W_t = (\frac{3}{2}T - \frac{J^2}{\rho^2})\rho_t + \frac{J}{\rho} \cdot J_t + \frac{3}{2}\rho T_t.$$

We derive (2.8) by replacing ρ_t using (2.3a) and J_t using (2.1b). Note that only the third equation (2.1c) is changed. If we then neglect the convection term in equation (2.1b) of the full HD model in this stage, we obtain (2.13) which corresponds to what we called the SHD model using the variables $(\rho, J, T)^t$. Changing $(\rho, J, T)^t$ back to $(\rho, J, W)^t$, this model turns into (2.3) with the appearance of an extra term A_c^*. The structure of the matrices in (2.13) is simpler than that of the corresponding matrices for the RHD model. For example, the last row of A_1 corresponding to the RHD model is

$$e_4^t A_1 = (-\frac{J_1 T}{\rho} - \frac{|J|^2 J_1}{\rho^3}, T + \frac{|J|^2 + J_1^2}{\rho^2}, \frac{J_1 J_2}{\rho^2}, \frac{3}{2}J_1).$$

while other rows are the same as those of A_1 in (2.13). There is another simplification of the full HD model, the so-called energy balance model (EB), which is used widely by engineers [7, 8]. In this model, the kinetic energy is assumed to be negligible. Therefore the total energy is equal to the thermal energy, i.e.,

$$W = \frac{3}{2}\rho T.$$

It is very simple to express the last row of A_1 corresponding to the EB model as

$$e_4^t A_1 = (0, T, 0, \frac{5}{2}J_1),$$

which is simpler than that of the SHD model. However, the eigenvalue-eigenvector problems for the EB model as well as for the RHD model are very complicated as compared with those for the full HD and SHD models.

2.3.3 Eigenvalue-Eigenvector Problem

Let us define

$$A_\mu = \mu_1 A_1 + \mu_2 A_2,$$

where $\mu = (\mu_1, \mu_2)^t$ is an arbitrary parameter vector satisfying $\mid \mu \mid_2 = (\mu_1^2 + \mu_2^2)^{1/2} = 1$. Consider the generalized eigenvalue-eigenvector problem

$$(A_\mu - \lambda_\mu A_0) Y_{\mu,i} = 0 \tag{2.14}$$

$(i = 1, \ldots, 4)$, then the generalized eigenvalues of A_μ are:

Type	Eigenvalues			
HD	$v \cdot \mu$	$v \cdot \mu$	$v \cdot \mu - c$	$v \cdot \mu + c$
SHD	0	$v \cdot \mu$	$-c$	c

In the above, $c = \sqrt{5T/3}$, the "sound speed" for $\kappa = 0$.

With the order of eigenvalues as above, A_μ has the following generalized eigen-matrix

$$Y_\mu = \begin{pmatrix} 0 & 1 & 1 & 1 \\ -\mu_2 & v_1 & v_1 - c\mu_1 & v_1 + c\mu_1 \\ \mu_1 & v_2 & v_2 - c\mu_2 & v_2 + c\mu_2 \\ 0 & -\frac{3c^2}{5\rho} & \frac{2c^2}{5\rho} & \frac{2c^2}{5\rho} \end{pmatrix} \tag{2.15}$$

for the full HD model, and

$$Y_\mu = \begin{pmatrix} 0 & 1 & 1 & 1 \\ -\mu_2 & \mu_1 v\cdot\mu & -c\mu_1 & c\mu_1 \\ \mu_1 & \mu_2 v\cdot\mu & -c\mu_2 & c\mu_2 \\ 0 & \frac{(v\cdot\mu)^2 - T}{\rho} & \frac{2c^2}{5\rho} & \frac{2c^2}{5\rho} \end{pmatrix} \tag{2.16}$$

for the SHD model. The matrices Y_μ are formed by assembling eigenvectors $Y_{\mu,i}$ ($i = 1, \ldots, 4$) as columns. The inverse matrices of Y_μ for the HD and SHD models are

$$Y_\mu^{-1} = \begin{pmatrix} v\times\mu & -\mu_2 & \mu_1 & 0 \\ \frac{2}{5} & 0 & 0 & -\frac{\rho}{c^2} \\ \frac{v\cdot\mu}{2c} + \frac{3}{10} & -\frac{\mu_1}{2c} & -\frac{\mu_2}{2c} & \frac{\rho}{2c^2} \\ -\frac{v\cdot\mu}{2c} + \frac{3}{10} & \frac{\mu_1}{2c} & \frac{\mu_2}{2c} & \frac{\rho}{2c^2} \end{pmatrix}, \tag{2.17}$$

where $\times$ is the cross product operator, and

$$Y_\mu^{-1} = \begin{pmatrix} 0 & \mu_2 & \mu_1 & 0 \\ \frac{2T}{3(c^2-(v\cdot\mu)^2)} & 0 & 0 & \frac{\rho}{(v\cdot\mu)^2-c^2} \\ \frac{5v\cdot\mu+3c}{10(c+v\cdot\mu)} & -2c\mu_1 & -2c\mu_2 & \frac{\rho}{2c(c+v\cdot\mu)} \\ \frac{3c-5v\cdot\mu}{10(c-v\cdot\mu)} & 2c\mu_1 & 2c\mu_2 & \frac{\rho}{2c(c-v\cdot\mu)} \end{pmatrix}, \tag{2.18}$$

respectively. Therefore, we can diagonalize the matrix $A_0^{-1}A_\mu$ to Λ_μ with eigenvalues of (2.14) forming its entries.

2.3.4 Properties

We have the following results which enable construction of a suitable non-symmetric SD formulation for the HD models in the next chapter.

Proposition 2.1 *For the HD model, there exists a diagonal matrix* $\Lambda_\beta = diag(\beta_1, \ldots, \beta_{d+2})$ *with constants* $\beta_i > 0$ $(i = 1, \ldots, d+2)$ *, such that* $\Lambda_\beta Y_\mu^{-1} A_0^{-1} K Y_\mu$ *is symmetric positive semi-definite.*

Proof. Here we only prove the typical case where $d = 2$ without loss of generality. From the definitions of Y_μ, A_0 and K we have

$$Y_\mu^{-1} A_0^{-1} K Y_\mu = \frac{9\kappa}{10} \begin{pmatrix} 0 \\ -1 \\ \frac{1}{2} \\ \frac{1}{2} \end{pmatrix} (0, -1, \frac{2}{3}, \frac{2}{3}), \tag{2.19}$$

which is independent of μ. It is easy to see that if we select

$$\Lambda_\beta = diag(1, 1, \frac{4}{3}, \frac{4}{3}), \tag{2.20}$$

then the matrix $\Lambda_\beta Y_\mu^{-1} A_0^{-1} K Y_\mu$ is symmetric positive semi-definite with rank 1. □

Proposition 2.2 *For the SHD model, if* $|v| < \sqrt{T}$*, then there exists a diagonal matrix* $\Lambda_\beta = diag(\beta_1, \ldots, \beta_{d+2})$ *with* $\beta_i > 0$ $(i = 1, \ldots, d+2)$*, such that* $\Lambda_\beta Y_\mu^{-1} A_0^{-1} K Y_\mu$ *is symmetric positive semi-definite.*

Proof. Similar to the argument in the proof of Proposition 2.1 $(d = 2)$,

$$Y_\mu^{-1} A_0^{-1} K Y_\mu = \frac{2\kappa}{3} \begin{pmatrix} 0 \\ \frac{1}{(v\cdot\mu)^2 - c^2} \\ \frac{1}{2c(c+v\cdot\mu)} \\ \frac{1}{2c(c-v\cdot\mu)} \end{pmatrix} (0, (v\cdot\mu)^2 - T, \frac{2c^2}{5}, \frac{2c^2}{5}). \tag{2.21}$$

We select

$$\Lambda_\beta = diag(1, \frac{(v\cdot\mu)^2 - c^2}{(v\cdot\mu)^2 - T}, \frac{5(c + v\cdot\mu)}{c}, \frac{5(c + v\cdot\mu)}{c}), \tag{2.22}$$

then the matrix $\Lambda_\beta Y_\mu^{-1} A_0^{-1} K Y_\mu$ is symmetric positive semi-definite. Since $|v| < \sqrt{T}$, all β_i $(i = 1, \ldots, 4)$ are positive. □

For system (2.1) with primitive variables, a similar result to that of Proposition 2.1 can be obtained. This can be found in Appendix A.

2.4 Boundary Conditions

The semiconductor device equations in Section 2.2 are posed in a bounded domain Ω representing the device geometry. The boundary Γ of Ω is piecewise smooth for the two-dimensional problem and trivially consists of two points for the one-dimensional problem. The boundary can generally be split into two disjoint parts:

$$\Gamma = \Gamma_1 \bigcup \Gamma_2.$$

For devices under consideration, such as the ρ^+-ρ-ρ^+ and the MESFET, Γ_1 and Γ_2 represent those parts of the boundary which correspond to metal Ohmic contacts and insulating parts, respectively. In the one-dimensional case, it reduces to $\Gamma = \Gamma_1$. For the MESFET device, Γ_1 can be further split into two disjoint parts:

$$\Gamma_1 = \Gamma_1^O \bigcup \Gamma_1^S,$$

where Γ_1^O denotes the parts of Γ_1 corresponding to Ohmic contacts and Γ_1^S corresponding to Schottky contacts.

2.4.1 Ohmic and Schottky Contacts

The concept of Ohmic and Schottky contacts are very important in modern device technology. The investigation and description of these contacts can be found in many published works (see, e.g., [72, 58, 66, 79] and the references therein).

A Schottky contact is a special metal-semiconductor contact which produces a so-called Schottky barrier with a significantly large barrier height $e\phi_B$ (the definition of ϕ_B will be given in detail in Chapter 6). It influences the device by forming a so-called depletion region, where the current is negligible.

An Ohmic contact possesses a negligible resistance. In principle, there is a potential barrier at the contact, with a very low height. The usual formation of the Ohmic contact is to dope the semiconductor heavily, so that it does not significantly perturb the device performance.

For the pure voltage driven contacts, the electrostatic potential can be expressed by (see [72])

$$\psi|_{\Gamma_1^S} = \psi_{bi} - \psi_{S0} + V_G, \tag{2.23}$$

$$\psi|_{\Gamma_1^O} = \psi_{bi} + V_D. \tag{2.24}$$

ψ_{bi} is a built-in potential, which is given by

$$\psi_{bi} = \frac{mT_0}{e} \ln \frac{\rho_D}{\rho_i}, \tag{2.25}$$

where ρ_i is the intrinsic electron density. ψ_{S0} is the potential related to the barrier height and V_G, V_D are external biased voltages at Γ_1^S and Γ_1^O, respectively. The typical value of ψ_{S0} is usually between half a volt and one volt.

The thermionic emission and diffusion theory [79] leads to the current expression at the Schottky contact,

$$J = -v_{th}(\rho - \rho_0), \tag{2.26}$$

where v_{th} is the thermionic emission velocity and ρ_0 is the surface electron density in thermal equilibrium ($V_G = V_D = 0$), which admits the following expression:

$$\rho_0 = \rho_D \exp(-\frac{e}{mT_0}\psi_{S0}). \tag{2.27}$$

When the Schottky contact operates in the reverse biased mode, the leakage current is small, i.e.,

$$J \approx 0, \tag{2.28}$$

at Γ_1^S. Therefore we can simply use the following boundary condition for ρ at the Schottky contact:

$$\rho|_{\Gamma_1^S} = \rho_0, \tag{2.29}$$

if the contact is in the reverse biased mode [72].

2.4.2 Traditional Boundary Conditions

We now write the traditional boundary conditions as follows, according to [69],

$$T|_{\Gamma_1} = T_0 \tag{2.30}$$

and

$$J \cdot n|_{\Gamma_2} = 0, \tag{2.31}$$

$$\nabla T \cdot n|_{\Gamma_2} = 0, \tag{2.32}$$

$$E \cdot n|_{\Gamma_2} = 0. \tag{2.33}$$

In the above, n denotes the unit normal vector on Γ. Besides these, we specify

At the Ohmic contact:

$$\rho|_{\Gamma_1^O} = \rho_D, \tag{2.34}$$

$$\psi|_{\Gamma_1^O} = \psi_{bi} + V_D. \tag{2.35}$$

At the Schottky contact:

$$\rho|_{\Gamma_1^S} = \rho_0, \tag{2.36}$$

$$\psi|_{\Gamma_1^O} = \psi_{bi} - \psi_{S0} + V_G. \tag{2.37}$$

We later take $V_G = 0$. ψ_{S0} will be specified in Chapter 6.

Remark 2.1 *The boundary condition (2.31) implies (see [69]) that*

$$\nabla\rho \cdot n|_{\Gamma_2} = 0. \tag{2.38}$$

Conditions (2.31) and (2.38) are equivalent only in the DD models. □

The boundary conditions (2.30)-(2.37) are physical boundary conditions. They turn out to be sufficient only for the SHD and DD models [80]. Mathematically, we need an extra "in-flow" boundary condition in case the two-dimensional HD model is used. This issue will be discussed in the next subsection.

2.4.3 "In-Flow" Boundary Condition

System (2.1) is an incompletely parabolic problem. General well-posed boundary conditions for such a system were analyzed in [31] in the fluid dynamics context. In the context of the semiconductor device problem, Thomann and Odeh [80] carried out a discussion on the well-posedness of the boundary conditions for the two-dimensional full HD model. They found that an extra "in-flow" boundary condition according to the eigenvalue $v \cdot n$ of A_n (taking $\mu = n$ at the boundary) is needed in the case that the contact Γ_1 is subsonic, i.e.,

$$\mid v \mid |_{\Gamma_1} \leq c^*|_{\Gamma_1}, \tag{2.39}$$

where

$$c^* = \sqrt{T} \tag{2.40}$$

stands for the "sound speed" for $\kappa \neq 0$. In order to describe the "in-flow" boundary condition, we define Γ_{in}, a part of Γ_1, as an "in-flow" boundary, i.e., it satisfies

$$J \cdot n|_{\Gamma_{in}} < 0.$$

Then the "out-flow" boundary is $\Gamma_{out} = \Gamma_1 \backslash \Gamma_{in}$.

According to [80] and [73], instead of (2.34) and (2.36), we can take

$$J \cdot \tau|_{\Gamma_{in}} = 0, \qquad \rho|_{\Gamma_{out}} = \rho_D, \tag{2.41}$$

where τ is a unit vector tangential to Γ, and the "in-flow" boundary condition

$$J \cdot n|_{\Gamma_{in}} = f(\rho) \tag{2.42}$$

for a proper function f, derived from the so-called "maximal dissipative" principle. Two observations were made in [80]:

1. The "in-flow" condition (2.42) is satisfied by (2.26) at the Schottky contact with a defined f.

2. When the device size tends to infinity (i.e., the HD model reduces to the DD model), (2.41) and (2.42) lead to the normal Dirichlet boundary condition for ρ.

Unfortunately, since no explicit function f is suggested in general, this approach is impractical for implementation. Moreover, there is still some doubt about the necessity of this condition in many real case simulations, especially when the convection term in (2.1b) does not play a significant role. So far there is no general agreed-upon "in-flow" boundary condition available in practice. A problem dependent "in-flow" boundary condition will be proposed in Chapter 5.

Chapter 3

Non-Symmetric Streamline-Diffusion Method

3.1 Introduction

Let us consider the convection-diffusion system of l partial differential equations in d spatial variables,

$$\mathcal{L}U \triangleq A_0 U_t + A \cdot \nabla U - \nabla \cdot \mathcal{K} \nabla U - F = 0 \tag{3.1}$$

where A_0 (mass matrix) is an $l \times l$ symmetric positive definite matrix, and

$$\begin{aligned} U^t &= (U_1, U_2, \ldots, U_l), && \text{(solution vector)} \\ A^t &= (A_1, A_2, \ldots, A_d), && \text{(convection matrix)} \\ \mathcal{K} &= diag(K, \cdots, K) && \text{(diffusion matrix)} \end{aligned}$$

with $l \times l$ matrices A_j and K. The term F in (3.1) is a source term.

System (3.1) is parabolic if K is nonsingular and hyperbolic when $K \equiv 0$. We are interested here in a more general case where K is allowed to be a singular nonzero matrix. This gives a so-called incompletely parabolic system.

Definition 3.1 *If A_j $(j = 1, \ldots, d)$ and K are all symmetric, then system (3.1) is said to be symmetric, otherwise it is said to be non-symmetric.* □

For some physical systems, such as the Euler equations of gas dynamics, the compressible Navier-Stokes equations and the hydrodynamic model of semiconductors, a symmetrization procedure exists such that a symmetric form of (3.1) can be obtained (e.g.,

[33, 38, 16, 73]). However, even in such cases where a symmetrizing transformation is known, the advantage of using the symmetric form in numerical computation doesn't seem to be obvious. In [9], streamline-diffusion (SD) methods based on both symmetric and non-symmetric forms of Euler equations were investigated and compared intensively for subsonic, transonic and supersonic flow problems. It was shown that solutions obtained using the two formulations are very close. In practice, people often prefer not to use the symmetric form due to the added complexity of the resulting formulation. This is the case, for example, in semiconductor device simulations, where the symmetrization is seldom used. For these reasons, it is useful to consider the SD formulation for non-symmetric systems.

The SD formulation for the symmetric convection-diffusion system was discussed by Hughes and Mallet [40] for the semi-discrete finite element scheme. An even more generalized design was given by Shakib *et al.* [77] for the full discrete scheme. The study of one-dimensional model problems is crucial in order to obtain proper formulations since some previous studies failed to treat the problem appropriately even in such a case.

It seems that the analysis for the non-symmetric case may not be carried out by a straightforward extension of the argument in [40]. In this chapter, a brief review of the SD method and some previous relevant results are presented in Section 3.2. Semi-discrete SD formulations for non-symmetric convection-diffusion systems of model problems are discussed in Section 3.3. A proper SD operator is derived in such a manner that it gives an optimal behavior if the system can be decoupled. In Section 3.4, the result in Section 3.3 is further generalized to full discretization schemes, including space-time SD formulations and methods of lines. Linear stability of commonly employed transient schemes is discussed in Section 3.5. In Section 3.6, numerical tests are presented, which support our arguments. From now on, we assume throughout this chapter that (3.1) is a linear constant coefficient system unless otherwise specified.

3.2 Brief Review

A brief review of SD methods relevant in our context is given in this section. For convenience, only problem (3.1) in steady state is considered.

3.2.1 Concept of the SD Method

To introduce the concept, we consider the scalar convection-diffusion equation of (3.1) in the form

$$a \cdot \nabla u = \kappa \Delta u + f, \tag{3.2}$$

which is defined in Ω with $\Omega \subset I\!R^d$. We prescribe mixed boundary condition on the boundary Γ of the domain Ω

$$u|_{\Gamma_1} = g, \tag{3.3}$$

$$\nabla u \cdot n|_{\Gamma_2} = 0. \tag{3.4}$$

Let $T_h = \{\Omega_e\}$ be a finite element triangulation of Ω, where Ω_e, $(e = 1, \ldots, n_{el})$, are typically triangles or quadrilaterals. We define the following finite element subspace, with spacing parameter h,

$$\mathcal{V}_g^h = \{v^h \mid v^h \in C^0(\Omega),\, v^h\,|_{\Omega_e} \in P_k(\Omega_e),\, v^h|_{\Gamma_1} = g\}, \tag{3.5}$$

where P_k is a polynomial space of degree at most k.

The essence of the SD method is a Petrov modification of the usual test function $v^h \in \mathcal{V}_0^h$ in the classical Galerkin method by adding a perturbation term along the streamline direction a, i.e.,

$$v^h \longleftarrow v^h + \tau a \cdot \nabla v^h,$$

where $\tau > 0$ is a scaling parameter. To denote the above perturbation term, we define the SD operator P^h by

$$P^h(v^h) = \tau a \cdot \nabla v^h.$$

Let $(f,g)_{\Omega_S}$ denote the usual inner product of functions f and g, and $\|f\|_{\Omega_S}$ be the corresponding L^2-norm on a space domain Ω_S. We customize $(f,g) = (f,g)_\Omega$ and $\|f\| = \|f\|_\Omega$ if $\Omega_S = \Omega$. Then the SD variational form for (3.2) reads: Find $u^h \in \mathcal{V}_g^h$ such that for all $\varphi \in \mathcal{V}_0^h$

$$\begin{aligned} &(a \cdot \nabla u^h, \varphi) + (\kappa \nabla u^h, \nabla \varphi) && \text{(Galerkin)} \\ &\quad + \sum_{e=1}^{n_{el}} (a \cdot \nabla u^h - \nabla \cdot (\kappa \nabla u^h) - f, P^h(\varphi))_{\Omega_e} && \text{(SD)} \\ &\quad = (f, \varphi). \end{aligned} \tag{3.6}$$

Note that the second line of (3.6) yields

$$\sum_{e=1}^{n_{el}} (a \cdot \nabla u^h + \cdots, P^h(\varphi))_{\Omega_e} = \underbrace{\sum_{e=1}^{n_{el}} (a \cdot \nabla u^h, \tau a \cdot \nabla \varphi)_{\Omega_e}}_{\text{streamline-diffusion}} + \cdots. \tag{3.7}$$

The first term of (3.7) introduces an upwinding effect so that it enhances the stability of the scheme. The choice of τ is important: either too small or too large a value may cause problems of oscillatory or overly diffused behavior of numerical solutions, respectively.

We define the element Peclet number

$$\alpha_e = \frac{1}{2} |a|_2 h_e / \kappa, \tag{3.8}$$

where $|a|_2 = (\sum_{i=1}^d a_i^2)^{1/2}$ and h_e is the element spacing parameter. A suitable choice of τ in [42] satisfies: if α_e is small (diffusion-dominated), then

$$\tau|_{\Omega_e} \sim O(h_e)^2/\kappa \tag{3.9}$$

and, if α_e is large (convection-dominated), then

$$\tau|_{\Omega_e} \sim O(h_e/|a|_2). \tag{3.10}$$

For example, when Ω_e is a rectangle element, the optimal choice of τ is

$$\tau = \frac{1}{2} h_e \xi(\alpha_e)/|a|_2 \tag{3.11}$$

with

$$\xi(\alpha_e) = \coth(\alpha_e) - {\alpha_e}^{-1}.$$

This leads to the following error estimate for the steady state case.

Theorem 3.1 *Let $\alpha_{max} = \max_e(\alpha_e)$. (1) If $\alpha_{max} \gg 1$ (convection-dominated), then*

$$\|u^h - u\| = O(h^{k+1/2}). \tag{3.12}$$

(2) If $\alpha_{max} \ll 1$ (diffusion-dominated), then

$$\|u^h - u\| = O(h^{k+1}). \ \square \tag{3.13}$$

The error estimate in (3.12) is a half-order lower than in (3.13). It may not be improved in general (along the line of the argument in [64]), but in many cases, the sharp error estimate $O(h^{k+1})$ is often observed.

3.2.2 SD Methods for Systems

We now consider extensions of the scalar SD formulation for the convection-diffusion system (3.1). We assume that the problem is defined in $\Omega = I\!R^d$ to ease our analysis.

Remark 3.1 *If problem (3.1) is defined in a bounded domain, we need to prescribe boundary conditions. Unfortunately, it is extremely difficult, in general, to find a set of*

well-posed boundary conditions for such an incompletely parabolic system. Only for some special cases, for instance the Friedrichs' system [47], are we able to specify boundary conditions suitable for a numerical analysis. □

For later purposes, let us define $[A]$ the 'pseudo-transpose' of A by

$$[A]^t = (A_1^t, A_2^t, \ldots, A_d^t). \tag{3.14}$$

Introducing

$$A_\mu = \mu_1 A_1 + \mu_2 A_2 + \cdots + \mu_d A_d, \tag{3.15}$$

where $\mu = (\mu_1, \mu_2, \ldots, \mu_d)^t$ with $\mu_i \geq 0$ $(j = 1, \ldots, d)$ is an arbitrary parameter vector satisfying $|\mu| = 1$, we assume in the following that A_μ is diagonalizable, i.e., there exist a non-singular matrix Y_μ and a diagonal matrix Λ_μ such that

$$Y_\mu^{-1} A_0^{-1} A_\mu Y_\mu = \Lambda_\mu \tag{3.16}$$

with diagonal elements forming eigenvalues λ_i, $(i = 1, \ldots, l)$, of $A_0^{-1} A_\mu$.

A finite element subspace analogous to (3.5) is given by

$$\mathcal{V}^h = \{V^h \mid V^h \in (C^0(\Omega))^l,\ V^h\ |_{\Omega_e} \in (P_k(\Omega_e))^l\}. \tag{3.17}$$

The counterpart of (3.6) for (3.1) in steady state reads: Find $U^h \in \mathcal{V}^h$ such that for all $\Psi \in \mathcal{V}^h$

$$\begin{aligned} &(A \cdot \nabla U^h, \Psi) + (\mathcal{K} \nabla U^h, \nabla \Psi) && \text{(Galerkin)} \\ &\quad + \sum_{e=1}^{n_{el}} (\mathcal{L} U^h, P^h(\Psi))_{\Omega_e} && \text{(SD)} \\ &\quad = (F, \Psi). \end{aligned} \tag{3.18}$$

For the coupled system (3.1), we lose the vision of streamline directions. Therefore, an appropriate generalization of the operator P^h is not trivial for system (3.1), even in the

symmetric case. Some previous attempts fail to treat each component equation properly even for a decoupled one-dimensional problem [43].

The two common nonzero choices of P^h (when $A_0 = I_l$, an identity matrix) are

Choice (a):

$$P^h(\Psi) = \tau A \cdot \nabla \Psi = \sum_{j=1}^{d} \tau A_j \Psi_{x_j}; \tag{3.19}$$

Choice (b):

$$P^h(\Psi) = \tau [A] \cdot \nabla \Psi = \sum_{j=1}^{d} \tau A_j^t \Psi_{x_j}, \tag{3.20}$$

where $\tau \geq 0$. When (3.1) is symmetric, (a) and (b) are identical. At a first glance, choice (a) of P^h may seem to be more attractive than choice (b). This is because if we take a look at the artificial diffusion term in (3.18), i.e.,

$$(A \cdot \nabla U^h, P^h(\Psi)) = \int_\Omega (\nabla U^h)^t D_s \nabla \Psi dx \tag{3.21}$$

using choice (a), we find that the artificial diffusion matrix $D_s = A\tau A^t$ is symmetric positive semi-definite, which is normally expected as in the symmetric system case. In contrast, the artificial diffusion matrix $D_s = A\tau A$ using choice (b) is indefinite. However, the choice of (a) was criticized, for example, by [42] and [83]. In [83], the choice of (b) was actually used to compute one-dimensional Euler flow. Numerical computations in [43] showed better results with choice (b) than with choice (a).

With the detailed investigation that follows, we are able to understand the intrinsic behavior of the above choices. Furthermore, a suitable operator P^h can be generated for the incompletely parabolic system (2.6) that we are concerned with in semiconductor device simulations. For clarity, we carry out the discussion only for the finite element space $\mathcal{V}^h$ with uniform rectangular elements Ω_e. The obtained results can be extended in a straightforward manner to more general cases using element-wise local coordinate transformations (see [77, 40]).

3.3 Semi-Discrete SD Formulations

Let us consider the convection-diffusion system (3.1). The problem is defined in $\Omega \times (0, T]$ (with $\Omega = I\!R^d$). Then we require that (3.1) be subject to the initial condition

$$U(\cdot, 0) = U_0, \tag{3.22}$$

with U_0 having compact support in $I\!R^d$. For convenience, we define $Z_\mu = A_0^{1/2} Y_\mu$ so that

$$Z_\mu^{-1} A_0^{-1/2} A_\mu A_0^{-1/2} Z_\mu = \Lambda_\mu. \tag{3.23}$$

The following assumption on the matrix K is needed for our discussion.

Assumption 3.1 *There exists a diagonal matrix $\Lambda_\beta = diag(\beta_1, \ldots, \beta_l)$, with $\beta_i > 0$ ($i = 1, \ldots, l$), such that $\Lambda_\beta^{1/2} Z_\mu^{-1} A_0^{-1/2} K A_0^{-1/2} Z_\mu \Lambda_\mu^{-1/2}$ is symmetric positive semi-definite.* □

The validity of this assumption is justified by Propositions 2.1 and 2.2 for the HD and SHD models.

3.3.1 One-Dimensional Case

For the one-dimensional case $d = 1$, (3.1) can be written as

$$A_0 U_t + A U_x = K U_{xx} + F. \tag{3.24}$$

We first consider a simpler case, i.e., $A_0 = I_l$ and $K = \kappa I_l$, where I_l is the $l \times l$ identity matrix. Then (3.24) can be diagonalized by the transformation $U = ZV$, to read

$$V_t + \Lambda V_x = \kappa V_{xx} + \tilde{F}, \tag{3.25}$$

where $\tilde{F} = Z^{-1} F$. It is easy to see that (3.25) is fully decoupled. Each component equation of (3.25) has the form

$$v_{i,t} + \lambda_i v_{i,x} = \kappa v_{i,xx} + \tilde{f}_i. \tag{3.26}$$

This is a scalar advection-diffusion equation. The semi-discrete SD-type variational form for (3.26) can be obtained using the SD method (3.6) with τ_i given by (3.11) (replacing a in (3.11) by λ_i). Thus the optimal behavior of the scheme is attained. If we assemble (3.26) in vector form for all i ($i = 1, \ldots, l$), we obtain the SD formulation for (3.25)

$$\begin{aligned}(\Lambda V_x^h, \Phi) + (\kappa V_x^h, \Phi_x) + \sum_{e=1}^{n_{el}} (\Lambda V_x^h - \kappa V_{xx}^h - \tilde{F} + V_t^h, \Lambda_\tau \Lambda \Phi_x)_{\Omega_e} \\ = (\tilde{F} - V_t^h, \Phi). \end{aligned} \tag{3.27}$$

In (3.27),

$$\Lambda_\tau = diag(\tau_1, \tau_2, \ldots, \tau_l). \tag{3.28}$$

After employing the change of variables $V^h = Z^{-1}U^h$ and $\Phi = Z^t\Psi$, (3.27) converts to the semi-discrete SD formulation for the system (3.24), that is,

$$\begin{aligned}(AU_x^h, \Psi) + (\kappa U_x^h, \Psi_x) + \sum_{e=1}^{n_{el}} (\mathcal{L}U^h, (A\tau)^t \Psi_x)_{\Omega_e} \\ = (F - U_t^h, \Psi), \end{aligned} \tag{3.29}$$

where

$$\tau = Z\Lambda_\tau Z^{-1}. \tag{3.30}$$

Thus, the proper choice of P^h in this case should be

$$P^h = (A\tau)^t \Psi_x. \tag{3.31}$$

It is clear now that choice (a) of P^h is not suitable and choice (b) of P^h, which indeed is better, needs to be further rescaled by a more general τ.

Next, we will consider the case when $A_0 \neq I_l$ and K is more general, possibly even singular. Under Assumption 3.1, our previous argument can be adjusted corresponding

to this more general case. Similar to the derivation of (3.25), (3.24) becomes, by the transformation $V = \Lambda_\beta^{1/2} Z^{-1} A_0^{1/2} U$,

$$V_t + \Lambda V_x = \tilde{K} V_{xx} + \tilde{F}, \tag{3.32}$$

where $\tilde{F} = \Lambda_\beta^{1/2} Z^{-1} A_0^{-1/2} F$ and

$$\tilde{K} = \Lambda_\beta^{1/2} Z^{-1} A_0^{-1/2} K A_0^{-1/2} Z \Lambda_\beta^{-1/2} \tag{3.33}$$

is symmetric positive semi-definite. Noting that (3.32) is a special symmetric system, the symmetric SD formulation for (3.32) can be derived according to [40], yielding

$$\begin{aligned} (\Lambda V_x^h, \Phi) + (\tilde{K} V_x^h, \Phi_x) + \sum_{e=1}^{n_{el}} (\Lambda V_x^h - \tilde{K} V_{xx}^h - \tilde{F} + V_t^h, \Lambda_\tau \Lambda \Phi_x)_{\Omega_e} \\ = (\tilde{F} - V_t^h, \Phi), \end{aligned} \tag{3.34}$$

where Λ_τ can still be defined by (3.28) and its entries are defined by

$$\tau_i = \frac{1}{2} h \xi(\alpha_i) / |\lambda_i|, \tag{3.35}$$

$$\alpha_i = \frac{1}{2} |\lambda_i| h / \kappa_i, \tag{3.36}$$

$$\xi(\alpha_i) = \coth(\alpha_i) - {\alpha_i}^{-1}, \tag{3.37}$$

$$\begin{aligned} \kappa_i &= e_i^t \Lambda_\beta^{1/2} Z^{-1} A_0^{-1/2} K A_0^{-1/2} Z \Lambda_\beta^{-1/2} e_i \\ &= e_i^t Z^{-1} A_0^{-1/2} K A_0^{-1/2} Z e_i. \end{aligned} \tag{3.38}$$

In the above, $\kappa_i \geq 0$ is ensured by Assumption 3.1. Employing the change of variables $V^h = \Lambda_\beta^{1/2} Z^{-1} A_0^{1/2} U^h$ and $\Phi = \Lambda_\beta^{-1/2} Z^t A_0^{1/2} \Psi$, we obtain the semi-discrete SD formulation for system (3.24)

$$\begin{aligned} (A U_x^h, \Psi) + (K U_x^h, \Psi_x) + \sum_{e=1}^{n_{el}} (\mathcal{L} U^h, (A\tau)^t \Psi_x)_{\Omega_e} \\ = (F - A_0 U_t^h, \Psi). \end{aligned} \tag{3.39}$$

The matrix τ in (3.39) is given by

$$\tau = A_0^{-1/2} Z \Lambda_\tau Z^{-1} A_0^{-1/2}. \tag{3.40}$$

From the above, we obtain P^h in such a case as

$$P^h(\Psi) = (A\tau)^t \Psi_x. \tag{3.41}$$

As we have observed, the above definition of τ is independent of the particular form of Λ_β. Therefore, Λ_β is just an auxiliary matrix which is not involved in actual computations.

3.3.2 Multi-Dimensional Case

In this subsection, we attempt to extend our construction of P^h from the one-dimensional case to the multi-dimensional case. A reasonable extension seems to be

$$P^h(\Psi) = [A]\tau \cdot \nabla \Psi. \tag{3.42}$$

The scaling matrix τ above is defined by

$$\tau = A_0^{-1/2} Z_{\mu_d} diag(\tau_1, \cdots, \tau_l) Z_{\mu_d}^{-1} A_0^{-1/2}, \tag{3.43}$$

where for $i = 1, \ldots, l$,

$$\mu_d = \frac{1}{\sqrt{d}} (\overbrace{1, \cdots, 1}^{d})^t, \tag{3.44}$$

$$\tau_i = \frac{1}{2} h \xi_i / |\lambda_i|_2 \tag{3.45}$$

and

$$|\lambda_i|_2 = (\sum_{j=1}^{d} (\lambda_{i,j})^2)^{1/2}, \tag{3.46}$$

$$\xi_i = \coth(\alpha_i) - \alpha_i^{-1}, \tag{3.47}$$

$$\alpha_i = \frac{1}{2} |\lambda_i|_2 h / \kappa_i \tag{3.48}$$

$$\kappa_i = e_i^t Z_{\mu_d}^{-1} A_0^{-1/2} K A_0^{-1/2} Z_{\mu_d} e_i. \tag{3.49}$$

Here $\lambda_{i,j}$ is the ith eigenvalue of $A_0^{-1}A_j$. The above $\kappa_i \geq 0$ is again ensured by Assumption 3.1. The definition of P^h satisfies three design criteria suggested in [40], i.e.,

(1) For $l > 1$ and $d = 1$, it reduces to the optimal form presented in Subsection 3.3.1.

(2) For $l = 1$ and $d > 1$, it coincides with that in (3.11).

(3) For $l > 1$, $d > 1$, and simultaneously diagonalizable coefficient matrices A_j, it satisfies criterion 2, with respect to each uncoupled scalar equation.

In addition to the above three criteria, the definition of P^h also satisfies

(4) If the system is symmetric, it gives an analogue to those defined in [40] in the sense that $A\tau A^t$ is symmetric positive semi-definite, since the matrix τ given by (3.43) reduces to

$$\tau = Y_{\mu_d} diag(\tau_1, \cdots, \tau_l) Y_{\mu_d}^t.$$

The verification of claims (1)-(4) is not difficult and is omitted here.

Remark 3.2 *For the two-dimensional (d=2) HD model of the semiconductor device equations with the (singular) diffusion matrix K given by (2.12), the corresponding κ_i in expression (3.49) can be obtained explicitly as*

$$\kappa_i = \begin{cases} \kappa_1 = 0 \\ \kappa_2 = \frac{2\kappa}{5} \\ \kappa_3 = \kappa_4 = \frac{2\kappa}{15}. \end{cases} \qquad (3.50)$$

□

3.4 Full Discrete SD Formulations

Let us define

$$\mathcal{B}(U^h, \Psi) = (A \cdot \nabla U^h, \Psi) + (\mathcal{K}\nabla U^h, \nabla\Psi) + \sum_{e=1}^{n_{el}} (A \cdot \nabla U^h - \nabla \cdot (\mathcal{K}\nabla U^h), P^h(\Psi))_{\Omega_e} \qquad (3.51)$$

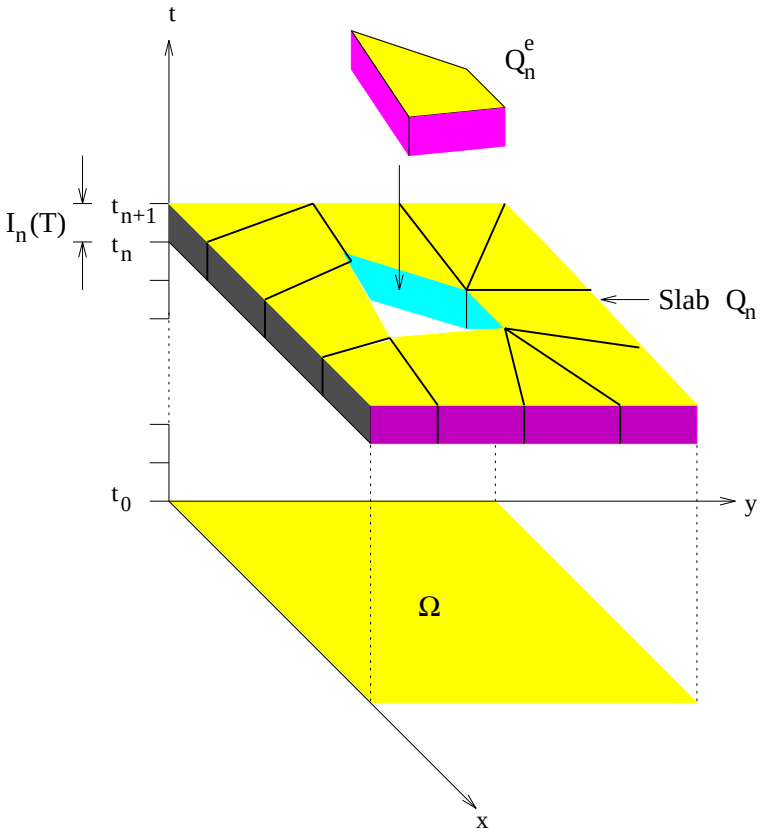

Figure 3.1: A space-time slab.

and

$$\mathcal{F}(\Psi) = (F, \Psi + P^h(\Psi)) \tag{3.52}$$

then the semi-discrete SD formulation (3.18) can be written as

$$(A_0 U_t^h, \Psi + P^h(\Psi)) + \mathcal{B}(U^h, \Psi) = \mathcal{F}(\Psi). \tag{3.53}$$

3.4.1 Space-Time Finite Element Methods

Simply consider a uniform partition $0 = t_0 < t_1 < \cdots < t_N = T$ of the time interval $I(T) = (0, T)$. Denote by $I_n(T) = (t_n, t_{n+1})$ the nth time subinterval with $\Delta t = t_{n+1} - t_n$

being the length of the subinterval. A space-time "slab" is then defined as (see Fig 3.1).

$$Q_n = \Omega \times I_n(T). \tag{3.54}$$

For the nth space-time slab, we define space-time element domains as

$$Q_n^e = \Omega_e \times I_n(T) \tag{3.55}$$

$(e = 1, \ldots, n_{el})$. We define the following finite element subspace

$$\mathcal{T}^h = \{V^h \mid V^h \in (C^0(Q_n))^l,\ V^h \mid_{Q_n^e} \in (P_k(Q_n^e))^l\}. \tag{3.56}$$

Note that any test function in $\mathcal{T}^h$ is continuous within each space-time slab Q_n, but is discontinuous across the interface of slabs. Considering this, let

$$V^h(t^{\pm}) = \lim_{\epsilon \to 0\pm} V^h(t_n + \epsilon), \tag{3.57}$$

and the jump in time of V^h

$$[\![V^h(t_n)]\!] = V^h(t_n^+) - V^h(t_n^-). \tag{3.58}$$

Given $U^h(t_0^-)$, a projection of the initial value U_0 on $\mathcal{V}^h$, the space-time SD formulation is as follows. Within each Q_n $(n = 0, \ldots, N-1)$, find $U^h \in \mathcal{T}^h$ such that for all $\Psi \in \mathcal{T}^h$,

$$\begin{aligned}
&\int_{Q_n} (A_0 U_t^h \cdot \Psi + A \cdot \nabla U^h \cdot \Psi + \mathcal{K} \nabla U^h \cdot \nabla \Psi)\, dxdt \qquad \text{(Galerkin)} \\
&\quad + \int_\Omega A_0 [\![U^h(t_n)]\!] \cdot \Psi(t_n^+)\, dx \qquad \text{(Jump Condition)} \\
&\quad + \sum_{e=1}^{n_{el}} \int_{Q_n^e} \mathcal{L} U^h \cdot P^h(\Psi)\, dxdt \qquad \text{(SD)} \\
&\quad = \int_{Q_n} F \cdot \Psi\, dxdt.
\end{aligned} \tag{3.59}$$

The operator P^h in (3.59) can be determined using the results in Section 3.3 as we show below. By the change of variables $U^h = A_0^{-1/2} V^h$ and $\Psi = A_0^{-1/2} \Phi$, (3.59) becomes

$$\int_{Q_n} (V_t^h \cdot \Phi + \bar{A} \cdot \nabla V^h \cdot \Phi + \bar{\mathcal{K}} \nabla V^h \cdot \nabla \Phi)\, dxdt$$

$$+\int_{\Omega}[\![V^h(t_n)]\!]\cdot\Phi(t_n^+)\,dx+\sum_{e=1}^{n_{el}}\int_{Q_n^e}\bar{\mathcal{L}}V^h\cdot\bar{P^h}(\Phi)\,dxdt$$
$$=\int_{Q_n}\bar{F}\cdot\Phi dxdt, \tag{3.60}$$

where, $\bar{P^h}=A_0^{-1/2}P^hA_0^{-1/2}$, $\bar{F}=A_0^{-1/2}FA_0^{-1/2}$ and

$$\bar{A}^t=(\bar{A}_1,\cdots,\bar{A}_d)=(A_0^{-1/2}A_1A_0^{-1/2},\cdots,A_0^{-1/2}A_dA_0^{-1/2})$$
$$\bar{\mathcal{K}}=diag(\bar{K},\cdots,\bar{K})=diag(A_0^{-1/2}KA_0^{-1/2},\cdots,A_0^{-1/2}KA_0^{-1/2}).$$

First we consider the case when $\Delta t=h$. Let

$$\mu_{d+1}=\frac{1}{\sqrt{d+1}}(\overbrace{1,\ldots,1}^{d+1})^t. \tag{3.61}$$

The operator P^h in Subsection 3.3.2 is only suitable for the steady state case. However, we can incorporate it in the space-time finite element methodology. We take $\bar{P^h}$ in (3.60) to be

$$\bar{P^h}(\Phi)=[\bar{A}]\bar{\tau}\cdot\nabla\Phi+\bar{\tau}\cdot\Phi_t \tag{3.62}$$

with

$$\bar{\tau} \;=\; Z_{\mu_{d+1}}diag(\tau_1,\cdots,\tau_l)Z^{-1}_{\mu_{d+1}}, \tag{3.63}$$

if we considered (3.60) to be a formulation for the "(d+1)-dimensional" steady state convection-diffusion system. In (3.63), τ_i $(i=1,\ldots,l)$ can still be defined by (3.45), but $|\lambda_i|_2$ should be changed to

$$|\lambda_i|_2=(1+\sum_{j=1}^{d}(\lambda_{i,j})^2)^{1/2}, \tag{3.64}$$

where $\lambda_{i,j}$ is the ith eigenvalue of $\bar{A}_j$. We notice that the matrix $(I_l+\sum_{i=1}^{d}\bar{A}_i)/\sqrt{d+1}$ is diagonalizable by its eigen-matrix $Z_{\mu_{d+1}}$, as is the matrix $(\sum_{i=1}^{d}\bar{A}_i)/\sqrt{d}$. Hence

$$Z_{\mu_{d+1}}=Z_{\mu_d}. \tag{3.65}$$

If $\Delta t \neq h$, we scale the time subinterval by $h/\Delta t$. Therefore, the above formulation remains the same except that $|\lambda_i|_2$ in (3.64) must be revised to

$$|\lambda_i|_2 = ((\frac{h}{\Delta t})^2 + \sum_{j=1}^{d}(\lambda_{i,j})^2)^{1/2}.$$

However, we prefer to make the following change heuristically

$$|\lambda_i|_2 = (C_r(\frac{h}{\Delta t})^2 + \sum_{j=1}^{d}(\lambda_{i,j})^2)^{1/2}, \tag{3.66}$$

where $C_r = 1$ except $C_r = 0$ for constant-in-time space-time finite elements.

Transforming from (3.60) back to (3.59), we obtain the corresponding term P^h in (3.59). To summarize, we give the expression for P^h as follows.

$$\begin{aligned}
P^h(\Psi) &= [A]\tau \cdot \nabla\Psi + \tau \cdot \Psi_t, && (3.67)\\
\tau &= A_0^{-1/2} Z_{\mu_d} diag(\tau_1, \cdots, \tau_l) Z_{\mu_d}^{-1} A_0^{-1/2}, && (3.68)\\
\mu_d &= \frac{1}{\sqrt{d}}(\overbrace{1, \cdots, 1}^{d})^t, , && (3.69)\\
\tau_i &= \frac{1}{2} h\xi_i/|\lambda_i|_2 && (3.70)\\
|\lambda_i|_2 &= (C_r(\frac{h}{\Delta t})^2 + \sum_{j=1}^{d}(\lambda_{i,j})^2)^{1/2}, && (3.71)\\
\xi_i &= \coth(\alpha_i) - \alpha_i^{-1}, && (3.72)\\
\alpha_i &= \frac{1}{2}|\lambda_i|_2 h/\kappa_i, && (3.73)\\
\kappa_i &= e_i^t Z_{\mu_d}^{-1} A_0^{-1/2} K A_0^{-1/2} Z_{\mu_d} e_i. && (3.74)
\end{aligned}$$

Here, $\lambda_{i,j}$ is the ith eigenvalue of $A_0^{-1}A_j$.

We point out that for general non-symmetric convection-diffusion systems, the so-called Galerkin/least-squares algorithm introduced in [35] is not appropriate, since we have to use $[A]$ in the definition of P^h instead of A in such cases.

3.4.2 Methods of Lines

Let $U^{h(n)}$ be the approximate solution vector of U^h at the time $t_n = n\Delta t$ with a uniform time step Δt. With $U^{h(0)}$ being a projection of the initial value U_0 on $\mathcal{V}^h$, we are interested in two simple time discretizations below.

SD-backward Euler:

$$(A_0\frac{U^{h(n+1)} - U^{h(n)}}{\Delta t}, \Psi + P^h(\Psi)) + \mathcal{B}(U^{h(n+1)}, \Psi) = \mathcal{F}(\Psi), \tag{3.75}$$

for any $\Psi \in \mathcal{V}^h$.

SD-trapezoidal:

$$(A_0\frac{U^{h(n+1)} - U^{h(n)}}{\Delta t}, \Psi + P^h(\Psi)) + \mathcal{B}(\frac{1}{2}(U^{h(n+1)} + U^{h(n)}), \Psi) = \mathcal{F}(\Psi), \tag{3.76}$$

for any $\Psi \in \mathcal{V}^h$.

The above schemes are not strict SD schemes in the sense of the space-time finite element idea, but they are simple to use.

3.5 Stability Arguments

From now on, we consider $k = 1$ in definitions of the finite element subspaces (see (3.17) and (3.56)). For definiteness, we set $F = 0$, i.e., no external force is prescribed.

3.5.1 Space-Time Finite Element Methods

To simplify our analysis, we carry out the stability discussions only for the constant-in-time space-time SD scheme without loss of generality. It is convenient for our discussion to set $A_0 = I_l$, otherwise we can simply eliminate it by working on the switched formulation (3.60).

With $A_0 = I_l$, the constant-in-time version of (3.59) is reduced to

$$(U^{h(n+1)} - U^{h(n)}, \Psi) + \Delta t\mathcal{B}(U^{h(n+1)}, \Psi) = 0, \tag{3.77}$$

where $U^{h(n+1)} = U^h(t_n^+)$ and $U^{h(n)} = U^h(t_n^-)$. Recall that τ is given by (3.68) and Z_{μ_d} is the eigen-matrix of the eigenvalue-eigenvector problem

$$(A_{\mu_d} - \lambda I_l) Z_{\mu_d,i} = 0. \tag{3.78}$$

The stability analysis of (3.77) is not easy in general, but at least we can handle it if the following normal symmetrization exists.

Suppose there exist non-singular matrices B and C such that

$$\tilde{A}_0 = CB \qquad \text{(Symm. Pos. Def.)} \tag{3.79}$$

$$\tilde{A}_i = CA_iB \qquad \text{(Symm.)} \quad i = 1, \ldots, d \tag{3.80}$$

$$\tilde{K} = CKB \qquad \text{(Symm. Pos. Semi-Def.)} \tag{3.81}$$

By the change of variables $U^{h(n)} = BV^{h(n)}$ and $\Psi = C^t\Phi$, (3.77) becomes

$$\begin{aligned} &\Delta t\,(\tilde{A}\cdot\nabla V^{h(n+1)}, \Phi) + \Delta t\,(\tilde{\mathcal{K}}\nabla V^{h(n+1)}, \nabla\Phi) + (\tilde{A}_0(V^{h(n+1)} - V^{h(n)}), \Phi) \\ &+ \Delta t\,(\tilde{A}\cdot\nabla V^{h(n+1)}, \tilde{A}\tilde{\tau}\cdot\nabla\Phi) = 0, \end{aligned} \tag{3.82}$$

where

$$\tilde{\tau} = B^{-1}\tau C^{-1} = B^{-1} Z_{\mu_d}\, diag(\tau_1, \cdots, \tau_l)\, Z_{\mu_d}^{-1} C^{-1}. \tag{3.83}$$

Considering the transformed eigenvalue-eigenvector problem

$$(\tilde{A}_0^{-1/2}\tilde{A}_{\mu_d}\tilde{A}_0^{-1/2} - \lambda I_l)\tilde{Z}_{\mu_d,i} = 0, \tag{3.84}$$

we claim that the above $\tilde{\tau}$ is appropriate, i.e., it can be expressed by

$$\tilde{\tau} = \tilde{A}_0^{-1/2}\tilde{Z}_{\mu_d}\, diag(\tau_1, \cdots, \tau_l)\, \tilde{Z}_{\mu_d}^{-1}\tilde{A}_0^{-1/2} \tag{3.85}$$

which corresponds to the transformed symmetric system. Thus, $\tilde{\tau}$ given by (3.83) is a symmetric positive definite matrix. It is easy to see, by comparing (3.78) and (3.84),

that

$$Z_{\mu_d} = B\tilde{A}_0^{1/2}\tilde{Z}_{\mu_d} = B(CB)^{-1/2}\tilde{Z}_{\mu_d}. \tag{3.86}$$

Using the above, $\tilde{\tau}$ given by (3.85) turns into

$$\begin{aligned}\tilde{\tau} &= CB^{-1/2}((CB)^{1/2}B^{-1}Z_{\mu_d})\,diag(\tau_1,\cdots,\tau_l)\,((CB)^{1/2}B^{-1}Z_{\mu_d})^{-1}(CB)^{-1/2} \\ &= B^{-1}Z_{\mu_d}\,diag(\tau_1,\cdots,\tau_l)\,Z_{\mu_d}^{-1}C^{-1},\end{aligned} \tag{3.87}$$

which proves the claim.

The stability of scheme (3.82) is now easy to prove. Rewrite (3.82) as

$$(\tilde{A}_0(V^{h^{(n+1)}} - V^{h^{(n)}}), \Phi) + \Delta t\mathcal{B}(V^{h^{(n+1)}}, \Phi) = 0. \tag{3.88}$$

It is obvious that

$$\begin{aligned}\mathcal{B}(V^{h^{(n+1)}}, V^{h^{(n+1)}}) &= (\tilde{A}\cdot\nabla V^{h^{(n+1)}}, V^{h^{(n+1)}}) + (\tilde{\mathcal{K}}\nabla V^{h^{(n+1)}}, \nabla V^{h^{(n+1)}}) \\ &+ (\tilde{A}\cdot\nabla V^{h^{(n+1)}}, \tilde{A}\tilde{\tau}\cdot\nabla V^{h^{(n+1)}}) \geq 0.\end{aligned} \tag{3.89}$$

If we take $\Phi = V^{h^{(n+1)}}$ in (3.88), then

$$\|V^{h^{(n+1)}}\|_{\tilde{A}_0} \leq \|V^{h^{(n)}}\|_{\tilde{A}_0}, \tag{3.90}$$

where $\|\cdot\|_{\tilde{A}_0}$ is a weighted L^2-norm defined by $\|V\|_{\tilde{A}_0}^2 = (V, \tilde{A}_0 V)$. The stability of (3.82) and therefore the stability of (3.77) are proven.

We are interested in two symmetrizing cases:

Case 1: $C = I_l$

This symmetrization corresponds, for example, to those for Navier-Stokes equations and the semiconductor HD model (see [72, 77]).

Case 2: $C = B^{-1}$

The special situation in this case is that of simultaneously diagonalizable systems. If Assumption 3.1 holds, then the stability of scheme (3.59) can be obtained for 1-D problems.

We summarize the above discussion in the following theorem.

Theorem 3.2 *If problem (3.1) admits a normal symmetrization, then the space-time SD discretization scheme (3.59), with the operator P^h defined by (3.67)-(3.74), is unconditionally stable.* □

3.5.2 Methods of Lines

The stability proof for the SD-backward Euler scheme is more difficult than for the space-time SD scheme due to the existence of the term $(A_0(U^{h(n+1)} - U^{h(n)})/\Delta t, P^h(\Psi))$ in (3.75). We can only provide a proof for the one-dimensional case under Assumption 3.1 and $\tau = \delta h A_0^{-1}$ with the scalar parameter $\delta > 0$.

By transformations $U^{h(n)} = A_0^{-1/2} Z \Lambda_\beta^{-1/2} V^{h(n)}$ and $\Psi = A_0^{-1/2} Z^{-t} \Lambda_\beta^{1/2} \Phi$, (3.75) yields

$$\begin{aligned}(\frac{V^{h(n+1)} - V^{h(n)}}{\Delta t}, \Phi) + \delta h\,(\frac{V^{h(n+1)} - V^{h(n)}}{\Delta t}, \Lambda\Phi_x) + (\Lambda V_x^{h(n+1)}, \Phi) \\ + (\tilde{K} V_x^{h(n+1)}, \Phi_x) + \delta h\,(\Lambda V_x^{h(n+1)}, \Lambda\Phi_x) = 0,\end{aligned} \tag{3.91}$$

where, the symmetric positive semi-definite matrix $\tilde{K}$ is defined by (3.33). Taking $\Phi = V^{h(n+1)}$ in (3.91), we have

$$\begin{aligned}\frac{\|V^{h(n+1)}\|^2}{2\Delta t} - \frac{\|V^{h(n)}\|^2}{2\Delta t} + \delta h\,(\frac{V^{h(n+1)} - V^{h(n)}}{\Delta t}, \Lambda V_x^{h(n+1)}) \\ + \|V_x^{h(n+1)}\|_{\tilde{K}}^2 + \delta h\,\|\Lambda V_x^{h(n+1)}\|^2 \le 0.\end{aligned} \tag{3.92}$$

Taking $\Phi = \delta h\,(V^{h(n+1)} - V^{h(n)})/\Delta t$ in (3.91), we have

$$\begin{aligned}\frac{\delta h}{\Delta t^2}\|V^{h(n+1)} - V^{h(n)}\|^2 + \delta h\,(\frac{V^{h(n+1)} - V^{h(n)}}{\Delta t}, \Lambda V_x^{h(n+1)}) \\ + \frac{\delta h}{2\Delta t}(\|V_x^{h(n+1)}\|_{\tilde{K}}^2 - \|V_x^{h(n)}\|_{\tilde{K}}^2) + \frac{(\delta h)^2}{2\Delta t}(\|\Lambda V_x^{h(n+1)}\|^2 - \|\Lambda V_x^{h(n)}\|^2) \le 0.\end{aligned} \tag{3.93}$$

We define $|||\cdot|||$, an auxiliary norm, by

$$|||V|||^2 = \|V\|^2 + \delta h \|\Lambda V_x\|^2 + (\delta h)^2 \|V_x\|_{\tilde{K}}^2. \tag{3.94}$$

Then (3.92) + (3.93) yields

$$\frac{1}{2\Delta t}(|||V^{h(n+1)}|||^2 - |||V^{h(n)}|||^2) + \frac{2\delta h}{\Delta t}(V^{h(n+1)} - V^{h(n)}, \Lambda V_x^{h(n+1)}) + \frac{\delta h}{\Delta t^2}\|V^{h(n+1)} - V^{h(n)}\|^2 + \delta h \, \|\Lambda V_x^{h(n+1)}\|^2 \leq 0. \tag{3.95}$$

Applying the inequality $a^2 + b^2 \geq 2ab$ to the last three terms at the left hand side of the above, we conclude that

$$|||V^{h(n+1)}|||^2 \leq |||V^{h(n)}|||^2. \tag{3.96}$$

To summarize, we have the following theorem.

Theorem 3.3 *If Assumption 3.1 holds and $P^h = \delta h A_0^{-1} A^t \Psi_x$ with a scalar parameter $\delta \geq 0$, then the one-dimensional SD-backward Euler scheme (3.75) is unconditionally stable.* □

We notice that the SD-backward Euler scheme (3.75) is equivalent to the constant-in-time space-time SD scheme (3.59) if we drop the term

$$(A_0(U^{h(n+1)} - U^{h(n)}), P^h(\Psi)) \tag{3.97}$$

in (3.59). As we can see from the above stability discussion, the term (3.97) is difficult to handle in the analysis. The difficulty caused by this term is also prominent when we try the stability analysis for the SD-trapezoidal scheme (3.76) in the 1-D case. A result similar to Theorem 3.3 can be obtained but under an extra restrictive condition (see Appendix B). Existence of such a term is not only troublesome in the analysis but also exhibits poor behavior in computations, as we will see in the next section.

3.6 Numerical Tests

For the purpose of numerical comparisons, we use three different choices of P^h. Choices (a) and (b) are given by (3.19) and (3.20), respectively, with $\tau = \delta h A_0^{-1}$. We will refer

to our generalized P^h (3.67)-(3.74) as the (c)-type. Better performance was observed in [43] for the (b)-type than for the (a)-type. This can be explained now by our analysis in the previous sections: The (b)-type operator does have the upwinding effect in the correct direction. The (c)-type operator is different from the (b)-type in that it also gives a proper scaling.

Two examples are tested here. The first is a one-dimensional hyperbolic system with constant coefficients. The next is the nonlinear hydrodynamic semiconductor device model for both one and two space dimensions, in which case K is singular.

3.6.1 Test 1

Our test hyperbolic system is given by

$$U_t + AU_x = 0, \tag{3.98}$$

where

$$A = \begin{pmatrix} 1 & 1+\epsilon \\ 0 & -\epsilon \end{pmatrix}. \tag{3.99}$$

The eigenvalues of A are $1, -\epsilon$ with eigen-matrix

$$Y = \begin{pmatrix} 1 & 1 \\ 0 & -1 \end{pmatrix}. \tag{3.100}$$

The boundary condition is chosen to be periodic. System (3.98) can be diagonalized by the transformation $V = Y^{-1}U$. The initial-value function U_0 is set corresponding to the initial value V_0, a pulse function, of the V-system. In this example, we take $h = 0.01$ and $\Delta t = 0.005$. The SD operator for the (c)-type is given by $P^h(\Psi) = (A\tau)^t\Psi_x$ according to (3.67)-(3.74) and

$$A\tau = \frac{h}{2}\begin{pmatrix} 1 & 1+\frac{\epsilon}{\sqrt{C_r(h/\Delta t)^2+\epsilon^2}} \\ 0 & -\frac{\epsilon}{\sqrt{C_r(h/\Delta t)^2+\epsilon^2}} \end{pmatrix}. \tag{3.101}$$

Numerical tests are presented with $\epsilon = 0.01$. A typical value $\delta = 1$ is taken for the (a)- and the (b)-type operators. Comparison of the three types is shown in Fig. 3.2 and Fig. 3.3 using the constant-in-time space-time SD method (3.77). It is evident that the (c)-type gives the best result while the (a)-type gives the worst, with respect to oscillatory behavior.

The solutions of the (c)-type are clearly non-oscillatory. We can show that the (c)-type scheme is actually a monotone scheme in such a case. To verify this, it is sufficient to consider a scalar hyperbolic equation

$$u_t + a u_x = 0 \qquad (a > 0) \tag{3.102}$$

since (3.98) can be virtually decoupled. If we define $u_i^{h(n)}$, the value of $u^{h(n)}$ at the node x_i, the (c)-type scheme can be easily expressed by the following finite difference scheme employing the trapezoidal quadrature rule

$$(1 + \nu\theta) u_i^{h(n+1)} + \frac{\nu}{2}(1 - \theta) u_{i+1}^{h\ (n+1)} - \frac{\nu}{2}(1 + \theta) u_{i-1}^{h\ (n+1)} = u_i^{h(n)} \tag{3.103}$$

where $\nu = a\Delta t/h$ and $\theta = a/\sqrt{C_r(h/\Delta t)^2 + a^2}$. If we denote the solution vector $U^{(n)} = (u_1^{h(n)}, u_2^{h(n)}, \ldots)^t$, then, by choosing $C_r = 0$, (3.103) reads

$$M U^{(n+1)} = U^{(n)} \tag{3.104}$$

with

$$M = \begin{pmatrix} 1+\nu & & \\ -\nu & 1+\nu & \\ & \ddots & \ddots \end{pmatrix}. \tag{3.105}$$

The inverse of M is

$$M^{-1} = \frac{1}{1+\nu} \begin{pmatrix} 1 & & \\ \frac{\nu}{1+\nu} & 1 & \\ & \ddots & \ddots \end{pmatrix}, \tag{3.106}$$

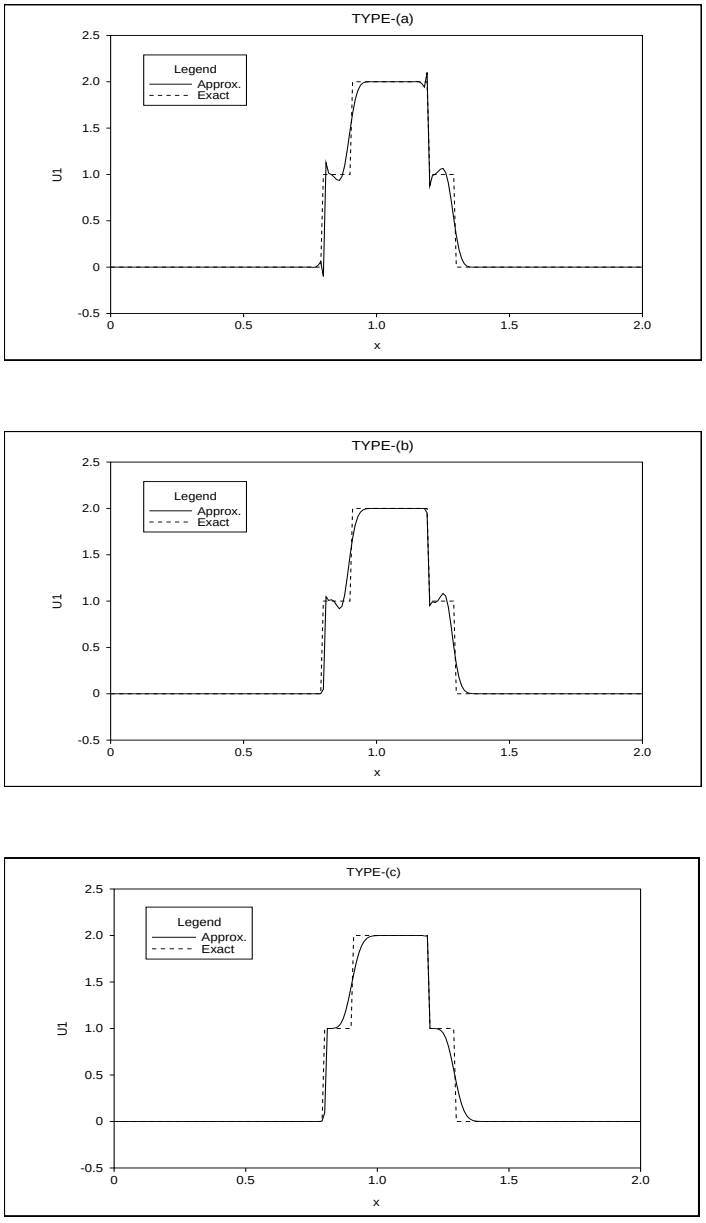

Figure 3.2: U_1 by (a), (b) and (c)-types of operators in test 1 using the constant-in-time space-time SD scheme.

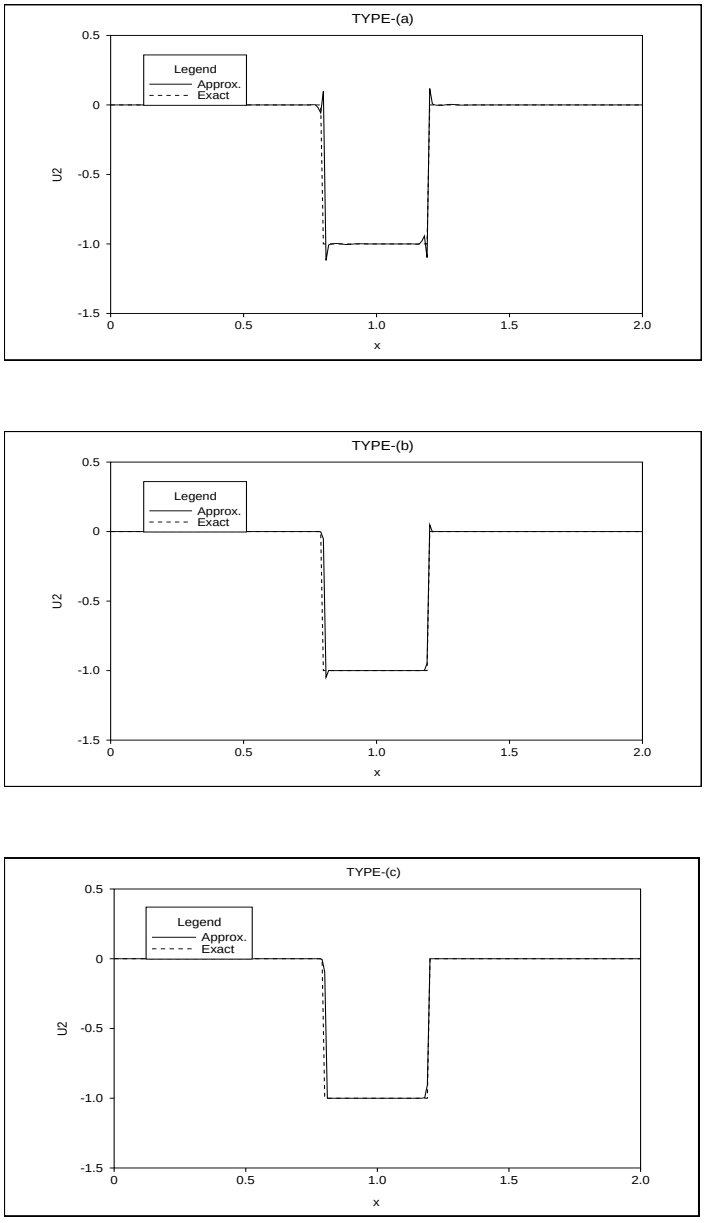

Figure 3.3: U_2 by (a), (b) and (c)-types of operators in test 1 using the constant-in-time space-time SD scheme.

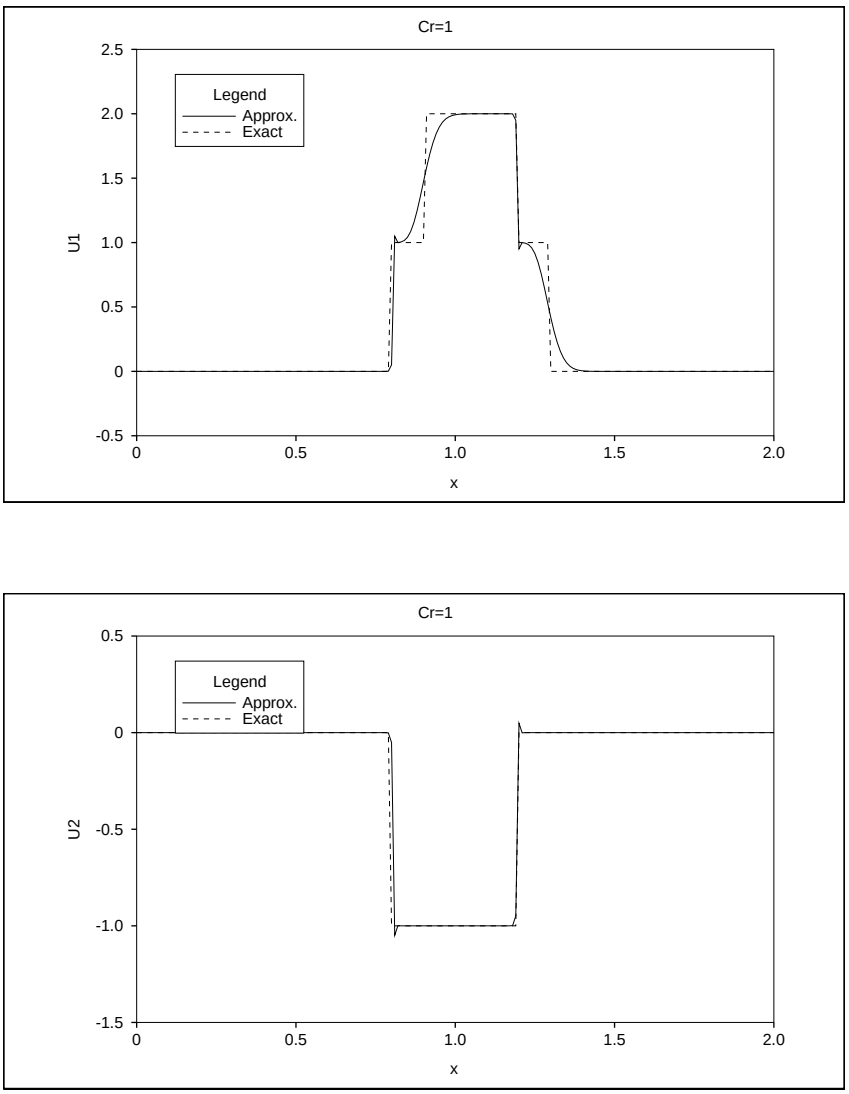

Figure 3.4: Solutions by (c)-type operator with $C_r = 1$ in test 1 using the constant-in-time space-time SD scheme.

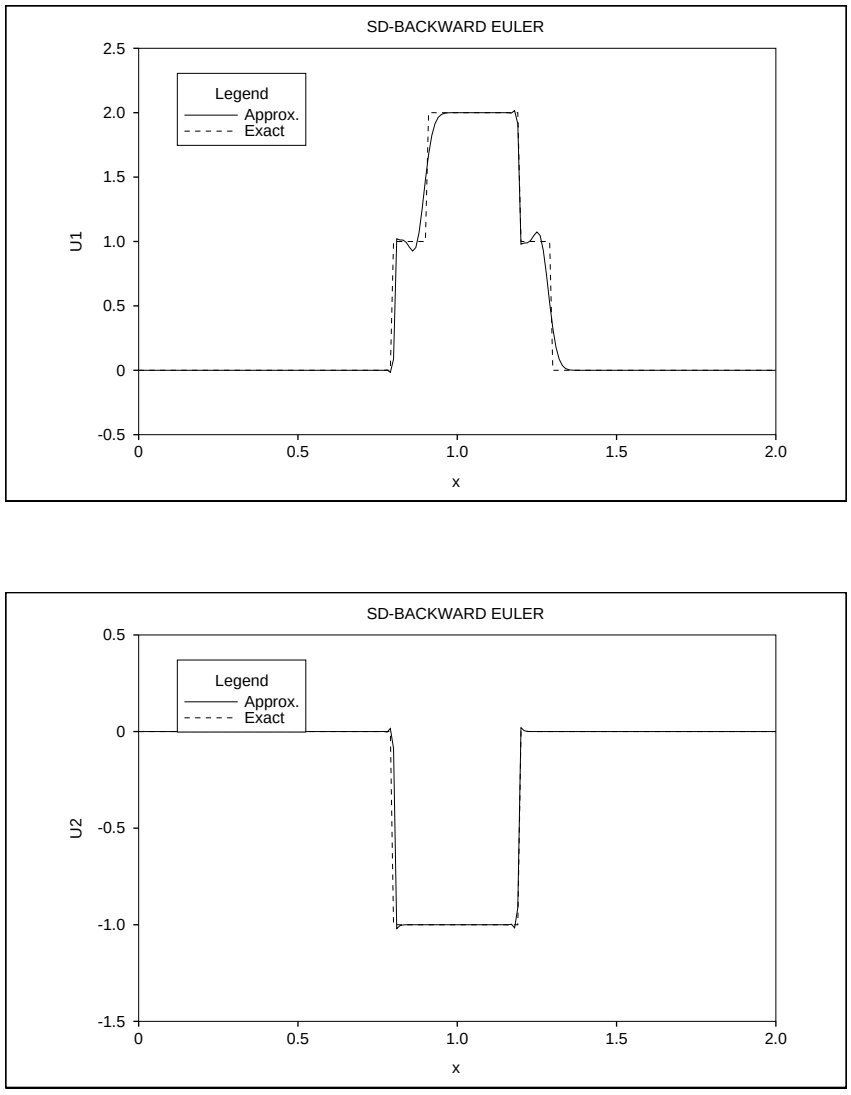

Figure 3.5: Solutions by (c)-type operator in test 1 using SD-backward Euler scheme.

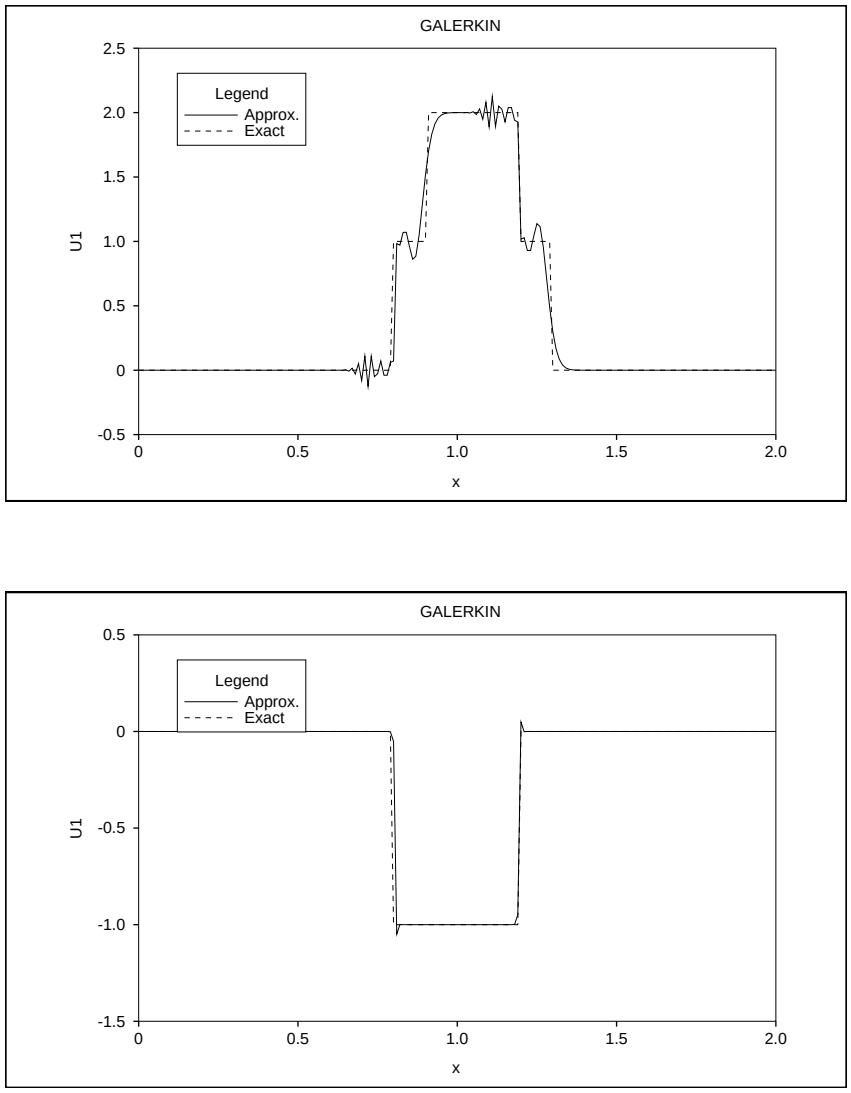

Figure 3.6: Solutions in test 1 using the Galerkin-backward Euler scheme.

which has non-negative entries. This proves the monotonicity of (3.103). If we use $C_r = 1$, instead of $C_r = 0$, the monotonicity is violated and therefore oscillations cannot be avoided. This is demonstrated in Fig. 3.4.

Remark 3.3 *For multi-dimensional convection-diffusion problems, the monotonicity of the SD method unfortunately does not hold. To further control the oscillatory behavior of the numerical solutions, the so-called nonlinear shock-capturing modification may be needed to introduce an amount of crosswind dissipation (see [15]).* □

Methods of lines are not suitable in the SD formulations as mentioned in the previous section. In this example, the SD-backward Euler scheme with the optimal P^h is also tested to support our argument. The numerical results are shown in Fig. 3.5, which have oscillations. As a reference, numerical solutions using the Galerkin-backward Euler scheme are provided in Fig. 3.6.

3.6.2 Test 2

Since the HD model is a system of nonlinear PDEs, a so-called predictor/multi-corrector algorithm with implicit-explicit nonlinear Newton type iterations is used (see [43, 77]). We delay the description of such a procedure to Chapter 5. Physical parameters of the model needed for the following computations are presented in Table 5.1. Extensive simulations of semiconductor devices will be carried out in Chapters 5 and 6.

We denote *ipass* the number of iterations required at each time step to relax to solutions within the design error tolerance, $tol = 10^{-4}$. We set $ipass \leq 40$; if more iterations are required then the scheme is considered to be divergent. In this example, the lattice temperature is set to be 300K.

1-D Case:

A 1.0-μm ρ^+-ρ-ρ^+ silicon diode is used with a 0.25-μm source, 0.5-μm channel and 0.25-μm drain regions. The doping profile ρ_D is given by $\rho_D = 10^{17} cm^{-3}$, if $0 \leq x \leq 0.25$ or $0.75 \leq x \leq 1.0$; $\rho_D = 10^{15} cm^{-3}$, if $0.35 \leq x \leq 0.65$. The above segments of ρ_D are connected smoothly by polynomial fits. The doping in this case is relatively mild. A uniform mesh of 100 points is used for this example. A comparison has been made between results of the (a)-type ($\delta = 1$) and the (c)-type. We first apply $1V$ biased voltage to the device. The steady state is reached by solutions of both types around time $t = 6$. We have observed that the iteration number *ipass* for the (a)-type is almost as twice as that for the (c)-type. When a $2V$ biased voltage is applied, the (a)-type diverges around time $t = 0.22$ and the (c)-type reaches the steady state at time $t = 6$. Numerical solutions for a 2-volt biased voltage are shown in Fig. 3.7.

2-D Case:

Let us consider a two-dimensional ρ^+-ρ-ρ^+ diode shown in Fig. 3.8 with the device domain [0, 1.0(μm)]$\times$[0, 0.5(μm)]. We set a 0.2-μm source and drain and the doping profile is defined by $\rho_D = 5 \times 10^{17} cm^{-3}$ in [0, 0.25(μm)]$\times$[0.25, 0.5(μm)] and in [0.75, 1.0(μm)]$\times$[0.25, 0.5(μm)] and $\rho_D = 2 \times 10^{15} cm^{-3}$ elsewhere, with abrupt junctions. A uniform mesh of 80×40 points is used. In this case, a $1V$ bias is prescribed. The (a)-type scheme fails to converge (producing an unphysical negative electron density). For the (c)-type, the solution tends to the steady state about $t = 10$. Typical solutions of this type are shown in Fig. 3.9.

The constant-in-time scheme is used in the above. It is first-order in time, but nevertheless it can be used to obtain the steady state solution with an overall accuracy of $O(h^{3/2})$. Moreover, we observe that in practice errors in spatial discretization often dominate those of the time discretization. It may be argued that a linear-in-time scheme would be preferable over the constant-in-time one, despite its additional complexity. However, we use the predictor/multi-corrector algorithm with explicit correction passes, so the

scheme is not unconditionally stable any more. The analysis in [75] showed that the linear space-time method might cause instability when the advection dominates.

We also have tested the above problems using the SD-backward Euler scheme. The evidence indicates that the SD-backward Euler scheme is even less stable than the classical Galerkin-backward Euler scheme. In contrast, the space-time SD scheme is much better. The method of lines with the semi-discrete SD approach is often used in the literature. For instance, they were employed for scalar equations in [15, 32] and for systems in [43]. However, the discussion and numerical experiments in this chapter suggest that we should use the space-time SD schemes, especially for systems.

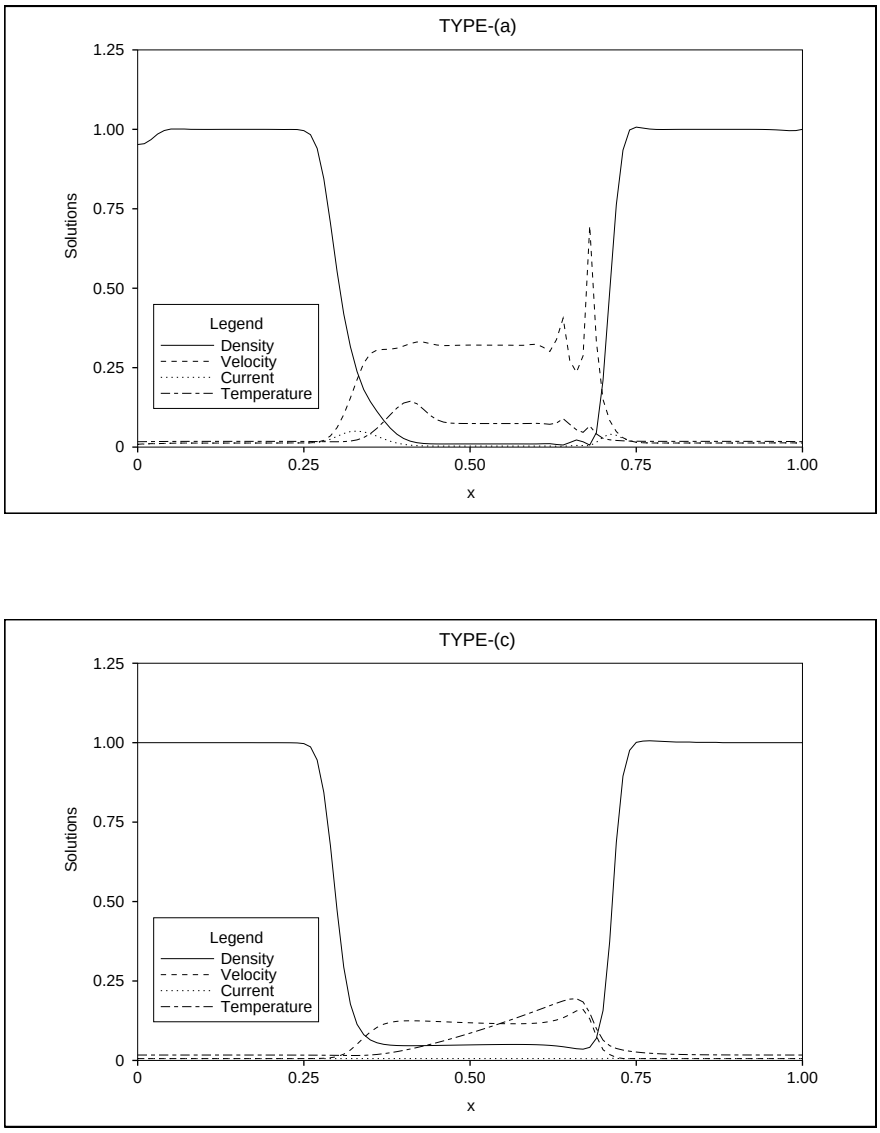

Figure 3.7: Solutions by (a) and (c)-types of operators in test 2 using the constant-in-time space-time SD scheme.

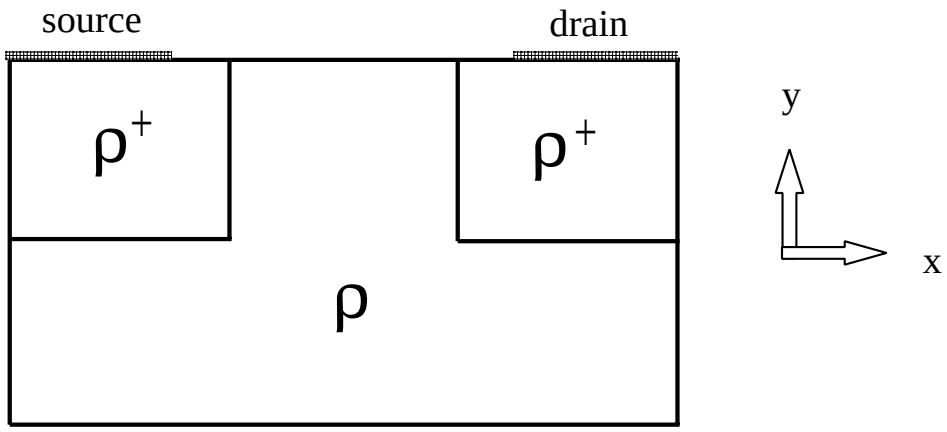

Figure 3.8: Geometry of a 2-D ρ^+-ρ-ρ^+ diode in test 2.

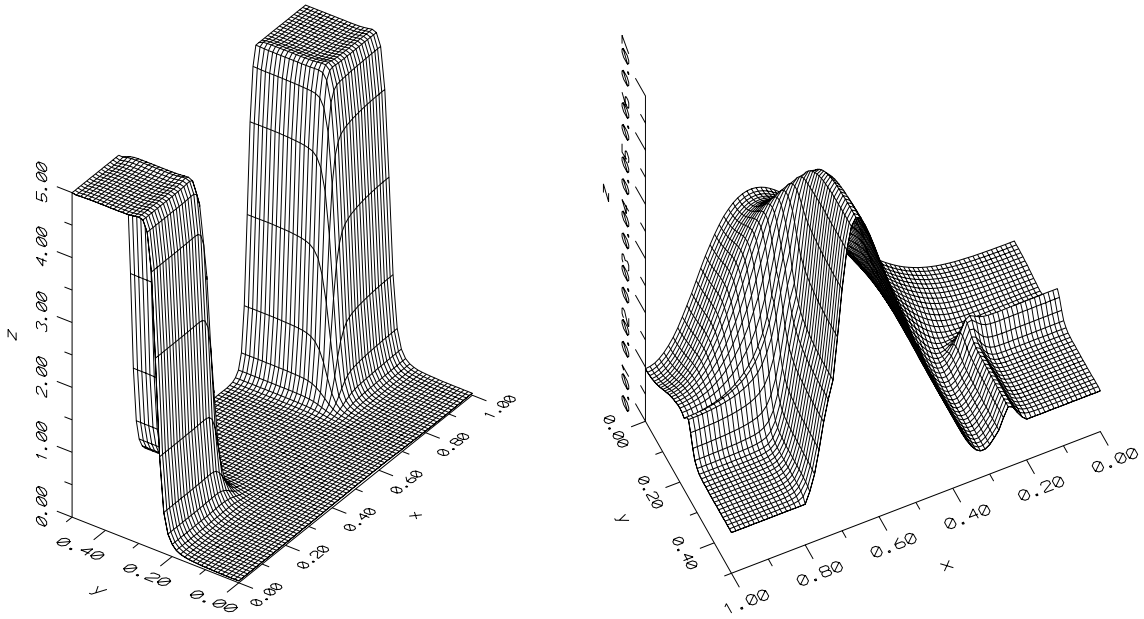

Figure 3.9: Electron density (left) and electron temperature (right) in test 2 using the constant-in-time space-time SD scheme.

Chapter 4

Potential Equation Solver

Let us consider the d-dimensional potential equation (2.2) in the form

$$\begin{cases} \nabla \cdot E = L, \\ E = -\nabla \psi \end{cases} \tag{4.1}$$

in Ω, assuming for this purpose that ρ is a known function. The equation (4.1) is subject to the mixed boundary conditions

$$\psi \mid_{\Gamma_1} = g_0, \tag{4.2}$$

$$E \cdot n \mid_{\Gamma_2} = 0. \tag{4.3}$$

Here, E is the electric field and g_0 is given by (2.35) and (2.37). The discussion that follows can be directly extended to the case where $E = -D\nabla\psi$ with $D(x) > 0$ known. But this extension is left to the reader because it is not strictly needed for our purposes.

4.1 Introduction

Upon elimination of E in (4.1) one obtains Poisson's equation for ψ. However, in our context, E is a more important physical variable than ψ. As far as the typical HD model is concerned for example, E is the only quantity that is needed in the system of conservation laws (2.1). Since the system of conservation laws is sensitive to the force of the electric field, an accurate approximation to E is desired. Finite element methods with high degree piecewise polynomials, of course, will achieve this goal. However, to

avoid the unnecessary complexity of using different settings in the finite element spaces, we prefer to stick with linear finite elements as used for the system of conservation laws. The classical Galerkin method only provides first-order accuracy for E. Thus it will cause a corresponding order reduction for all solution components even if the order of the SD method is higher. Therefore, a more accurate method whose order is compatible with that of the SD method is needed for our special purpose.

Normally, in order to obtain an accurate solution of E, we should treat E as an independent variable. It is natural to consider a mixed finite element method for (4.1). Unfortunately, this requires that the finite element spaces for ψ and E be compatible, i.e., that the space pair satisfies the Brezzi-Babuška condition (see [10]). Different settings of nodal points (staggered grids) have to be used for ψ and E. To circumvent this constraint, some alternative approaches were proposed, for example, the augmented finite element method in [10] and the div-rot finite element method in [52, 53]. The augmented method solves a coupled system for ψ and E simultaneously, so it is costly. The div-rot method solves a system of equations for E only, hence it could be more efficient than the augmented method. However, to guarantee the convergence of the div-rot method, the boundaries Γ_1 and Γ_2 must be connected, i.e., the segments of Γ_1 cannot be separated by Γ_2, and vice versa. Unfortunately this does happen in our device simulation problems. We therefore propose a new method that shares the advantages of both the augmented and div-rot methods.

The arrangement of the chapter is as follows. In Section 4.2, we provide formulations of the augmented and div-rot methods. We then propose a new formulation in Section 4.3 by combining ideas of these methods and carry out numerical experiments in Section 4.4.

4.2 Previous Work

4.2.1 The Div-Rot Method

The div-rot method was initially designed to solve the div-rot system such as the Maxwell equations using the so-called least-squares methodology. If we apply the rotation operator to the second equation of (4.1), we have

$$\nabla \times E = 0.$$

Then (4.1) can be converted to the div-rot system

$$\begin{cases} \nabla \cdot E - L = 0, \\ \nabla \times E = 0, \end{cases} \tag{4.4}$$

which eliminates the variable ψ. A finite element approximation for (4.4) was discussed by Křížek and Neittaanmäki (see [52, 53]). Before introducing the method, we define the finite element subspace

$$\tilde{\mathcal{Q}}^h = \{q^h \mid q^h \in (C^0(\Omega))^d,\ q^h \mid_{\Omega_e} \in (P_1(\Omega_e)^d,\ q^h \times n \mid_{\Gamma_1} = 0,\ q^h \cdot n \mid_{\Gamma_2} = 0\}. \tag{4.5}$$

If we assume that g_0 is constant, then the div-rot formulation reads: Find $E^h \in \tilde{\mathcal{Q}}^h$ such that for all $q^h \in \tilde{\mathcal{Q}}^h$

$$a(E^h, q^h) = (L, \nabla \cdot q^h), \tag{4.6}$$

where

$$a(p, q) = (\nabla \cdot p, \nabla \cdot q) + (\nabla \times p, \nabla \times q). \tag{4.7}$$

To ensure convergence, the bilinear form $a(\cdot, \cdot)$ must satisfy the $\tilde{\mathcal{Q}}^h$-ellipticity or the Lax-Milgram theorem (see [52, 18, 82]). Křížek and Neittaanmäki showed that for all $q^h \in \tilde{\mathcal{Q}}^h$,

$$\|q^h\| \leq C(\|\nabla \cdot q^h\| + \|\nabla \times q^h\|), \tag{4.8}$$

for some constant C independent of h, if and only if Γ_1 and Γ_2 are connected.

4.2.2 The Augmented Method

The idea of the augmented method originated from that of Franca and Hughes's Galerkin least-squares method in [23] (which is a counterpart of the SD method). Define a pair of finite element subspaces

$$\mathcal{W}_{g_0}^h = \{w^h \mid w^h \in C^0(\Omega),\ w^h \mid_{\Omega_e} \in P_1(\Omega_e),\ w^h \mid_{\Gamma_1} = g_0\}, \tag{4.9}$$

$$\mathcal{Q}^h = \{q^h \mid q^h \in (C^0(\Omega))^d,\ q^h \mid_{\Omega_e} \in (P_1(\Omega_e))^d,\ q^h \cdot n \mid_{\Gamma_2} = 0\}. \tag{4.10}$$

The augmented formulation reads (see [10]): Find $(\psi^h, E^h) \in \mathcal{W}_{g_0}^h \times \mathcal{Q}^h$ such that for all $(w^h, q^h) \in \mathcal{W}_0^h \times \mathcal{Q}^h$

$$\begin{cases} a(E^h, q^h) + b(\psi^h, q^h) = \beta(L, \nabla \cdot q^h) - \alpha \int_{\Gamma_1} g_0 q^h \cdot n ds, \\ b(w^h, E^h) + c(\psi^h, w^h) = (L, w^h), \end{cases} \tag{4.11}$$

where

$$a(p, q) = \alpha\,(p, q) + \beta\,(\nabla \cdot p, \nabla \cdot q), \tag{4.12}$$

$$b(w, q) = -(1 - \alpha)\,(w, \nabla \cdot q), \tag{4.13}$$

$$c(v, w) = \alpha\,(\nabla v, \nabla w). \tag{4.14}$$

The parameters α and β satisfy $0 \leq \alpha < 1$ and $\beta \geq 0$, respectively. Note that we have a coupled system to solve.

Remark 4.1 *Motivated by the div-rot method, we also can consider the bilinear form* $a(\cdot, \cdot)$ *as*

$$a(p, q) = \alpha\,(p, q) + \beta\,[(\nabla \cdot p, \nabla \cdot q) + (\nabla \times p, \nabla \times q)], \tag{4.15}$$

which enhances the stability of the method. If $\alpha = 0$*, the div-rot method is recovered.* □

4.3 A New Method

Based on the above work, we propose a new formulation that can be viewed as a balance of the augmented method and the div-rot method. The new approach reads: Find $\psi^h \in \mathcal{W}^h_{g_0}$ and $E^h \in \mathcal{Q}^h$, such that for any $w^h \in \mathcal{W}^h_0$ and $q^h \in \mathcal{Q}^h$,

$$\begin{cases} a(E^h, q^h) + b(\psi^h, q^h) = \beta(L, \nabla \cdot q^h) - \int_{\Gamma_1} g_0 q^h \cdot n ds, \\ c(\psi^h, w^h) = (L, w^h), \end{cases} \tag{4.16}$$

where

$$a(p,q) = (p,q) + \beta\left[(\nabla \cdot p, \nabla \cdot q) + (\nabla \times p, \nabla \times q)\right], \tag{4.17}$$

$$b(w,q) = -(w, \nabla \cdot q), \tag{4.18}$$

$$c(v,w) = (\nabla v, \nabla w). \tag{4.19}$$

Notice that (4.16) is actually decoupled, therefore it saves computation time (as compared with the augmented method). The parameter β determines the order of accuracy of the method as we will see later.

Remark 4.2 *The formula (4.16) can be interpreted formally as the finite element approximation of the problem*

$$\begin{cases} -\beta(\Delta E - \nabla L) + E + \nabla \psi = 0, \\ -\Delta \psi = L, \end{cases} \tag{4.20}$$

where

$$\Delta E = \nabla \nabla \cdot E - \nabla \times \nabla \times E. \tag{4.21}$$

If $\beta \to 0$, the classical Galerkin method is obtained. If $\beta \to \infty$, the div-rot method is obtained. In case that Γ_1 and Γ_2 are connected, $(\nabla \cdot p, \nabla \cdot q) + (\nabla \times p, \nabla \times q)$ is positive (cf. (4.8)). □

Denoting $e_\psi = \psi - \psi^h$ and $e_E = E - E^h$, we are ready to state the following theorem.

Theorem 4.1 *If $\beta \sim h$ and (ψ, E) are smooth enough, then*

$$\|e_\psi\| = O(h^2), \tag{4.22}$$

$$\|e_E\| = O(h^{3/2}). \tag{4.23}$$

Proof. Since (4.16) is decoupled, it is a straightforward matter to obtain (4.22) (see, e.g.,[18]). Now we prove (4.23). It is obvious that e_ψ and e_E satisfy

$$a(e_E, q^h) + b(e_\psi, q^h) = 0, \qquad \forall q^h \in \mathcal{Q}^h. \tag{4.24}$$

Let us define $\Pi_h E \in \mathcal{Q}^h$ as the interpolant of E, say at nodal points, and denote $\eta_E = E - \Pi_h E$, then the following standard approximation result holds:

$$\|\eta_E\| + h(\|\nabla \cdot \eta_E\| + \|\nabla \times \eta_E\|) = O(h^2). \tag{4.25}$$

By (4.24) and the Schwarz inequality,

$$\begin{aligned}
a(e_E, e_E) &= a(e_E, (E - \Pi_h E) + (\Pi_h E - E^h)) \\
&= a(e_E, \eta_E + (\Pi_h E - E^h)) \\
&= a(e_E, \eta_E) - b(e_\psi, \Pi_h E - E^h) \\
&= a(e_E, \eta_E) - b(e_\psi, e_E) + b(e_\psi, \eta_E) \\
&\leq \|e_E\| \, \|\eta_E\| + \beta \left(\|\nabla \cdot \eta_E\| \, \|\nabla \cdot e_E\| + \|\nabla \times \eta_E\| \, \|\nabla \times e_E\|\right) \\
&+ \|e_\psi\| \, \|\nabla \cdot e_E\| + \|e_\psi\| \, \|\nabla \cdot \eta_E\|.
\end{aligned} \tag{4.26}$$

Using (4.22) and (4.25), we derive estimates for the terms on the right hand sides of the above inequality as follows

$$\|e_E\| \, \|\eta_E\| \leq Ch^4 + \frac{1}{2}\|e_E\|^2 \tag{4.27}$$

$$\beta \left(\|\nabla \cdot \eta_E\| \, \|\nabla \cdot e_E\| + \|\nabla \times \eta_E\| \, \|\nabla \times e_E\| \right)$$
$$\leq C\beta h^2 + \beta \, (\frac{1}{4} \|\nabla \cdot e_E\|^2 + \frac{1}{2} \|\nabla \times e_E\|^2), \tag{4.28}$$
$$\|e_\psi\| \, \|\nabla \cdot e_E\| \leq C \, \frac{h^4}{\beta} + \frac{\beta}{4} \, \|\nabla \cdot e_E\|^2 \tag{4.29}$$

and

$$\|e_\psi\| \, \|\nabla \eta_E\| \leq C h^3. \tag{4.30}$$

The above positive constant C may depend on the solution ψ and E, but it is independent of h. Hence, we obtain

$$a(e_E, e_E) \leq C(h^4 + \beta h^2 + \frac{h^4}{\beta} + h^3) + \frac{1}{2} a(e_E, e_E). \tag{4.31}$$

Therefore

$$a(e_E, e_E) \leq 2C(h^4 + \beta h^2 + \frac{h^4}{\beta} + h^3). \tag{4.32}$$

The theorem is proved if we choose $\beta \sim h$. □

Remark 4.3 *From the proof of Theorem 4.1, it is easy to see that the convergence result still holds if we consider (4.16) without the rotation term* $(\nabla \times E^h, \nabla \times q^h)$*, which is used to stabilize the scheme.* □

Theorem 4.1 indicates that the convergence rate of the scheme (4.16) is consistent with that of the usual SD method. The scheme (4.16) adopts the idea of the least-squares finite element method, but the methods are different. In a recent paper by Pehlivanov *et al.* [63], a least-squares method was proposed and analyzed. The preconditioner there, which decouples the calculations for ψ^h and E^h, is quite similar to our method if we take $\beta = 1$ and drop the rotation term in (4.16). That method thus gives first-order accuracy in $\|e_E\|$, as was shown in [63] and also can be seen in the proof of Theorem 4.1.

We point out that the proof of Theorem 4.1 can be applied to a more general case in which a higher degree polynomial space P_k is used in the subspace pair (4.9) and (4.10). In such a case, the convergence results will be

$$\|e_\psi\| = O(h^{k+1}), \tag{4.33}$$

$$\|e_E\| = O(h^{k+1/2}). \tag{4.34}$$

4.4 Numerical Test

Let $\Omega \subset I\!R^2$ be a unit square with $\Gamma_1 = \Gamma_1^1 \bigcup \Gamma_1^2$, where $\Gamma_1^1 = \{x = 0\}$ and $\Gamma_1^2 = \{x = 1\}$, and $\Gamma_2 = \Gamma \backslash \Gamma_1$. Consider the following model problem:

$$-\Delta\psi = \frac{5}{4}\pi^2 \sin(\frac{\pi}{2}x)\cos(\pi y) \tag{4.35}$$

with mixed boundary conditions

$$\psi \mid_{\Gamma_1^1} = 0, \tag{4.36}$$

$$\psi \mid_{\Gamma_1^2} = \cos(\pi y), \tag{4.37}$$

$$\nabla\psi \cdot n \mid_{\Gamma_2} = 0. \tag{4.38}$$

The exact solution is provided by

$$\psi = \sin(\frac{\pi}{2}x)\cos(\pi y). \tag{4.39}$$

We use uniform partitions of Ω into rectangular elements. The finite element subspaces $\mathcal{W}_{g_0}^h$ and $\mathcal{Q}^h$ consist of piecewise bilinear polynomials. Denoting $E = -\nabla\psi$, Table 4.1 and 4.2 exhibit the numerical results for E^h using (4.16). They confirm that $\beta \sim h$ gives the best convergence results. We observe that the numerical convergence rates for our uniform mesh are higher than those predicted in Theorem 4.1 for general meshes. This is expected and can be explained along the arguments of Peterson in [64] and Lin

Mesh Size	$\|e_E\|$				
		Without Rotation Term		With Rotation Term	
	$\beta = 0$	$\beta = h$	$\beta = 1$	$\beta = h$	$\beta = 1$
$h = 0.2$	9.100D-2	2.529D-1	7.523D-1	1.807D-1	3.905D-1
$h = 0.1$	3.125D-2	4.280D-2	2.607D-1	3.439D-2	1.747D-1
$h = 0.05$	1.038D-2	7.191D-3	7.352D-2	6.059D-3	5.577D-2
$h = 0.025$	3.556D-3	1.384D-3	1.934D-2	1.254D-3	1.488D-2

Table 4.1: Errors of E^h with different parameter settings.

in [56]. The computed solution can have a higher convergence rate in many situations as compared with that from the theoretical estimation, except for some special mesh constructions. In particular, sharper error estimates are possible for the rectangular meshes by more subtle investigations (see [56]). Moreover, the bilinear mode xy in the finite element subspaces often raises the convergence rate, which is beyond the reach of our error estimations.

Mesh Size	Convergence Rate				
		Without Rotation Term		With Rotation Term	
	$\beta = 0$	$\beta = h$	$\beta = 1$	$\beta = h$	$\beta = 1$
$h = 0.1$	1.5420	2.5629	1.5289	2.3935	1.1604
$h = 0.05$	1.5900	2.5733	1.8261	2.5048	1.6473
$h = 0.025$	1.5454	2.3773	1.9265	2.2725	1.9061

Table 4.2: Convergence rates for E^h with different parameter settings.

Chapter 5

Simulation I: the ρ^+-ρ-ρ^+ Diode

5.1 Introduction

The ρ^+-ρ-ρ^+ diode, which simulates a channel of a metal oxide semiconductor field effect transistor (MOSFET), is a fundamental device which was used to understand the behavior of the hydrodynamic (HD) model and to optimize the HD modeling by simulations (e.g., overcoming the spurious velocity overshoot [30]). Recall that the HD model for semiconductor devices consists of a system of conservation laws for charge density, momentum and energy. Since there are hyperbolic modes (see Gardner *et al* [29] for a detailed discussion), it supports shocks or discontinuities of solutions. As a model problem, the one-dimensional ρ^+-ρ-ρ^+ diode was considered intensively by many researchers. For instance, uniqueness of subsonic solutions was proved by Degond and Markowich [19]; transonic solutions were analyzed mathematically by means of viscosity approximations by Gamba (see [24], [25]); Ascher *et al* [2] and Markowich and Pietra [59] studied shock phenomena for a current driven problem using a phase plane analysis, which gave a full explanation of how and when the shock occurs; shocks were found for the full system by Gardner [26] in a steady state case and by Fatemi *et al* [22] in a non-steady state case with low temperatures.

There are many numerical methods designed to handle the occurrence of shocks. For example, the so-called ENO (essentially nonoscillatory) scheme used in [22] is an efficient shock-capturing algorithm. But most of them are one-dimensional in nature although

they can be used for two-dimensional problems by operator splitting techniques. The streamline-diffusion (SD) method is suitable for handling multi-dimensional cases with theoretical backing. In this chapter, the SD method presented in Chapter 3 with a shock-capturing modification is used to simulate the silicon ρ^+-ρ-ρ^+ diode for both the subsonic and transonic electron flows. Shocks of the transonic flows are captured for one- and two-dimensional diodes.

In Section 5.2, a SD method with a shock-capturing modification as well as a numerical treatment of the "in-flow" boundary condition is presented. In Section 5.3, we describe the so-called predictor/multi-corrector algorithm applied to our problem. Physical parameters for device simulations are given in Section 5.4 and finally numerical experiments are carried out in Section 5.5.

5.2 SD Method for Devices

In this section, we consider the SD formulation for the d-dimensional ($d = 1$ or 2) HD model (2.6) in the form

$$\mathcal{L}U \triangleq A_0 U_t + A \cdot \nabla U + C(U) - \nabla \cdot (\mathcal{K} \nabla U) = 0, \tag{5.1}$$

where $U = (\rho, J, T)^t$ is the unknown vector of working variables.

We define the problem (5.1) in a bounded domain Ω with its boundary $\Gamma = \Gamma_1 \bigcup \Gamma_2$, the union of contact and insulating parts. The domain Ω is divided into three regions by junctions: the source, the channel and the drain regions (traversing Ω from left to right in Fig. 5.1 for example).

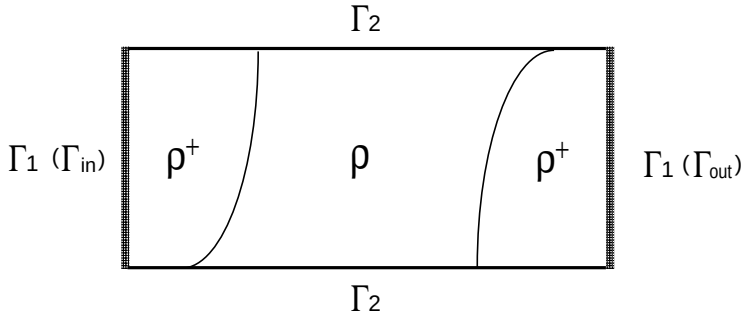

Figure 5.1: Geometry of ρ^+-ρ-ρ^+ diode.

5.2.1 Shock-Capturing SD Formulation

The SD formulation for system (5.1) follows that of Chapter 3 with minor adjustments. We use the following finite element subspace

$$\mathcal{T}_g^h = \{V^h \mid V^h \in (C^0(Q_n))^l,\ V^h\ |_{Q_n^e} \in (P_1(Q_n^e))^l,\ \mathcal{D}V^h\ |_{\Gamma_1 \times I_n(T)} = g\}, \tag{5.2}$$

where $l = d + 2$. The symbol $\mathcal{D}$ is a boundary condition operator and g is an expression standing for essential boundary conditions given by (2.30)-(2.31) and (2.41). It is understood that the subspace $\mathcal{T}_0^h$ is a special case of $\mathcal{T}_g^h$ with zero essential boundary conditions.

As we have mentioned in Section 2.4, an additional "in-flow" boundary condition is needed mathematically. Although this was noticed and analyzed in [80], no analytic expression was given there because no obvious related physical quantity is available. We therefore seek a reasonable approximation in our cases using the momentum equation (2.1b). We assume the current and velocity are almost constant near Γ_{in}, so the convection term $v\nabla \cdot J + J \cdot \nabla v$ is almost zero. This is true in many cases, for example when the doping profile is constant near Γ_{in}. If we further ignore J_t, we propose the following

approximation of the "in-flow" boundary condition:

$$J \cdot n|_{\Gamma_{in}} = -\mu_0(\rho E + \frac{mT_0}{e}\nabla\rho + \frac{m\rho_D}{e}\nabla T) \cdot n|_{\Gamma_{in}}, \tag{5.3}$$

in which we assume that the "in-flow" current is a sum of drift, diffusion and thermal currents. This may cause an error initially, but it soon dies out when t increases.

For any test function $\Psi \in \mathcal{T}^h$, if we denote $\bar{\Psi} = (\Psi_2, \ldots, \Psi_{d+1})^t$, the space-time SD formulation with a shock-capturing modification for the HD model (5.1) is as follows. Within each Q_n $(n = 0, \ldots, N-1)$, find $U^h \in \mathcal{T}_g^h$ such that for all $\Psi \in \mathcal{T}_0^h$,

$$\begin{aligned}
&\int_{Q_n} [(A_0 U_t^h + A \cdot \nabla U^h + C(U^h)) \cdot \Psi + \mathcal{K}\nabla U^h \cdot \nabla\Psi]\, dxdt && \text{(Galerkin)} \\
&+ \int_\Omega A_0[\![U^h(t_n)]\!] \cdot \Psi(t_n^+)\, dx && \text{(Jump Condition)} \\
&+ \sum_{e=1}^{n_{el}} \int_{Q_n^e} \mathcal{L}U^h \cdot P^h(\Psi)\, dxdt && \text{(SD)} \\
&+ \sum_{e=1}^{n_{el}} \int_{Q_n^e} \nu(U^h)\tilde{\nabla}U^h \cdot \bar{A}_0\tilde{\nabla}\Psi\, dxdt && \text{(SC)} \\
&+ \int_{\Gamma_{in}\times I_n(T)} J^h \cdot n\bar{\Psi} \cdot n\, dsdt && \text{(Weak In-Flow)} \\
&= -\int_{\Gamma_{in}\times I_n(T)} \mu_0\,(\rho_D E^h + \frac{mT_0}{e}\nabla\rho^h + \frac{m\rho_D}{e}\nabla T^h) \cdot n\bar{\Psi} \cdot n\, dsdt, && (5.4)
\end{aligned}$$

where $\bar{A}_0 = diag(A_0, A_0, A_0)$ and the generalized gradient operator $\tilde{\nabla}$ is given by

$$\tilde{\nabla} = \begin{pmatrix} \frac{\partial}{\partial t} I_{d+2} \\ \nabla I_{2(d+2)} \end{pmatrix}.$$

The second term to the last on the left-hand side of (5.4) is a so-called shock-capturing term which introduces a certain amount of crosswind diffusion near shocks. The coefficient $\nu(U^h)$ is defined as

$$\nu(U) = \delta h \max\{\frac{|\mathcal{L}U|_2^p}{h + |\tilde{\nabla}U|_{\bar{A}_0}^p},\ h^{1/2}\}, \tag{5.5}$$

where δ is a parameter, $|\cdot|_{\bar{A}_0}$ is an $\bar{A}_0$-weighted l^2-norm and the integer $p = 1$ or 2. The last terms at the left and right sides of (5.4) constitute a weak formulation of the "inflow" boundary condition (5.3). This will alleviate the possible discrepancy introduced by (5.3) as compared with (2.1b) at nearby points (though this discrepancy should be small anyway). Moreover, it enhances the stability of the numerical scheme.

5.2.2 Concept of the Shock Capturing SD Method

Although the SD method in its basic form discussed in Chapter 3 gives a dramatic improvement as compared with the standard Galerkin method, oscillations cannot be entirely prevented near the discontinuities or sharp layers of solutions. As a remedy, a shock-capturing (SC) modification is used to achieve the goals: (1) preserving high accuracy in the regions where the solutions are smooth; (2) suppressing oscillations near the discontinuities or sharp gradients of the solutions. The method is a true nonlinear one even if the problem considered is linear.

A shock-capturing SD method was first proposed for the steady state convection-diffusion problem by Hughes *et al.* [42]. The extension to a system was studied in [41]. The method was adapted by Johnson and Szepessy [51] using the space-time finite element discretization for the nonlinear Burgers equation. There were many efforts along this line afterwards (e.g., see [77, 15, 12]). Now the shock-capturing SD method has become a standard formulation.

Let us consider again the scalar convection-diffusion problem (3.2) in Section 3.2:

$$\mathcal{L}u \triangleq a \cdot \nabla u - \kappa \Delta u - f = 0. \tag{5.6}$$

Compared to the basic SD Petrov modification, the shock-capturing SD Petrov modification of the usual test function $v^h \in \mathcal{V}_0^h$ in the classical Galerkin method reads

$$v^h \longleftarrow v^h + \tau\, a \cdot \nabla v^h + \tau_{||}\, a_{||} \cdot \nabla v^h,$$

where the parameter $\tau_{||} > 0$. Similar to the SD operator, we define the SC operator by

$$P^h_{||}(v^h) = \tau_{||}\, a_{||} \cdot \nabla v^h.$$

Different from the SD operator, the SC operator needs to satisfy only a few design conditions [77]: in order to control the oscillations, this operator should act in the direction of the gradient; for consistency it should be proportional to the residual $\mathcal{L}^h u^h$; and for accuracy it should vanish quickly or remain within the order of accuracy of the basic SD scheme in smooth regions of the solutions.

Quadratic SC Operator :

For $|\nabla u^h|_2 \neq 0$, the projection $a_{||}$, which projects the residual $\mathcal{L}u^h$ onto the direction of the gradient ∇u^h, is given by

$$a_{||} = \frac{\mathcal{L}u^h}{|\nabla u^h|_2^2} \nabla u^h. \tag{5.7}$$

Clearly

$$a_{||} \cdot \nabla u^h = \mathcal{L}u^h, \tag{5.8}$$

$$a_{||} \cdot v^h = 0, \qquad \forall v^h \in \text{null}(\nabla u^h). \tag{5.9}$$

The inner product of the SD operator $P^h_{||}(v^h)$ and $\mathcal{L}u^h$ on each element Ω_e gives the following quadratic SC form

$$\int_{\Omega_e} \tau_{||} \frac{|\mathcal{L}u^h|_2^2}{|\nabla u^h|_2^2} \nabla u^h \cdot \nabla v^h \, dx. \tag{5.10}$$

Linear SC Operator:

The SC operator satisfying the design conditions is not unique. We can also consider the following linear SC form

$$\int_{\Omega_e} \tau_{||} \frac{|\mathcal{L}u^h|_2}{|\nabla u^h|_2} \nabla u^h \cdot \nabla v^h \, dx. \tag{5.11}$$

For system (5.1), we can revise the above SC operators according to [77] involving appearances of the matrix A_0 and the time derivative. The added h in the denominator of (5.5) is to prevent division by zero in case that $|\tilde{\nabla} U^h|_{\bar{A}_0} = 0$. In (5.5) we require, according to [44], that

$$\nu(U^h) \geq \delta h^{3/2} \tag{5.12}$$

which does not degrade the order of accuracy of the scheme.

5.3 Predictor/Multi-Corrector Algorithm

For each n, the discretization scheme (5.4) leads to a system of nonlinear algebraic equations. A predictor/multi-corrector algorithm (see [43, 77] for details) is used here to reduce the resulting nonlinear system to a sequence of linear systems. Moreover, we shall incorporate the potential equation solver presented in Chapter 4 within this algorithm.

For simplicity, we only consider the constant-in-time finite element subspace $\mathcal{T}^h$ here. The procedure is similar for the linear-in-time case though it is more complicated. Within each space-time slab Q_n, the trial solution U^h can be expressed by

$$U^{h(n+1)} = \sum_{P=1}^{n_d} \Psi_P(x) u_P^{(n+1)}, \tag{5.13}$$

where n_d is the number of nodal points of the space finite element mesh, $u_P^{(n+1)}$ is the vector of nodal unknowns at node P for the nth space-time slab and Ψ_P is the shape function associated with node P.

Define

$$u^{(n)} = ((u_1^{(n)})^t, (u_2^{(n)})^t, \ldots, (u_{n_d}^{(n)})^t)^t. \tag{5.14}$$

Substituting (5.13) into (5.4) and taking $\Psi = \Psi_P$ for $P = 1, \ldots, n_d$, (5.4) leads to a nonlinear algebraic system

$$G(u^{(n)}, u^{(n+1)}) = 0 \tag{5.15}$$

with $u^{(n)}$, associated with the solution in the (n-1)st slab, coming from the jump condition in (5.4). Newton's iteration applied to (5.15) yields

$$G(\cdot, u_{(i+1)}) \cong G(\cdot, u_{(i)}) + \frac{\partial G(\cdot, u_{(i)})}{\partial u} \Delta u_{(i)} = 0, \tag{5.16}$$

where

$$u_{(i+1)} = ((u_{1,(i+1)})^t, (u_{2,(i+1)})^t, \ldots, (u_{n_d,(i+1)})^t)^t \tag{5.17}$$

is the (i+1)st iterative approximation of $u^{(n+1)}$ with $u_{(0)} = u^{(n)}$. $\Delta u_{(i)}$ is defined by

$$\Delta u_{(i)} = u_{(i+1)} - u_{(i)}. \tag{5.18}$$

Denote by

$$R^{(i)} = G(\cdot, u_{(i)}), \tag{5.19}$$

the residual vector. Then

$$R^{(i)} = ((R_1^{(i)})^t, (R_2^{(i)})^t, \ldots, (R_{n_d}^{(i)})^t)^t, \tag{5.20}$$

where

$$\begin{aligned}
R_P^{(i)} = \Delta t \int_\Omega & [(A \cdot \nabla U_{(i)}^h + C(U_{(i)}^h)) \cdot \Psi_P + \mathcal{K} \nabla U_{(i)}^h \cdot \nabla \Psi_P] \, dx && \text{(Galerkin)} \\
+ \int_\Omega & A_0 [U_{(i)}^h - U^{h\,(n)}] \cdot \Psi_P \, dx && \text{(Jump Condition)} \\
+ \Delta t \sum_{e=1}^{n_{el}} & \int_{\Omega_e} \mathcal{L} U_{(i)}^h \cdot P^h(\Psi_P) \, dx && \text{(SD)} \\
+ \Delta t \sum_{e=1}^{n_{el}} & \int_{\Omega_e} \nu(U_{(i)}^h) \nabla U_{(i)}^h \cdot \bar{A}_0(U_{(i)}^h) \nabla \Psi_P \, dx && \text{(SC)} \\
+ \Delta t & \int_{\Gamma_{in}} J_{(i)}^h \cdot n \bar{\Psi}_P \cdot n \, ds && \text{(Weak In-Flow)} \\
+ \Delta t & \int_{\Gamma_{in}} \mu_0 \left(\rho_D E_{(i)}^h + \frac{m T_0}{e} \nabla \rho_{(i)}^h + \frac{m \rho_D}{e} \nabla T_{(i)}^h\right) \cdot n \bar{\Psi}_P \cdot n \, ds
\end{aligned} \tag{5.21}$$

with $U^h_{(i)}$, the ith iterative approximation to $U^{h^{(n+1)}}$, defined by

$$U^h_{(i)} = \sum_{P=1}^{n_d} \Psi_P(x) u_{P,(i)}. \tag{5.22}$$

To keep the notation simple, we denote the algebraic system from (4.16) of the Poisson solver at each time step by

$$(\psi^{(n)}, E^{(n)}) = P_{sol}(u^{(n)}), \tag{5.23}$$

where the pair $(\psi^{(n)}, E^{(n)})$ here stands for a pair of nodal unknown vectors for the pair $(\psi^{h^{(n)}}, E^{h^{(n)}})$ as $u^{(n)}$ for $U^{h^{(n)}}$ without causing any confusion. We can now describe the following algorithm.

Predictor/Multi-Corrector Algorithm:

Given initial data, for $n = 0, 1, \ldots, N-1$, do

(Predictor)

$u_{(0)} = u^{(n)}$

$(\psi_{(0)}, E_{(0)}) = P_{sol}(u^{(n)})$

(Multi-corrector loop)

For $i = 0, 1, \ldots, ipass - 1$, do

$M^* \Delta u_{(i)} = -R^{(i)}$

$u_{(i+1)} = u_{(i)} + \Delta t \Delta u_{(i)}$

$(\psi_{(i+1)}, E_{(i+1)}) = P_{sol}(u_{(i+1)})$

Continue

$u^{(n+1)} = u_{(ipass)}$

$(\psi^{(n+1)}, E^{(n+1)}) = (\psi_{(ipass)}, E_{(ipass)})$

End.

In the above box, we use an explicit pass in the multi-corrector loop. The parameter *ipass* can be either fixed or determined by $R^{(i)}$. The mass lump matrix is

$$M^* = (M_{JK}), \tag{5.24}$$

where

$$M_{JK} = \begin{cases} \int_\Omega A_0 \Psi_J \cdot \Psi_J \, dx & \text{if } J = K, \\ 0 & \text{if } J \neq K. \end{cases} \tag{5.25}$$

This method is conditionally stable. The algorithm CFL condition is of $O(\Delta t/h^2)$ due to the thermal conductivity and the artificial diffusivity [77]. The algorithm is simple in implementation because the matrix M^* is easy to invert.

5.4 Physical Parameters

For the subsequent device simulations, we adopt the following system of units:

Classification	Unit
Length	$10^{-6}\ m$ ($1\ \mu m$)
Time	$10^{-12}\ s$ ($1\ ps$)
Mass	$10^{-10}\ Kg$
Potential	Volt
Energy	$10^{-18}\ J$
Charge	$10^{-18}\ C$
Temperature	Kelvin (unscaled)
Capacitance	$10^{-18}\ F$

Typical values of physical parameters for silicon devices that we use are given in Table 5.1 under such a unit system.

Physical Parameters	Value
m_e	0.9109
κ_b	0.138046×10^{-4}
e	0.1602
λ	11.7×8.85418
κ_0	0.4

Table 5.1: Values of physical parameters.

In Table 5.1, m_e is the electron mass. The effective mass of the electron $m = 0.26m_e$ at $T_0 = 300K$ and $0.24m_e$ at $T_0 = 77K$; the intrinsic electron density $\rho_i = 1.45 \times 10^{10} cm^{-3}$ at $T_0 = 300K$ and $2.84 \times 10^{20} cm^{-3}$ at $T_0 = 77K$. We point out that κ_0 in Table 5.1 is heuristically the best for the diode we consider. If κ_0 is away from this value, a spurious velocity overshoot will appear (see [22, 29]).

The models for μ_0 and v_s are those used in [26]:

$$\mu_0 = \mu_{min} + \frac{\Delta\mu}{1 + (\rho_D/\rho_{ref})^\gamma}, \tag{5.26}$$

where

$$\mu_{min} = 80 cm^2/V \cdot s \times \begin{cases} (300K/T_0)^{0.45} & T_0 \geq 200K \\ 1.5^{0.45}(200K/T_0)^{0.15} & T_0 < 200K, \end{cases} \tag{5.27}$$

$$\Delta\mu = (300K/T_0)^2 1430 \frac{cm^2}{V \cdot s} - \mu_{min}, \tag{5.28}$$

$$N_{ref} = (T_0/300K)^{3.2} 1.12 \times 10^{17} cm^{-3}, \tag{5.29}$$

$$\gamma = 0.72(T_0/300K)^{0.065}. \tag{5.30}$$

and

$$v_s = \frac{2.4}{1 + 0.8\exp(0.5T_0/300K)} \times 10^7 \text{cm/s}. \tag{5.31}$$

5.5 Numerical Simulations

In this section, numerical experiments for the one- and two-dimensional ρ^+-ρ-ρ^+ silicon diodes are performed for both the subsonic and transonic electron flows. The SD scheme (5.4) with the constant-in-time finite element subspace $\mathcal{T}^h$ is used throughout the section. This will not degrade the entire order of accuracy of solutions since the explicit predictor/multi-corrector algorithm introduced in Section 5.3 requires that Δt be proportional to h^2.

5.5.1 One-Dimensional Simulations

In this subsection, we use uniform meshes with $h = 0.05$, $\Delta t = 0.2\,h$. The shock-capturing term in (5.4) is not included, i.e., δ is set to be zero.

Case 1: $T_0 = 300K$

A 0.6-μm silicon diode is used with a 0.1-μm source, 0.4-μm channel and 0.1-μm drain. The doping profile is given by

$$\begin{aligned} \rho_D(x) &= 5 \times 10^{17}\ \mathrm{cm}^{-3}, \qquad \text{if } 0 \le x \le 0.05 \text{ or } 0.55 \le x \le 0.6, \\ \rho_D(x) &= 2 \times 10^{15}\ \mathrm{cm}^{-3}, \qquad \text{if } 0.15 \le x \le 0.45. \end{aligned}$$

The above segments of ρ_D are connected smoothly by a scaled version of the polynomial:

$$Q(x) = (x+1)^4(-5x^3 + 20x^2 - 29x + 16). \tag{5.32}$$

Steady state solutions are obtained by letting solutions evolve in time. Solutions with biased voltages V_D =1, 1.5 and 2V are shown in Fig. 5.2.

Remark 5.1 *We set the biased voltage to be zero at the source as a reference. Therefore, whenever we say we apply a biased voltage V_D to the device, it means that the bias is prescribed for the drain.* □

The Mach number $|v|/c^*$ is less than 1 for all x, so the electron flow is a subsonic one. It is worth noticing that no spurious velocity overshoot is observed using the parameters presented in Section 5.4. For comparison, numerical solutions with spurious velocity overshoots are given in Appendix C using a different set of parameters.

Case 2: $T_0 = 77K$

We take Gardner's example in [26]. A 1.2-μm silicon diode is used with 0.1-μm source, 1.0-μm channel and 0.1-μm drain. The doping profile is given by

$$\begin{aligned} \rho_D(x) &= 10^{18}\ \mathrm{cm}^{-3}, \qquad \text{if } 0 \le x \le 0.05 \text{ or } 1.15 \le x \le 1.2, \\ \rho_D(x) &= 10^{15}\ \mathrm{cm}^{-3}, \qquad \text{if } 0.15 \le x \le 1.05. \end{aligned}$$

The above segments of ρ_D are connected smoothly by a scaled version of the polynomial (5.32). The biased voltage $V_D = 1V$ is applied.

Evolutions of velocity and temperature in time are shown in Fig. 5.3. Solutions reach the steady state at about 11 ps. We notice strong initial layers for the solutions. A steady state shock wave with Mach number 4.1 is shown in Fig. 5.4. A shock wave is developed at $x \simeq 0.43$. It can only be formed at the transition for the electron flow from the supersonic region to the subsonic region. The cooling of electrons, when the flow enters the channel, is stronger in this case as compared with the above $T_0 = 300K$ case. The resulting velocity and temperature profiles are typical and are qualitatively the same as those in [26] and [21].

Case 3: HD vs SHD

To compare solutions of the full HD and SHD models, we plot the $J - V_D$ (at $T_0 = 300K$) and $J - T_0$ (at $V_D = 2V$) curves of both models in Fig. 5.6 using the same 1.2-μm diode as in case 2 except

$$\begin{aligned} \rho_D(x) &= 5 \times 10^{17}\ \mathrm{cm}^{-3}, \qquad \text{if } 0 \le x \le 0.05 \text{ or } 1.15 \le x \le 1.2, \\ \rho_D(x) &= 2 \times 10^{15}\ \mathrm{cm}^{-3}, \qquad \text{if } 0.15 \le x \le 1.05. \end{aligned}$$

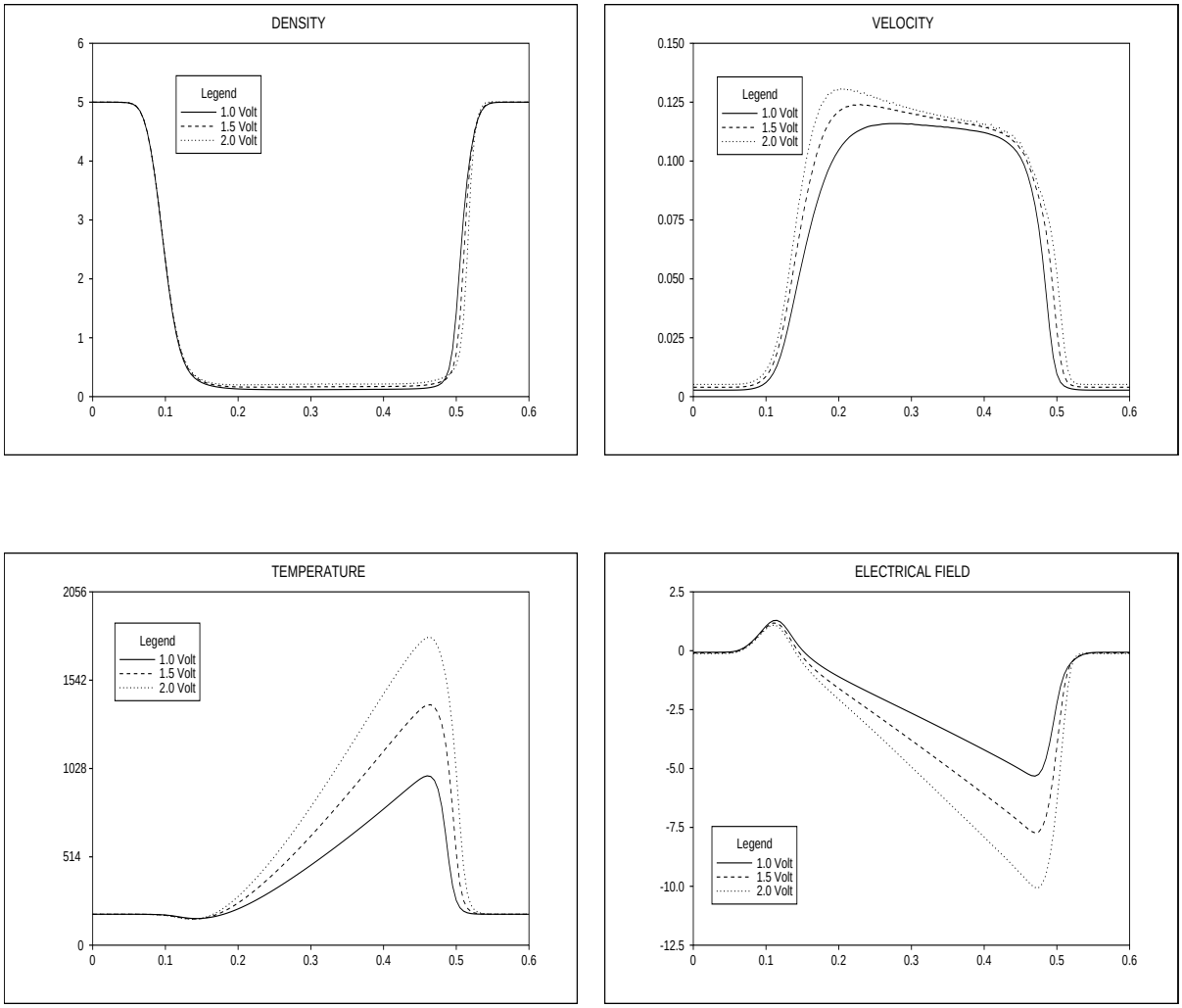

Figure 5.2: HD model at 300K: Electron densities in $10^{17}cm^{-3}$; velocities in $10^8 cm/s$; temperatures in Kelvin and electric fields in $10^4 V/cm$.

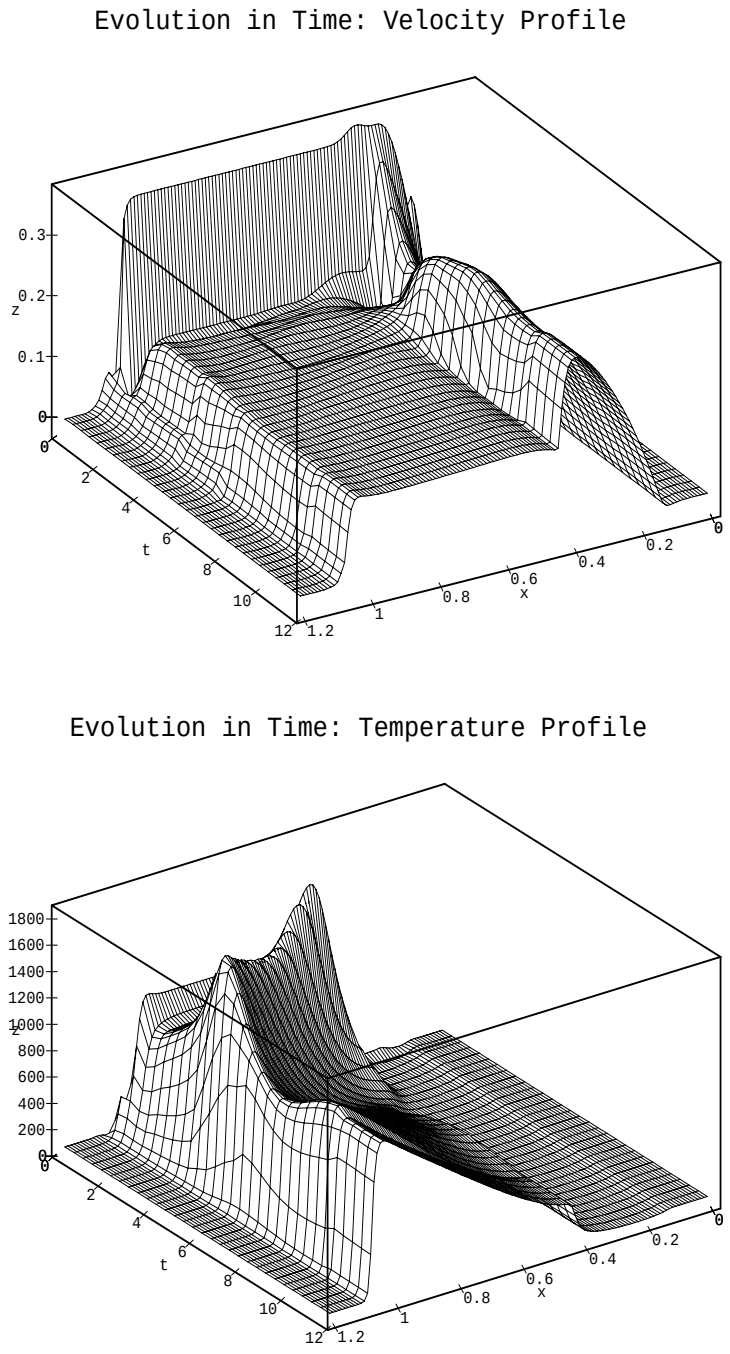

Figure 5.3: HD model at 77K: evolutions of selected solutions.

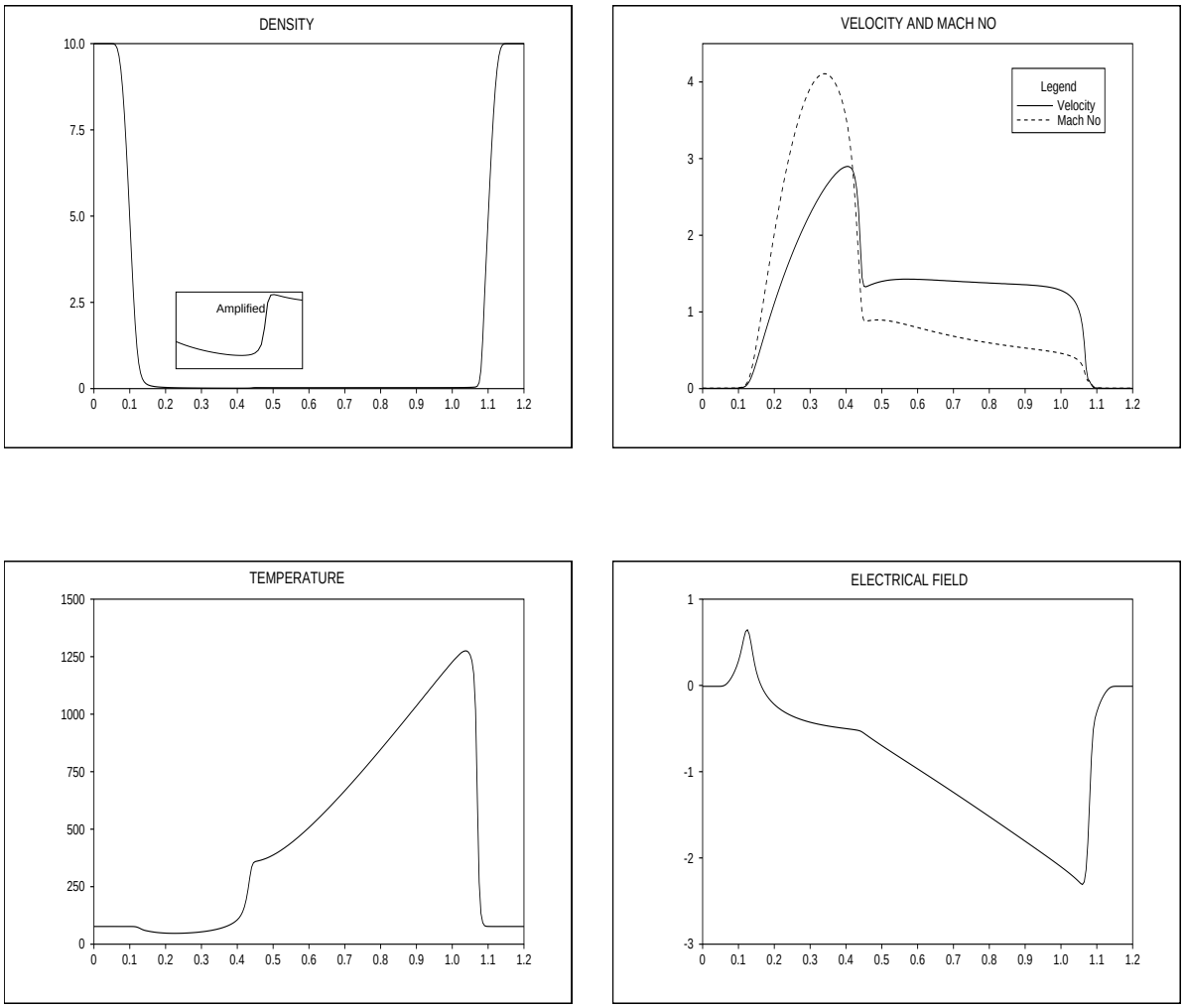

Figure 5.4: HD model at 77K: Electron density in $10^{17}cm^{-3}$; velocity in $10^7 cm/s$ and Mach number; electron temperature in Kelvin; electric field in $10^4 V/cm$ (from left to right and top to bottom).

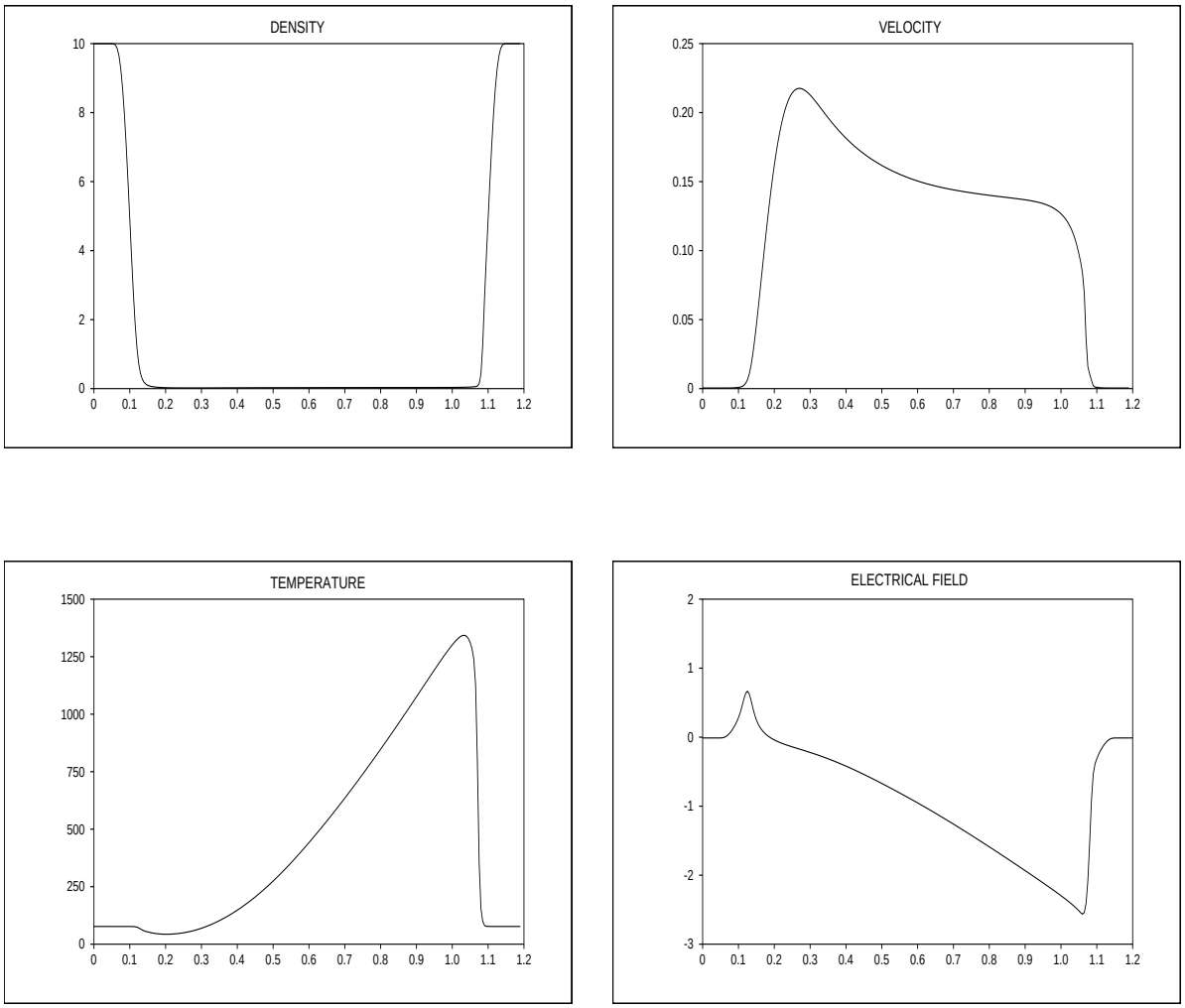

Figure 5.5: SHD model at 77K: Electron density in $10^{17}cm^{-3}$; velocity in $10^8 cm/s$; electron temperature in Kelvin; electric field in $10^4 V/cm$ (from left to right and top to bottom).

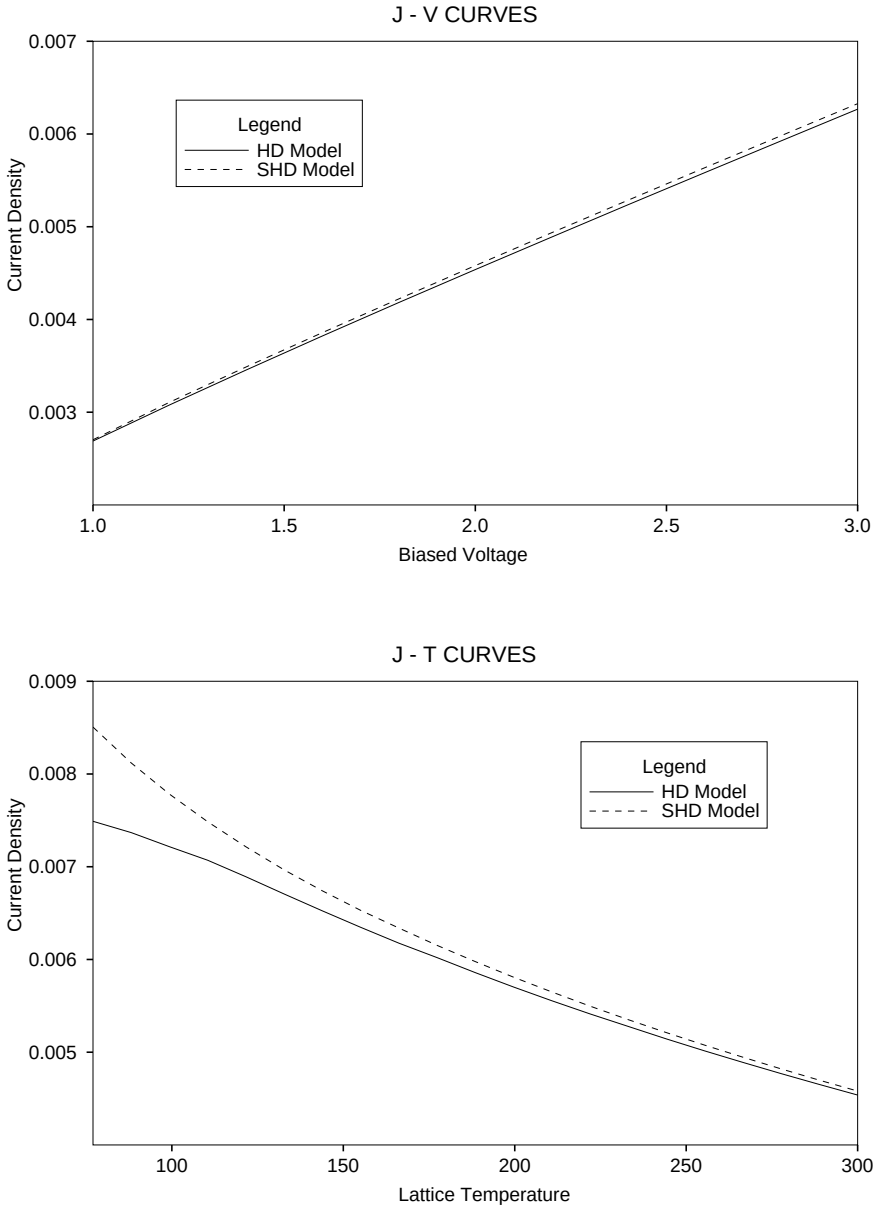

Figure 5.6: Comparisons of $J - V_D$ and $J - T_0$ curves using the HD and SHD models.

The difference is not very pronounced in the $J - V_D$ curves when the biased voltage V_D is increased. However, the difference is more pronounced in the $J - T_0$ curves when the ambient temperature T_0 reaches $77K$. We have observed that the current density of the full HD model is always smaller than that of the SHD model.

The steady state solutions of the SHD model at $T_0 = 77K$, which are noticeably different from those of the HD model, are presented in Fig. 5.5 with exactly the same parameter and geometry settings as in case 2.

5.5.2 Two-dimensional Simulations

Let us consider the HD model of the two-dimensional ρ^+-ρ-ρ^+ silicon diode shown in Fig. 5.1 with $\Omega = [0, 1(\mu m)] \times [0, 0.5(\mu m)]$. The two junctions are given by

$$x_1(y) = \frac{1}{4} - \frac{1}{2}(y - 1/2)^2, \tag{5.33}$$

$$x_2(y) = \frac{3}{4} + \frac{1}{2}y^2. \tag{5.34}$$

We define the doping profile (see Fig. 5.7):

$$\rho_D(x) = 5 \times 10^{17}\ \mathrm{cm}^{-3}, \qquad \text{if } 0 \le x \le x_1 \text{ or } x_2 \le x \le 1.0,$$

$$\rho_D(x) = 2 \times 10^{15}\ \mathrm{cm}^{-3}, \qquad \text{if } x_1 + 0.1 \le x \le x_2 - 0.1.$$

The above segments of ρ_D are, as in the one-dimensional case, connected by a scaled version of $Q(\xi)$ of (5.32), where

$$\xi = 200.0 \times (x_1(y) - x + 0.005) \qquad \text{for source-channel junction}$$

$$\xi = 200.0 \times (x - x_2(y) + 0.005) \qquad \text{for channel-drain junction}$$

An 80×40 uniform mesh is used in the following computations for the steady state solutions for the subsonic flow at $T_0 = 300K$ and the transonic flow at $T_0 = 77K$. The bias is $V_D = 1V$ in the following cases.

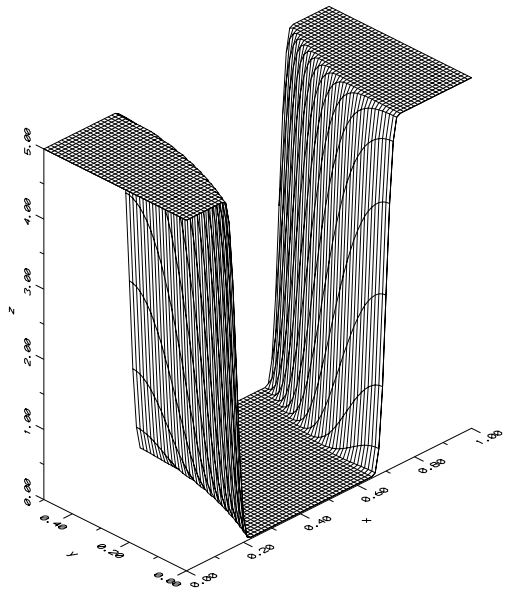

Figure 5.7: Doping profile in $10^{17}\ cm^{-3}$

Case 1: $T_0 = 300K$

In this case, we set $\Delta t = 0.002$ and $\delta = 0$. We present the electrical field and streamlines of the current in Fig. 5.8 and Fig. 5.9. Surface plots for the electron density and temperature are shown in Fig. 5.10. The Mach number in this case is 0.7.

We have observed oscillation of the current near junctions due to the sharp profile of the doping ρ_D. This (numerical) phenomenon was also reported in [22]. Since the current is small in comparison with other solutions, it is very sensitive to any small perturbations. Therefore it bears a relatively larger error than other quantities. The results show that the distortion of the current is more prominent at the ρ-ρ^+ junction than at the ρ^+-ρ junction. The error in the current is proportional to the order of accuracy of the numerical scheme, so higher order schemes or alternatively finer grids could help.

Case 2: $T_0 = 77K$

In this case, we set $\Delta t = 0.001$ and $\delta = 1$. A shock wave is presented with Mach

number 5.2 at the steady state (see Fig. 5.11). The shock profile develops in the channel and spreads over about 3 grid points. The peak value of Mach number can reach as high as 7.8 in evolution. The cooling effect is milder than that in the 300K case.

Numerical computations were applied to different geometries of the diode as well as different doping profiles. For some cases with shocks or abrupt junctions with sharp corners, we need to add the shock-capturing term defined in Section 5.3 with $\delta > 0$, which stabilizes the numerical scheme. Note, though, that we want to take δ as small as possible: if δ is large then it causes an overly diffused behavior of the solutions and, more seriously, it produces a poor current approximation as explained in the previous paragraph. The size of δ used here is still much smaller than what is required if the classical artificial viscosity method is employed.

5.5.3 Comments and Conclusions

Shocks of HD models are simulated for both one- and two-dimensional ρ^+-ρ-ρ^+ diodes by the shock-capturing SD method. Robustness of the employed SD method is evidenced by its performance and will be demonstrated again in the MESFET simulations in Chapter 6.

Although in many applications, such as the one in the following chapter, the solutions of the SHD model are close to those of the HD model, we observed an exceptional case. The prominent difference between these two models is that the HD model, but not the SHD model, supports shocks. With the same parameter setting, the behavior of the HD model is substantially different from that of the SHD model when shocks are developed in the HD model. Numerical experiments presented here have shown the influence of the shock on the solutions of the HD model. Failure to capture the shocks might cause serious error in the source-drain current.

We also examined different components of the current and found that the strength of the thermal current is less than that of the drift current or diffusion current.

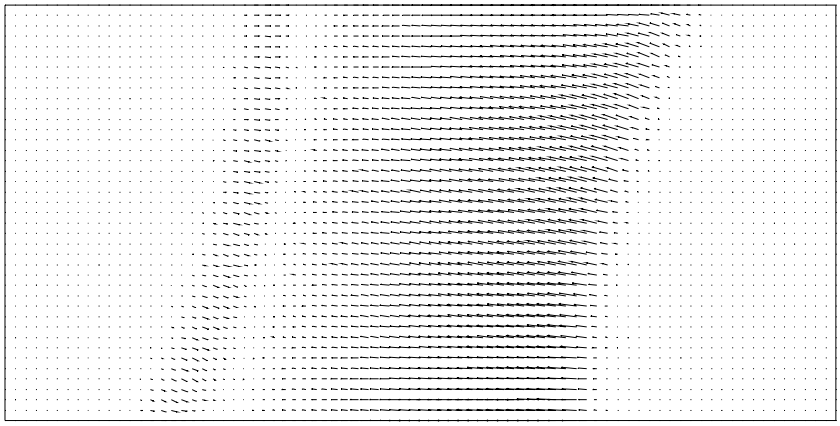

Figure 5.8: HD model at 300K: Electrical field.

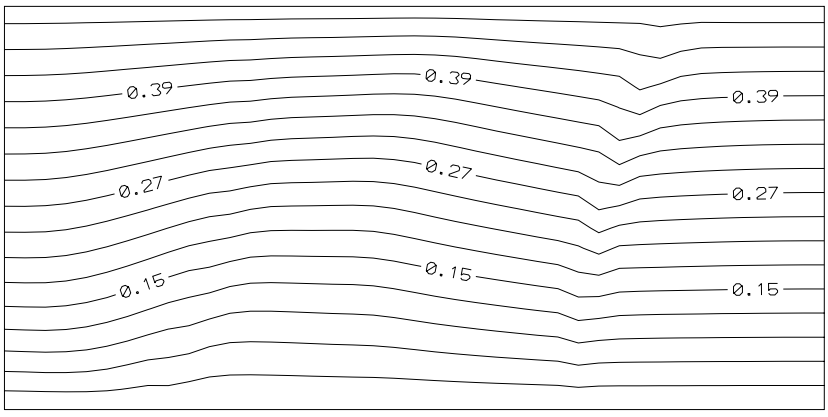

Figure 5.9: HD model at 300K: Streamlines of the current.

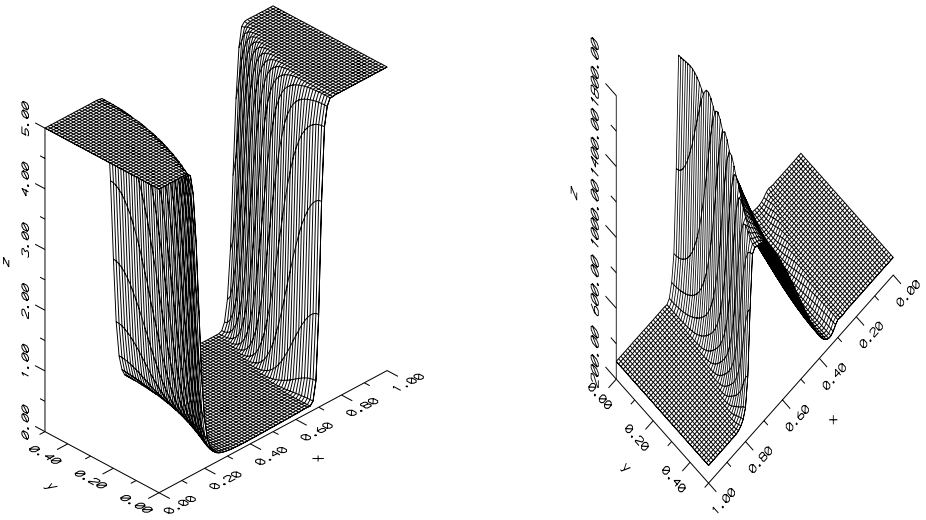

Figure 5.10: HD model at 300K: Electron density (left) in 10^{17} cm^{-3} and electron temperature (right) in Kelvin.

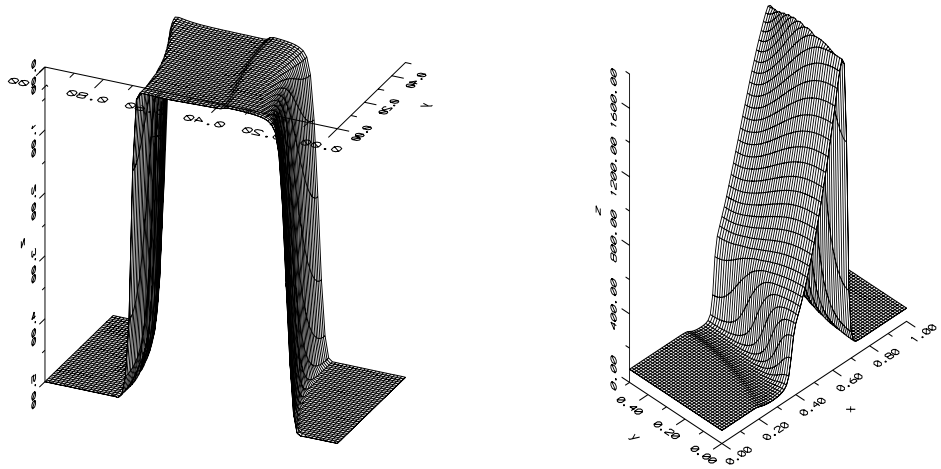

Figure 5.11: HD model at 77K: Electron density (left) in 10^{17} cm^{-3} (image is inverted) and electron temperature (right) in Kelvin.

Chapter 6

Simulation II: the MESFET Device

6.1 Introduction

The metal semiconductor field effect transistor (MESFET) is one of the important semiconductor devices. The physical characteristics of the device are manipulated by a rectifying metal-semiconductor contact at the the gate, known as a Schottky contact after Walter Schottky, who first proposed a model for the potential barrier formation in 1930s.

Although much progress has been made in the development of metallic contacts in semiconductor technology, a full understanding of the mechanism of barrier formation is far from complete. Therefore, a highly simplified model for simulation is used. The MESFET devices were simulated by Cook and Frey [17], Jerome and Shu [51] and Chen *et al.* [13] using the hydrodynamic (HD) model. Although there were no shocks observed, the shock-capturing algorithms in [51] and [13] proved to be useful when sharp layers occur. In this chapter, MESFET devices at room temperature are simulated effectively by our streamline-diffusion (SD) finite element methods using the HD models as well as the drift-diffusion (DD) models. We indicate that the SD method (without the shock-capturing term) for the conventional DD model is identical to the well-known Scharfetter-Gummel (SG) discretization [71] in one space dimension. Consequently, SD methods can be viewed as reasonable extensions of the SG formulation for the general convection-diffusion systems in multi-space dimensions.

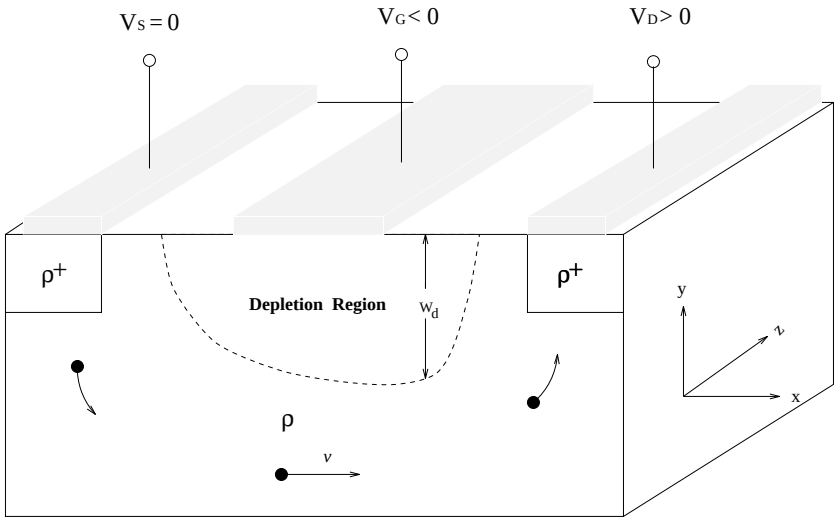

Figure 6.1: Schematic of MESFET operation.

Numerical experiments are implemented for models in an increasing order of complication: the conventional DD (DD1) model → the mixed-formulation DD (DD2) model → the simplified HD (SHD) model → the full HD model. Comparisons are made among solutions of the different models. We find a qualitative discrepancy between the solutions of the DD models and the HD models. A small difference, mainly in the temperature, is also found between the full HD and simplified HD models.

The arrangement of the chapter is as follows: In section 2, the physical aspect of the MESFET device (or essentially that of the Schottky diode), i.e., the formation of the Schottky barrier, is modeled. In section 3, the methodology of the SG discretization and close relationship with the SD concept are described. Numerical results and discussions are supplied in section 4. Good performance of the numerical method is demonstrated in this simulation.

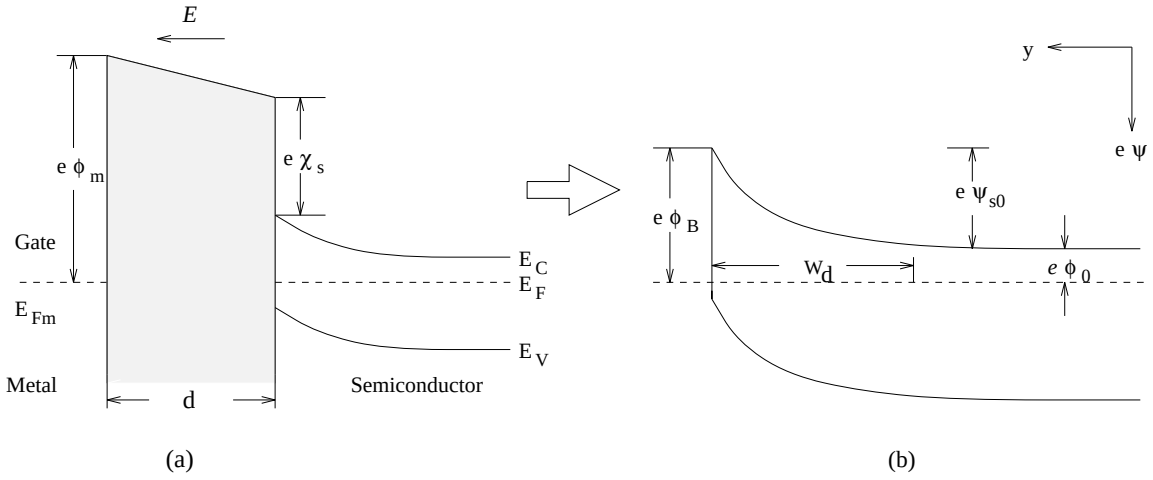

Figure 6.2: Formation of Schottky barrier

6.2 Schottky Barrier

A typical MESFET structure and its operation are shown in Fig. 6.1. The source, gate and drain regions are prescribed with external biased voltages V_S, V_G and V_D, respectively. We assume that the source is grounded, i.e., $V_S = 0$. The main feature of the device is the formation of the so-called Schottky barrier (of the potential) at the interface of the gate by intimately contacting the metal to the semiconductor. To derive the mathematical model reflecting the formation of the barrier, it is sufficient to consider the thermal equilibrium state of the device.

6.2.1 Formation of Schottky Barrier

The commonly employed energy band diagrams can be used to describe the physical characteristics of the device. Fig. 6.2 illustrates the process of barrier formation near the

gate (along the y direction) in thermal equilibrium. To depict this process, we introduce a metal working function ϕ_m with $e\phi_m$ being defined as the amount of energy required to raise an electron from the Fermi level E_F to the vacuum level. Vacuum level is the energy level of an electron just outside the metal with zero kinetic energy. Similarly, we can introduce a semiconductor working function ϕ_s with $\phi_s < \phi_m$. The working functions describe material differences. For a semiconductor, since ϕ_s (actually the Fermi level E_F) varies with the doping, therefore another parameter χ_s, the electron affinity, is employed instead. By the electron affinity, $e\chi_s$ is defined as the energy difference of an electron between the vacuum level and the lower edge of the conductor band E_C. According to the Schottky model, the barrier results from the difference in working functions of the two materials. When metal and semiconductor get closer than a very short distance d (see energy diagram (a) in Fig. 6.2), an electric field, as shown in Fig. 6.3, exists in the region between the metal and semiconductor due to the higher energy of electrons in the semiconductor side. The electrons flow into the metal until the Fermi levels on the two sides are brought into coincidence. As the electrons move out of the semiconductor into the metal, the free electron density in the semiconductor region near the boundary decreases. Note that in thermal equilibrium the Fermi level remains constant. Since the separation between conductor band edge E_C and the Fermi level E_F increases with decreasing electron density, the conductor band E_C and valence band E_V are bent upward. Typical electron density and potential barrier profiles near the gate are calculated in Fig. 6.4.

Energy diagram (b) in Fig. 6.2 shows the case after the full contact is made and thermal equilibrium is reached. To measure how much the energy bands bend up, we define ϕ_B, a quantity called the barrier height function. It is clear that

$$\phi_B = \phi_m - \chi_s. \tag{6.1}$$

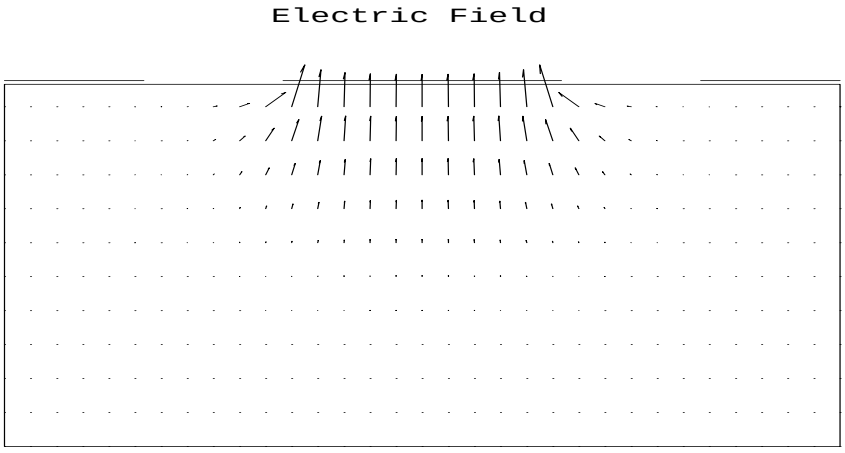

Figure 6.3: Electric field near the Schottky contact.

The region where the energy bands bend is called the depletion region since the electron density there is less than the doping density. W_d denotes the width of the region. From the thermionic-emission theory, only a very small leakage current exists in the gate region if a reverse bias voltage is applied to the gate (see [79, 66]). In this work, we are interested in the case where $\phi_B > 0$.

6.2.2 Mathematical Model

In thermal equilibrium, the external biased voltages are set to be zero ($V_G = 0$ and $V_D = 0$). In such a case, $J = 0$ and $T = T_0$. Then all the device models (2.1)-(2.5) in Chapter 2 reduce to the steady state as:

$$T_0 \nabla \rho + \tfrac{e\rho E}{m} = 0, \tag{6.2a}$$

$$\nabla(\lambda \cdot \nabla \psi) = \rho - \rho_D. \tag{6.2b}$$

Solutions of (6.2) are presented in Fig. 6.5 with $\phi_B = 0.8V$ and $\rho_D = 10^{17} cm^3$.

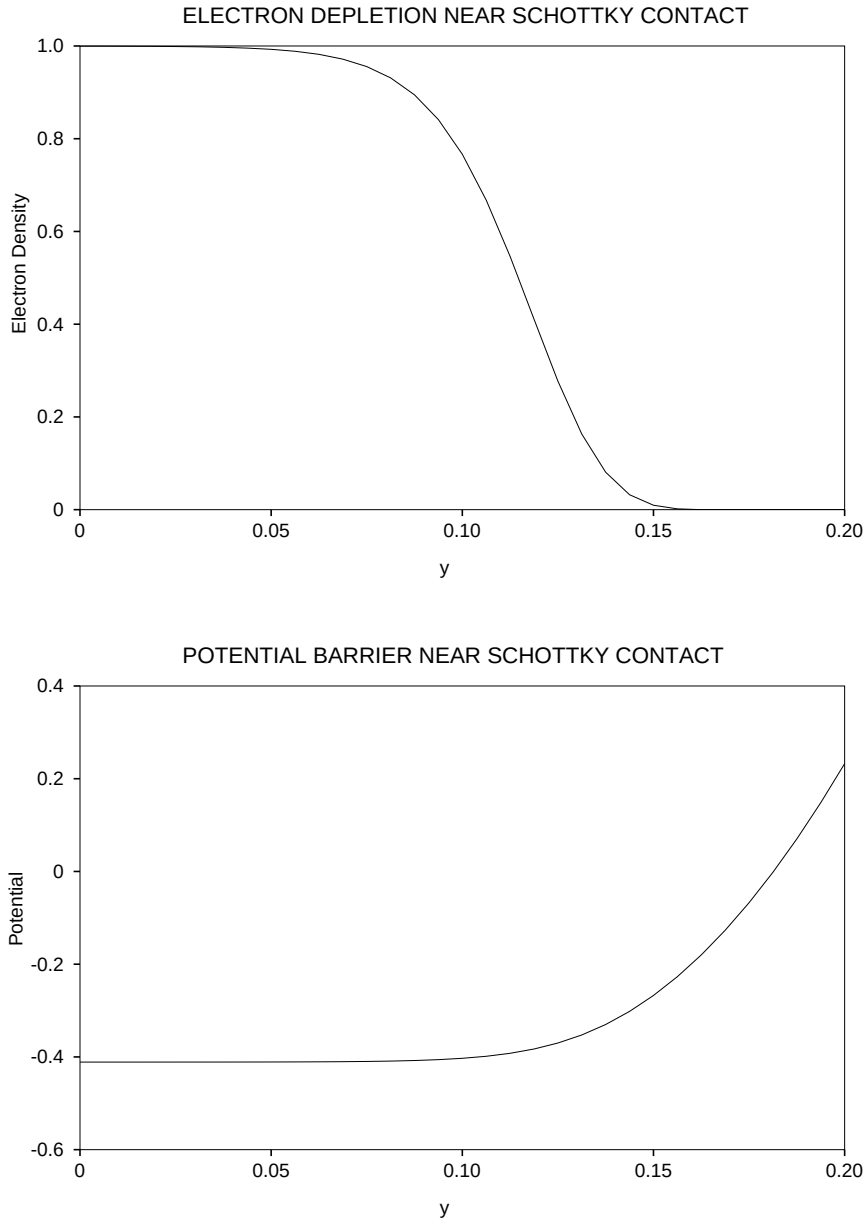

Figure 6.4: ρ and $-\psi$ with $\phi_B = 0.8V$ and $\rho_D = 10^{17} cm^3$. Schottky contact is at y=0.2.

Recall the quasi-Fermi level ϕ_n, which is a constant in the thermal equilibrium case. Integrating (6.2a) yields

$$\phi_n \triangleq -E_F/e = \psi - \frac{mT_0}{e} \ln \frac{\rho}{\rho_i}. \tag{6.3}$$

Equation (6.3) provides a potential-electron density relation

$$\psi = \frac{mT_0}{e} \ln \frac{\rho}{\rho_i}, \tag{6.4}$$

if we set $\phi_n = 0$ as a reference level.

For the Schottky contact, the electron density can be expressed by

$$\rho_0 = N_C \exp(-\frac{e}{mT_0}\phi_B), \tag{6.5}$$

defined as the surface electron density (see [72, 79]). N_C is termed the effective density of state in the conduction band, which has the typical value of $N_C = 4.07 \times 10^{19} cm^{-3}$ for silicon at room temperature. The above admits an alternative expression

$$\rho_0 = \rho_D \exp(-\frac{e}{mT_0}(\phi_B - \phi_0)), \tag{6.5$'$}$$

where $e\phi_0$ measures the energy difference between the conduction band edge and Fermi level, and

$$\phi_0 = \frac{mT_0}{e} \ln \frac{N_C}{\rho_D}. \tag{6.6}$$

Substituting ρ_0 in (6.4) by (6.5) or (6.5$'$), we obtain the built-in potential at the Schottky contact of the gate

$$\psi_{bi}^S = \frac{mT_0}{e} \ln \frac{N_C}{\rho_i}, \tag{6.7}$$

or

$$\psi_{bi}^S = \frac{mT_0}{e} \ln \frac{\rho_D}{\rho_i} - (\phi_B - \phi_0). \tag{6.7$'$}$$

In the source and drain, we have Ohmic contacts and $\rho = \rho_D$. Therefore

$$\psi_{bi}^O = \frac{mT_0}{e} \ln \frac{\rho_D}{\rho_i}. \tag{6.8}$$

Now the boundary conditions defined in Chapter 2 can be completed. ψ_{S0} in (2.37) is given by

$$\psi_{S0} = \phi_B - \phi_0. \tag{6.9}$$

In order that the semiconductor operates in the non-degenerated parameter domain (i.e., $E_C - E_F > 2mT_0$), we require

$$\rho_D < \exp(-2)N_C = 5.508 \times 10^{18}\text{cm}^{-3}. \tag{6.10}$$

Remark 6.1 *The boundary conditions we employed here are slightly different from those given in [51] and [13], where all variables are required to satisfy Neumann conditions on* Γ_2. *Those conditions are obviously over-determined and may cause formation of artificial boundary layers.* □

6.3 Discretizations for DD Models

It is convenient to express the DD models (2.4) and (2.5) in the uniform form

$$\mathcal{L}U \triangleq U_t + A \cdot \nabla U + C(U) - \nabla \cdot (\mathcal{K} \nabla U) = 0 \tag{6.11}$$

as equation (2.6) for the HD models, where $U = (\rho, J)^t$ for the DD2 model and $U = \rho$ for the DD1 model. For two-dimensional problems for example, $A = (A_1, A_2)^t$, $C(U)$ and $\mathcal{K}$ are given by,

for DD2 Model:

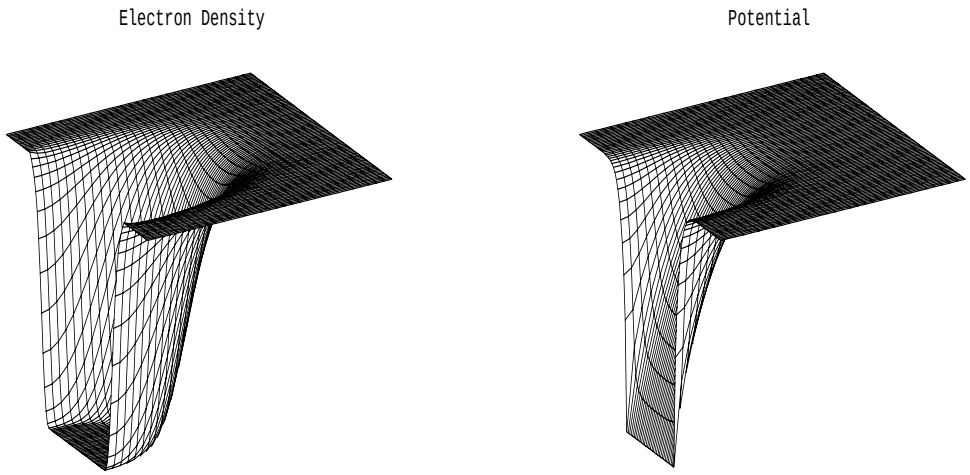

Figure 6.5: Electron density (left) and potential (right) with $\phi_B = 0.8V$ and $\rho_D = 10^{17} cm^3$ in thermal equilibrium.

$$A_1 = \begin{pmatrix} 0 & 1 & 0 \\ T_0 & 0 & 0 \\ 0 & 0 & 0 \end{pmatrix}, \qquad A_2 = \begin{pmatrix} 0 & 0 & 1 \\ 0 & 0 & 0 \\ T_0 & 0 & 0 \end{pmatrix},$$

$$C = \begin{pmatrix} 0 \\ \frac{e}{m}\rho E_1 + \frac{J_1}{\tau_J} \\ \frac{e}{m}\rho E_2 + \frac{J_2}{\tau_J} \end{pmatrix},$$

and $\mathcal{K} = 0$;

for DD1 model:

$A_1 = -\mu_0 \rho E_1$, $A_2 = -\mu_0 \rho E_2$, $C = -\mu_0 \rho \nabla \cdot E$ and $\mathcal{K} = D_0 I_2$.

6.3.1 The SD Method for DD Models

As in Section 5.2.1 for the HD models, we use the the following finite element subspace for the DD models

$$\mathcal{T}_g^h = \{V^h \mid V^h \in (C^0(Q_n))^l,\, V^h \mid_{Q_n^e} \in (P_1(Q_n^e))^l,\, \mathcal{D}V^h \mid_{\Gamma_1 \times I_n(T)} = g\}, \tag{6.12}$$

where $l = d + 1$ for the DD2 model and $l = 1$ for the DD1 model. Here g stands for essential boundary conditions given by (2.34) and (2.36) for the DD1 model, and in addition (2.31) for the DD2 model.

The DD models can be solved using the same scheme as (5.4) except that we drop the (SC) and (Weak In-Flow) terms, which reads

$$\begin{aligned} &\int_{Q_n} (U_t^h + A \cdot \nabla U^h + C(U^h)) \cdot \Psi + \mathcal{K} \nabla U^h \cdot \nabla \Psi \, dxdt && \text{(Galerkin)} \\ &\quad + \int_\Omega [\![U^h(t_n)]\!] \cdot \Psi(t_n^+) \, dx && \text{(Jump Condition)} \\ &\quad + \sum_{e=1}^{n_{el}} \int_{Q_n^e} \mathcal{L} U^h \cdot P^h(\Psi) \, dxdt = 0. && \text{(SD)} \end{aligned} \tag{6.13}$$

6.3.2 A SD Method for the Steady State DD1 Model

In the case when ρ^h is taken to be a piecewise linear polynomial approximation to ρ, the steady state SD scheme for the scalar DD1 model reduces to

$$\begin{aligned} &(\nabla \cdot (\mu_0 \rho^h E^h), \Psi) + (D_0 \nabla \rho^h, \nabla \Psi) && \text{(Galerkin)} \\ &\quad + (\nabla \cdot (\mu_0 \rho^h E^h), \tau \mu_0 E^h \cdot \nabla \Psi) = 0. && \text{(SD)} \end{aligned} \tag{6.14}$$

We see from the above that the streamline is along the direction of the electric field. Formulation (6.14) is similar to the multi-dimensional SD extension of Scharfetter-Gummel discretization by Sharma and Carey in [78], but the scaling parameter τ we use here is different from theirs. In [78] the numerical electric field E^h is assumed to be piecewise

constant, therefore the (SD) part in (6.14) can be simplified to

$$(\nabla \cdot (\mu_0 \rho^h E^h), \tau \mu_0 E^h \cdot \nabla \Psi) = (\mu_0 E^h \cdot \nabla \rho^h, \tau \mu_0 E^h \cdot \nabla \Psi). \tag{6.15}$$

However, we use a piecewise linear approach to E^h here.

6.3.3 SG Method for the 1-D Steady State DD1 Model

The steady state DD1 model in one space dimension

$$\frac{dJ}{dx} = 0 \tag{6.16}$$

yields a constant current J on the whole space domain Ω, where

$$J = \mu_0 \rho \frac{d\psi}{dx} - D_0 \frac{d\rho}{dx}. \tag{6.17}$$

Employing a uniform partition of Ω with grid points $x_j = x_0 + jh$ $(j = 1, \ldots, N)$, we discretize (6.16) and (6.17) by assuming that within each interval (x_j, x_{j+1}), the potential ψ is linear and the electric field $E = -d\psi/dx$ is constant. Integrating (6.17) on jth interval to obtain ρ explicitly as

$$\rho(x) = \rho_j \exp(\frac{\mu_0}{D_0}(\psi - \psi_j)) - \frac{J}{\mu_0 E_{i+1/2}} [1 - \exp(\frac{\mu_0}{D_0}(\psi - \psi_j))], \tag{6.18}$$

where ρ_j and ψ_j are approximate solutions at x_j, and $E_{1+1/2} = (\psi_{j+1} - \psi_j)/h$. Setting $\rho(x_{j+1}) = \rho_{j+1}$ on jth interval, (6.18) implies

$$J = -D_0 \frac{2\beta_{j+1/2}}{h} [\frac{\rho_{j+1} \exp(\beta_{j+1/2}) - \rho_j \exp(-\beta_{j+1/2})}{\exp(\beta_{j+1/2}) - \exp(-\beta_{j+1/2})}], \tag{6.19}$$

where $\beta_{j+1/2} = |\alpha_{j+1/2}|$ and $\alpha_{j+1/2}$ is the cell (element) Peclet number defined by (3.8). With the DD1 model in this case,

$$\alpha_{j+1/2} = \frac{\mu_0}{2D_0} h E_{j+1/2}. \tag{6.20}$$

Using (6.19) on jth and $(j+1)$st intervals, the constant J yields the SG discretization

$$\rho_{j+1}[\beta_{j+1/2}(\coth(\beta_{j+1/2})+1)] - \rho_j[\beta_{j+1/2}(\coth(\beta_{j+1/2})-1)$$
$$\beta_{j-1/2}(\coth(\beta_{j+1/2})+1)] + \rho_{j-1}[\beta_{j-1/2}[\coth(\beta_{j-1/2})-1)] = 0. \tag{6.21}$$

The above procedure is also known as an exponential fitting.

As for the one-dimensional SD method (6.14), the scaling parameter τ that follows (3.11) is

$$\tau = \frac{h}{2\mu_0 E_{j+1/2}}\,[\coth(\alpha_{j+1/2}) - \alpha_{j+1/2}^{-1}] \tag{6.22}$$

on the jth interval. We note that

$$\alpha_{j+1/2}[\coth(\alpha_{j+1/2}) - \alpha_{j+1/2}^{-1}] = \beta_{j+1/2}[\coth(\beta_{j+1/2}) - \beta_{j+1/2}^{-1}]. \tag{6.23}$$

Therefore, the (SD) term in (6.14) can be written as

$$(\mu_0 E^h \cdot \nabla\rho^h, \tau\mu_0 E^h \cdot \nabla\Psi) = (D_s \nabla\rho^h, \nabla\Psi) \tag{6.24}$$

with artificial diffusivity D_s given by

$$D_s = D_0\beta_{j+1/2}[\coth(\beta_{j+1/2}) - \beta_{j+1/2}^{-1}], \tag{6.25}$$

if we use a piecewise linear ψ^h and a piecewise constant E^h. Following the arguments in [78], it is not difficult to show that (6.21) can be recovered by (6.14) with the streamline diffusion (6.24). Therefore the SD methods are reasonable extensions of the SG method in the context of numerical solutions for semiconductor devices.

6.4 Numerical Simulations

We simulate two-dimensional silicon MESFET devices at room temperature $T_0 = 300K$ by using the HD, SHD, DD2 and DD1 semiconductor device models given in Chapter 2.

The HD and SHD models are solved by the shock-capturing SD method (5.4), but the finite element subspace $\mathcal{T}_g^h$ defined in (5.2) is changed to one with the function g representing essential boundary conditions (2.30)-(2.31), (2.34) and (2.36) corresponding to the MESFET. The DD2 and DD1 models are solved by the SD method (6.13). The finite element subspaces we use are the constant-in-time, linear-in-space types.

Numerical simulations are carried out on a device domain $\Omega = [0, 0.6\mu m] \times [0, 0.2\mu m]$. The source, gate and drain regions are given by segments of $[0, 0.1] \times \{y = 0.2\}$, $[0.2, 0.4] \times \{y = 0.2\}$ and $[0.5, 0.6] \times \{y = 0.2\}$, respectively.

The problem that we are interested in is the one with the gate in the state of reversed bias (i.e., $\phi_B > 0$). In such a case, a large depletion region occurs near the gate, such that the carrier movement in this region is negligible due to the formation of the potential barrier. Therefore electrons can flow from the source to drain only through a channel underneath the gate, if an external biased voltage is applied to the drain (see Fig. 6.1 for the depiction of the device operation). Unless otherwise specified, the potential barrier height function is $\phi_B = 0.8V$ and a biased voltage $V_D = 2V$ is applied to the drain in the following computations. Initial values are solutions of thermal equilibrium cases.

6.4.1 Example 1

The doping profile ρ_D is given by (see Fig. 6.6): $\rho_D = 3 \times 10^{17} cm^{-3}$ in $[0, 0.1] \times [0.15, 0.2]$ and in $[0.5, 0.6] \times [0.15, 0.2]$, and $\rho_D = 1 \times 10^{17} cm^{-3}$ elsewhere, with abrupt junctions. This was used in [51, 13]

Comparisons of numerical solutions of different models are made in this example. Steady state solutions are obtained by letting the solutions evolve in time.

A uniform grid of 96 $\times$ 32 points is used first. The time step Δt=1.D-3. Results with this grid are shown in Fig. 6.8 to Fig. 6.13. The surface electron density is about $\rho_0 = 1.567 \times 10^6 cm^{-3}$ in this case. The surface plots of electron densities of the four models

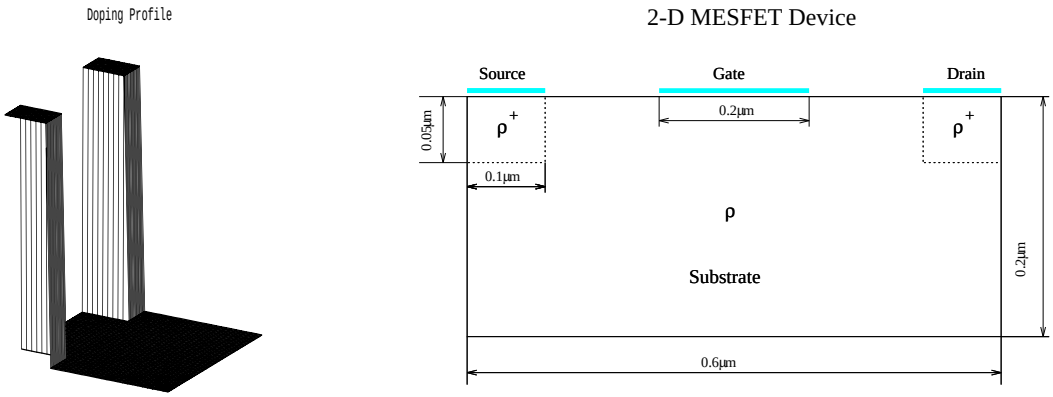

Figure 6.6: Doping and 2-D geometry of the device for example 1.

are shown in Fig. 6.8. We find that solutions of HD models are different from those of DD models. The HD and SHD models have boundary layers for ρ near the drain, whereas the DD2 and DD1 models do not exhibit such layers. This is a noticeable phenomenon of the hot electron effect in the hydrodynamic models. Mathematical analysis of the possible formation of a boundary layer near the outlet boundary of the device for the HD model was given by Gamba (see [24, 25]). Also, there are valleys in the solutions of the HD models, which stretch from the gate region through the substrate.

The electron current is an important component in device simulation. In Fig. 6.9, we present the current flows of models DD2, SHD and HD. It clearly shows the flow of electrons from the source to the drain. In our simulation, the leakage current of electrons is correctly reflected (from the semiconductor towards the gate, which is shown by the plot of the velocity component in y direction in Fig. 6.10), although it is very small. This is noticeably different from that of [13]. The width of the depletion region is about $W_d = 0.1\mu m$. We have observed that W_d for the HD models is smaller than that for the DD models. We detect an error in the current around the junction near the source, but not near the drain. This might be caused by numerical dissipation, which is mainly

manipulated by the shock-capturing term. Since the current is very sensitive, it is easily polluted by any perturbation. The parameter $\delta = 1$ is used in the example. We also experimented with different values of the parameter δ. When δ decreases, we get a better current approximation. In order to control the possible oscillation of solutions and achieve stability of the numerical computation, we pay the small price of slightly losing accuracy in the sharp change regions. However, the approximated electron current obtained does not exhibit non-physical behavior, i.e., there is no recirculation of the electron flow (cf. [13]).

We provide temperature profiles for the HD and SHD models in Fig. 6.11 and potentials for the HD and DD1 models in Fig. 6.12. There is a bigger cusp in the temperature of the SHD model around the point $x = 0.2, y = 0.2$ than in the HD model.

In Fig. 6.13, we show solutions of the HD model when $\phi_B - \phi_0 = 0.8V$. Correspondingly, the surface electron density is about $\rho_0 = 1.81 \times 10^4 cm^{-3}$. The solutions do not seem to have big differences to those in the $\phi_B = 0.8V$ case.

We make the following observations: (i) The solutions for the HD model and SHD model are close except for the temperatures. In the device simulation literature, engineers often prefer to use the SHD model, because it approximates the full HD model very well in many realistic situations and takes into account most important physical phenomena missing in the DD model. Such is the case in the simulation reported here. (ii) The SD method (6.13) for the DD1 model with τ defined in Chapter 3 (l=1), is optimal according to [42]. Comparisons were made by Sharma and Carey [78] for a diode and a MOSFET. Their evidence shows that the SD method causes less smearing than other SG extensions. The SD method for the DD2 model is reasonable although perhaps not optimal unless the system can be decoupled. The numerical experiments show that the results obtained for the DD2 model are no worse than those for the DD1 model. In Fig. 6.14, cross-sectional electron densities at y=1.75μm of DD1 vs DD2 models and HD vs SHD models are given

for the purpose of comparison.

A finer mesh of 192×64 points is used next. The time step Δt =5.D-4 and parameter $\delta = 1.5$ for this grid. The steady state electron density and current flow of the HD model are given in Fig. 6.15. The electron current is slightly improved after the refinement, while the improvement of the electron density is almost invisible.

6.4.2 Example 2

The doping profile ρ_D is given by (see Fig. 6.7): $\rho_D = 3\times 10^{17} cm^{-3}$ in $(x-0.2)^2+y^2 \leq 0.1^2$ and in $(x-0.2)^2 + (y-0.6)^2 \leq 0.1^2$, and $\rho_D = 1 \times 10^{17} cm^{-3}$ elsewhere. Now abrupt junctions are not aligned with mesh lines.

Uniform grids of 96×32 and of 192×64 are used again for this example. Simulated results for the steady state solutions of the HD model are shown in Fig. 6.16 and Fig. 6.17. The numerical solutions behave qualitatively very well near the junctions. In fact, the SD method is so designed that it deals with this situation effectively. We notice in this case that the boundary layer near the drain for the electron density is very mild, in contrast to that in example 1. This suggests that the formation of the boundary layers depends strongly on the geometric setting of the device. A similar phenomenon was simulated and analyzed using a 1-D current driven problem by Ascher *et al.* in [2].

Evolutions of the solutions are shown in Figs. 6.18- 6.21 using the 96 grid. We increase the biased voltage from $V_D = 0$ in the thermal equilibrium state, to $V_D = 2V$ within 0.1ps and then stay at this value for the rest of the time. It is found that solutions behave wildly in a short time interval right after t=0.1ps. We use $\delta = 1.5$ during this time interval in order to enhance the stability. We reduce it to 1 when the solutions are close to the steady state. The boundary layer of the electron density and the strength of the current density at the outlet become milder when the steady state is reached.

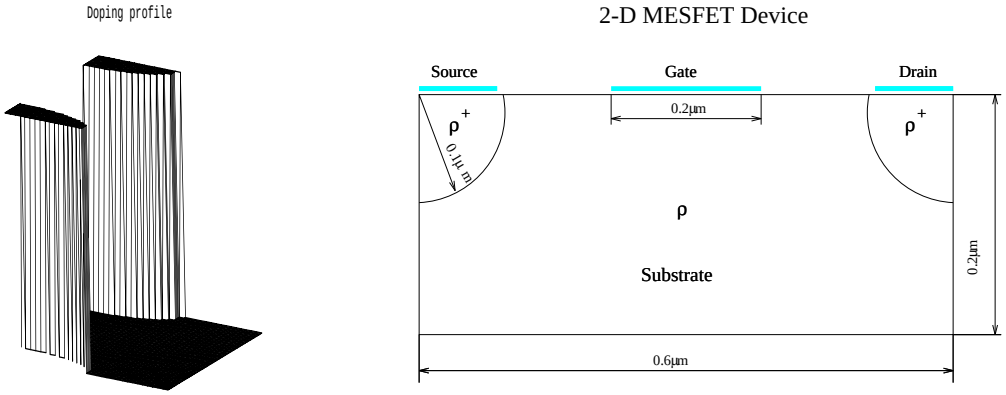

Figure 6.7: Doping and 2-D geometry of the device for example 2.

6.5 Comments and Conclusions

We have applied the SD method to 2-D MESFET devices by using the HD and DD models. The method extends the well-known SG formulation. The performance of the presented numerical schemes is very satisfactory and the computational results meet physical expectations well.

Comparisons of different models are made in the numerical simulations. They indicate that the results of the HD and DD models are qualitatively different. However, the results of the SHD and full HD models are relatively close in this simulation, especially for the electron density and current.

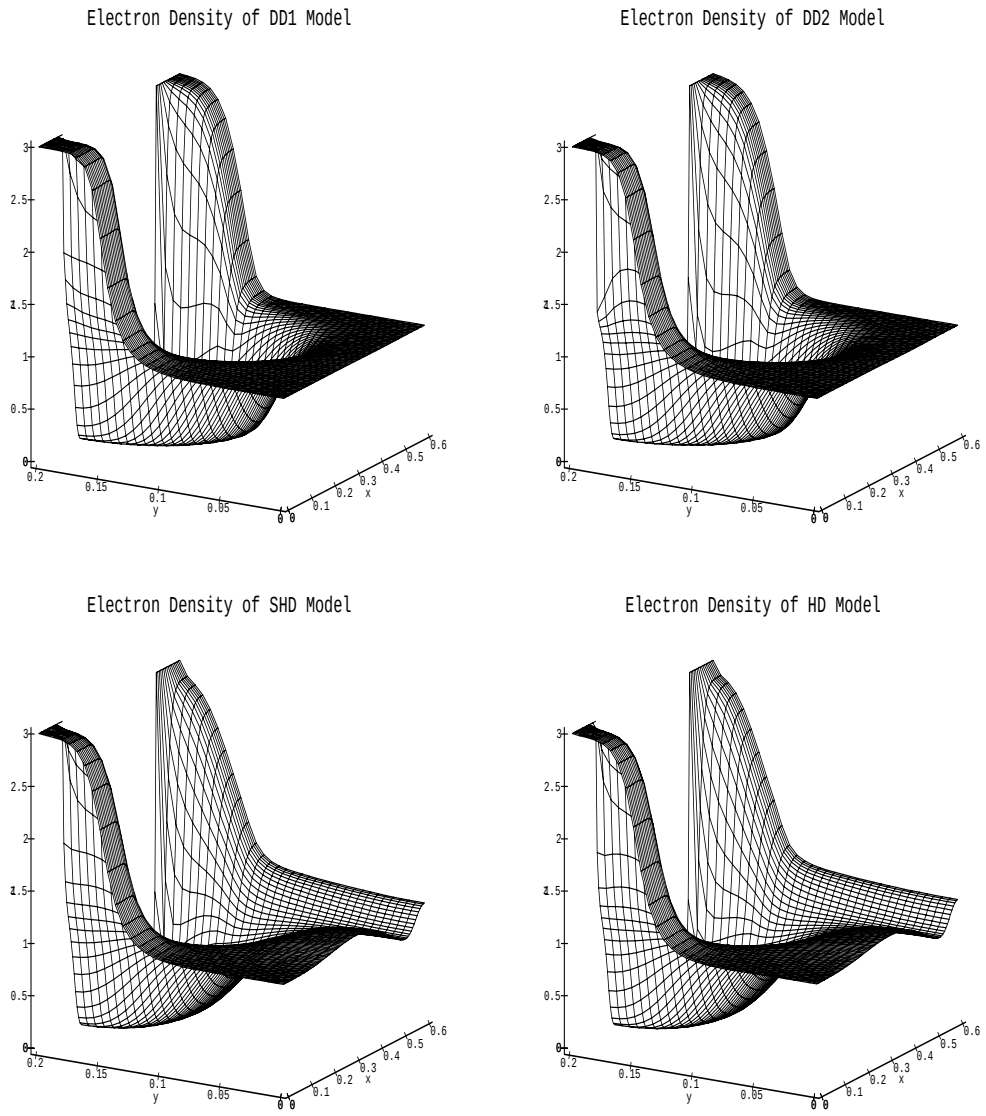

Figure 6.8: Electron densities in $10^{17} cm^{-3}$ for example 1.

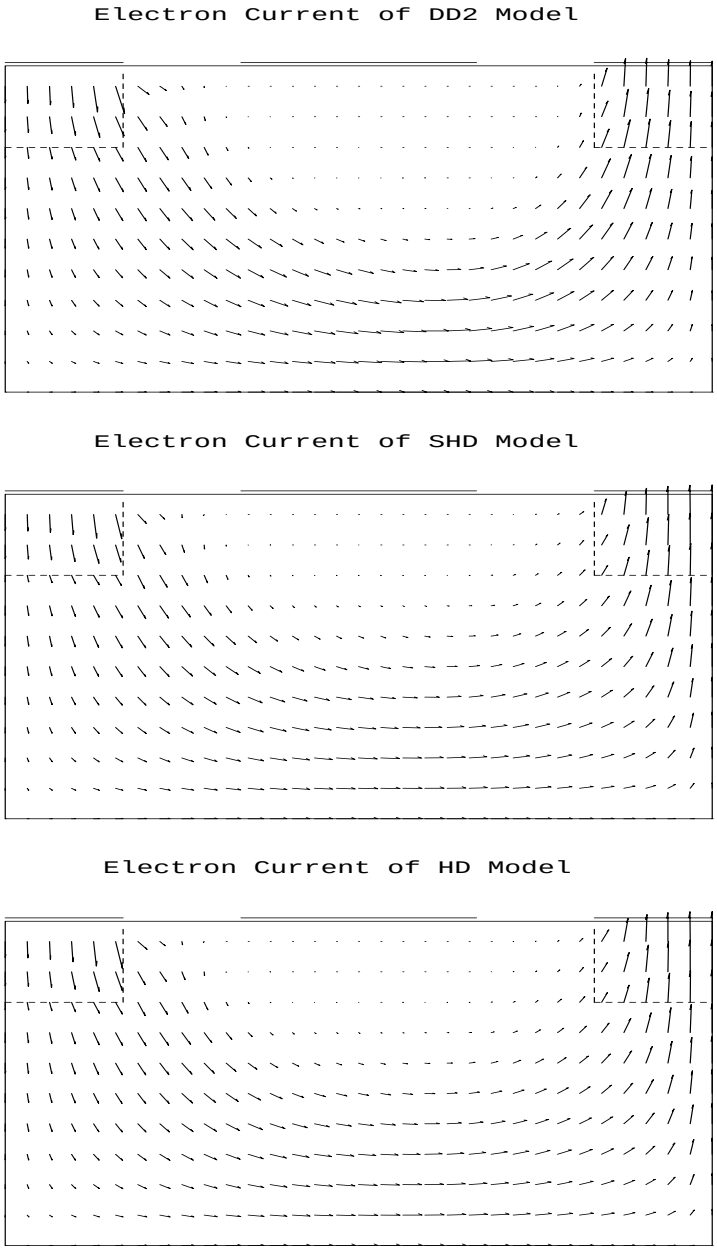

Figure 6.9: Electron currents for example 1.

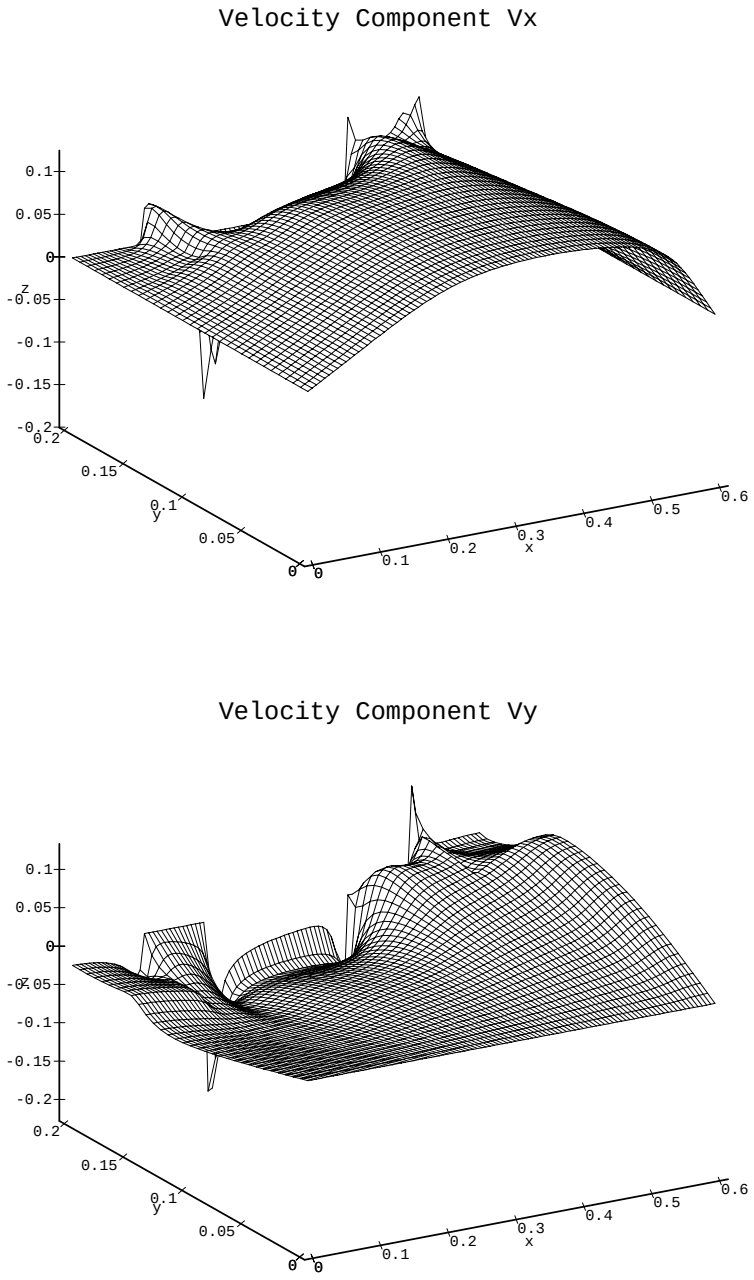

Figure 6.10: Mean velocity components for example 1.

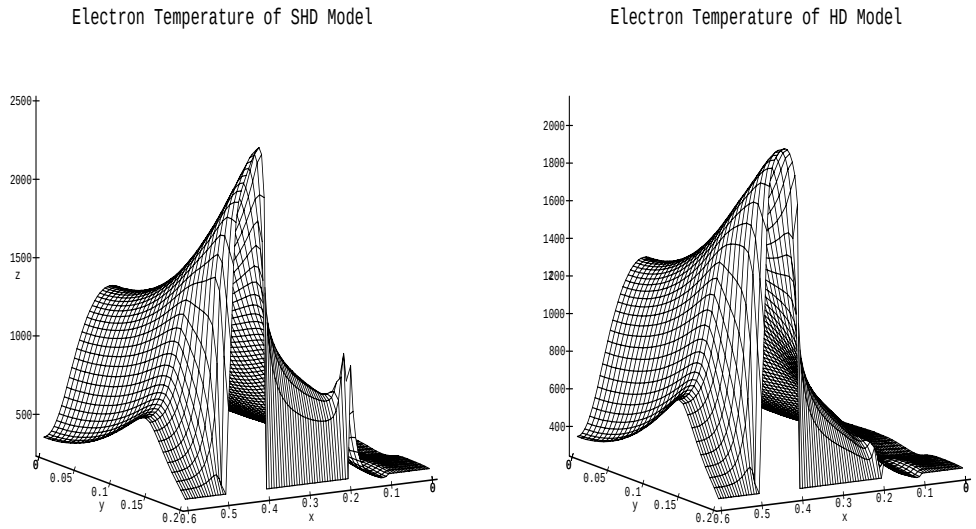

Figure 6.11: Electron temperature in Kelvin for example 1.

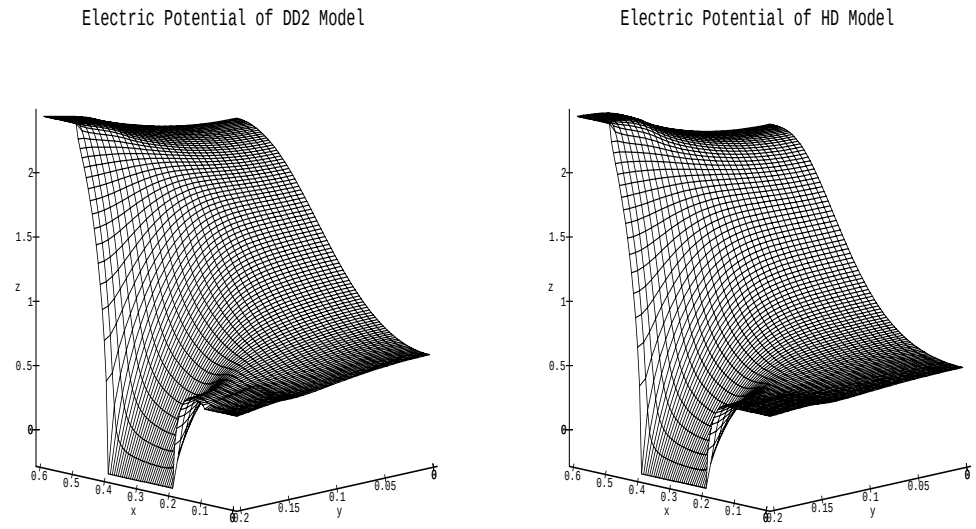

Figure 6.12: Electric Potential for example 1.

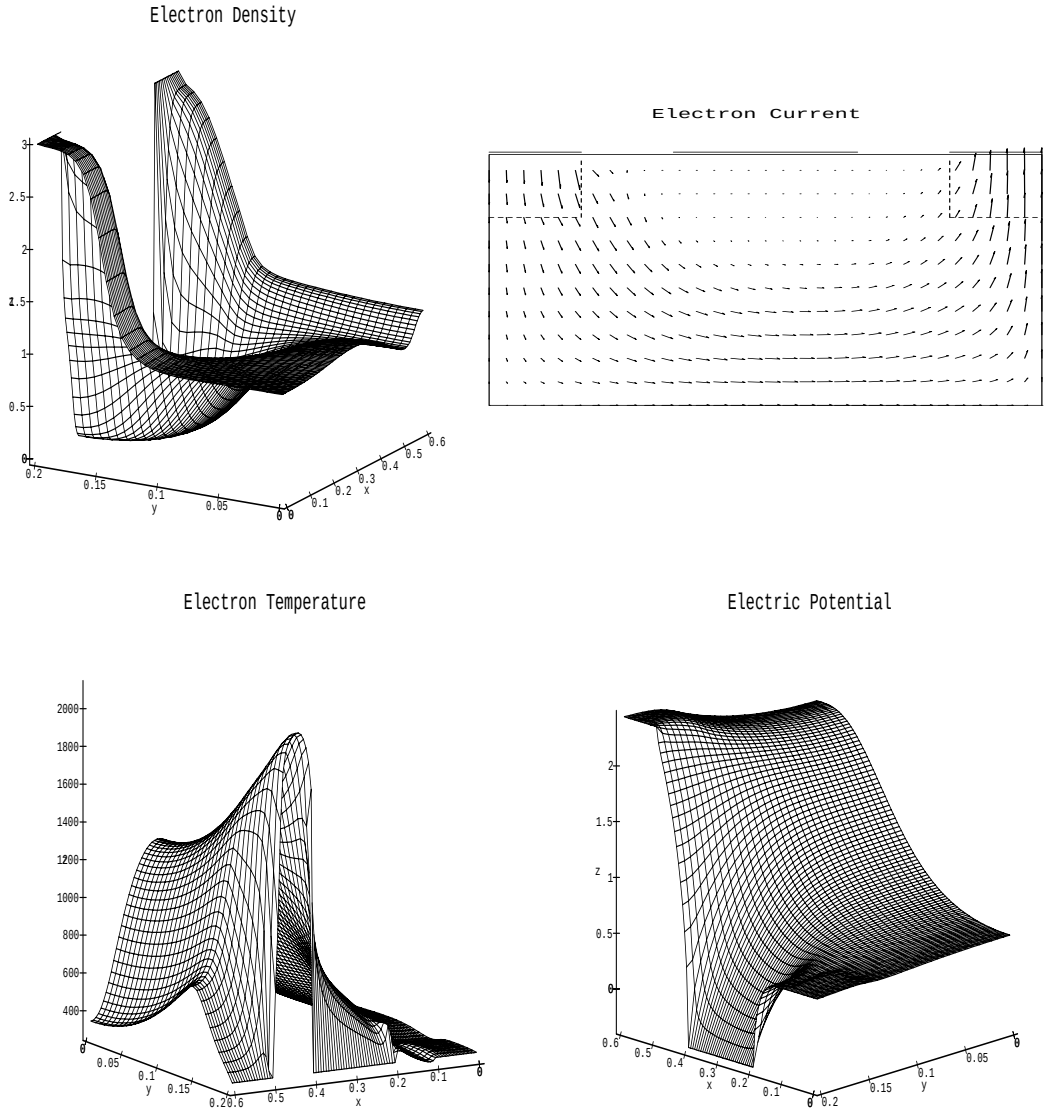

Figure 6.13: Solutions for $\phi_B - \phi_0 = 0.8V$.

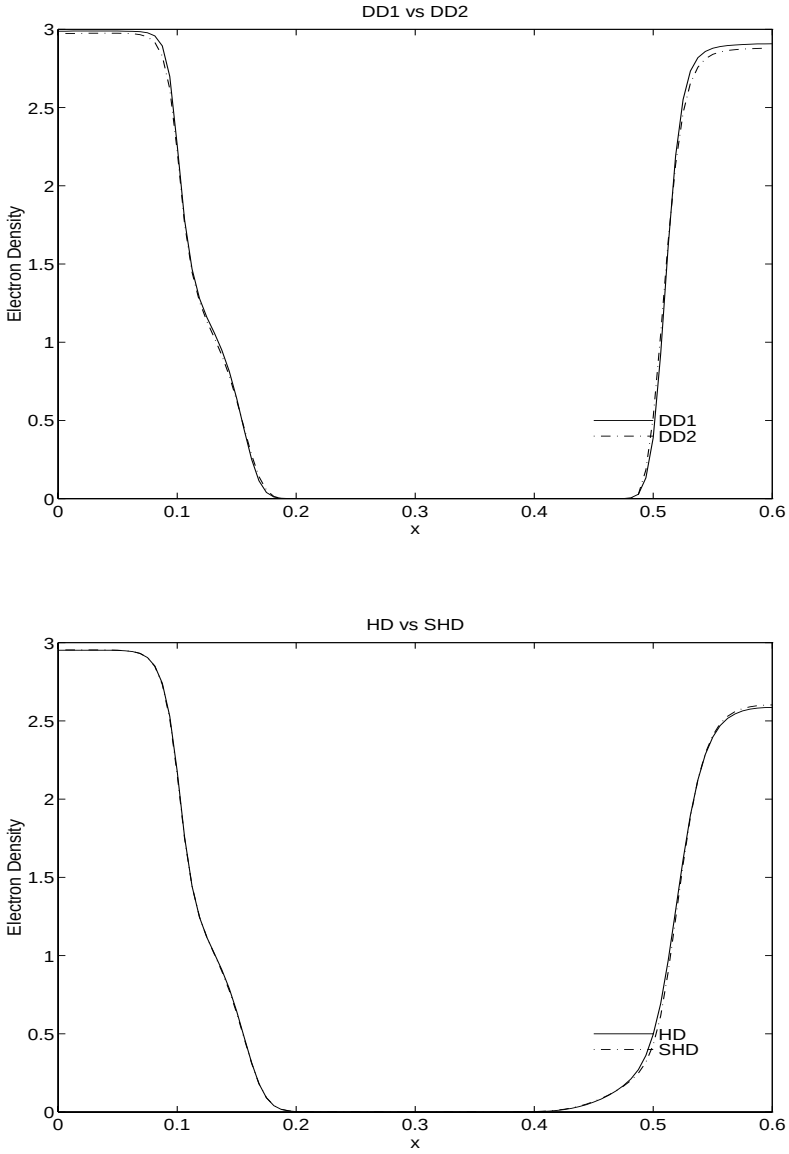

Figure 6.14: Comparison of electron densities at $y = 0.175\mu m$ for example 1.

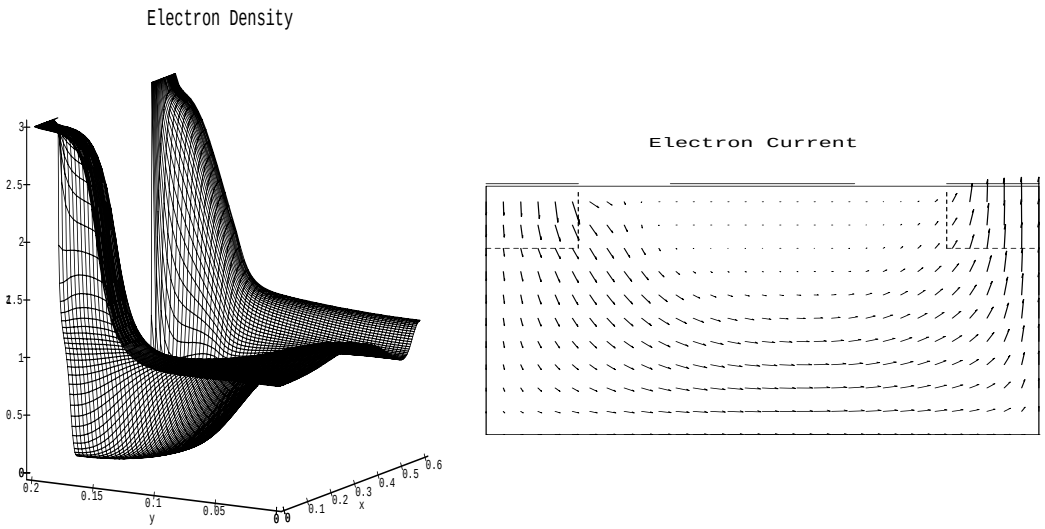

Figure 6.15: Electron density and current with the finer mesh for example 1.

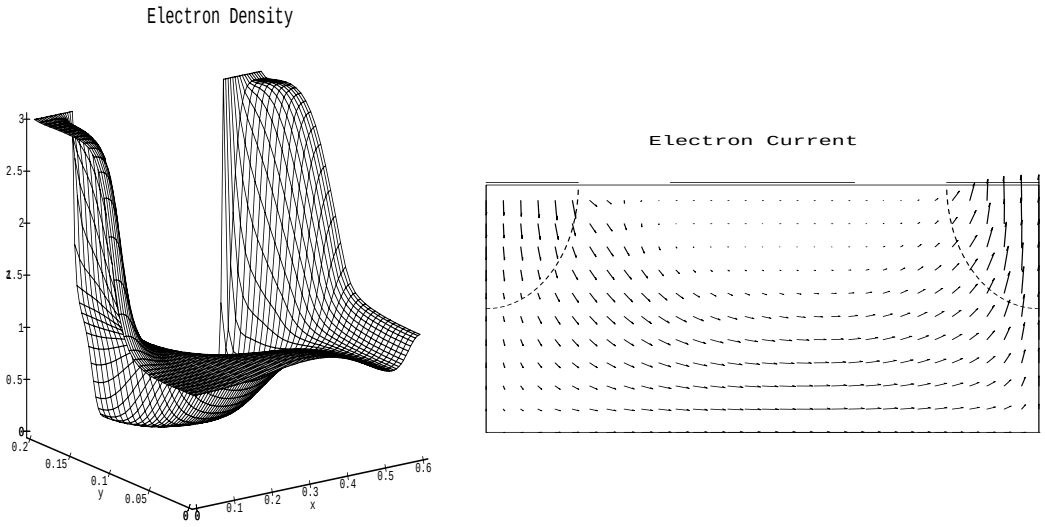

Figure 6.16: Electron density and current for example 2: a grid of 96×32 points.

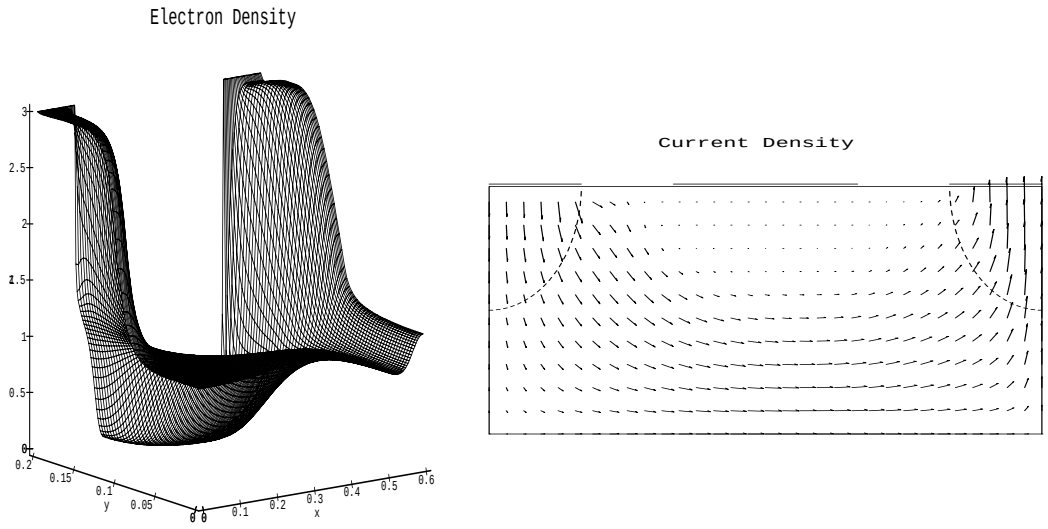

Figure 6.17: Electron density and current for example 2: a grid of 192×64 points.

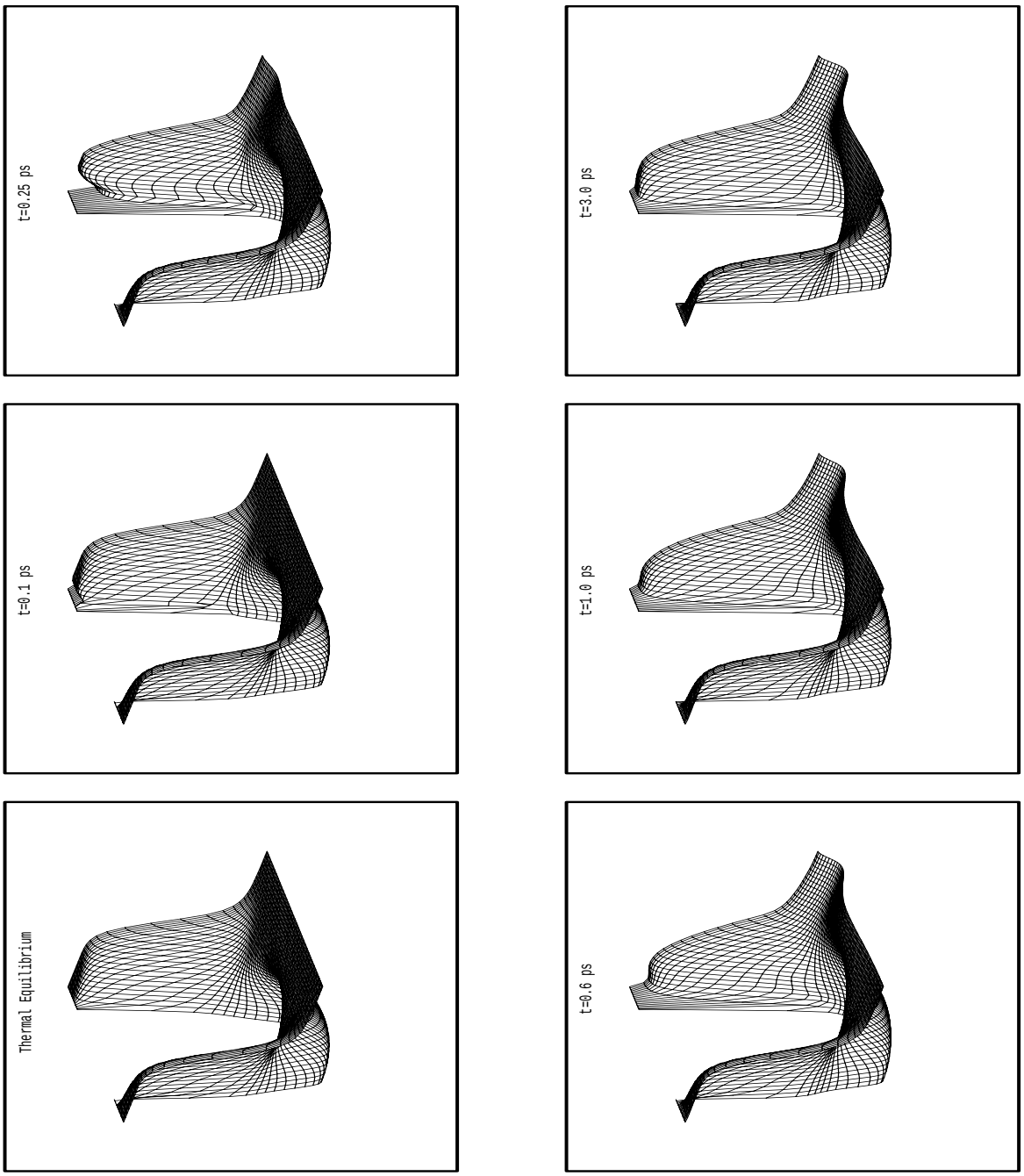

Figure 6.18: Evolution of the electron density for example 2.

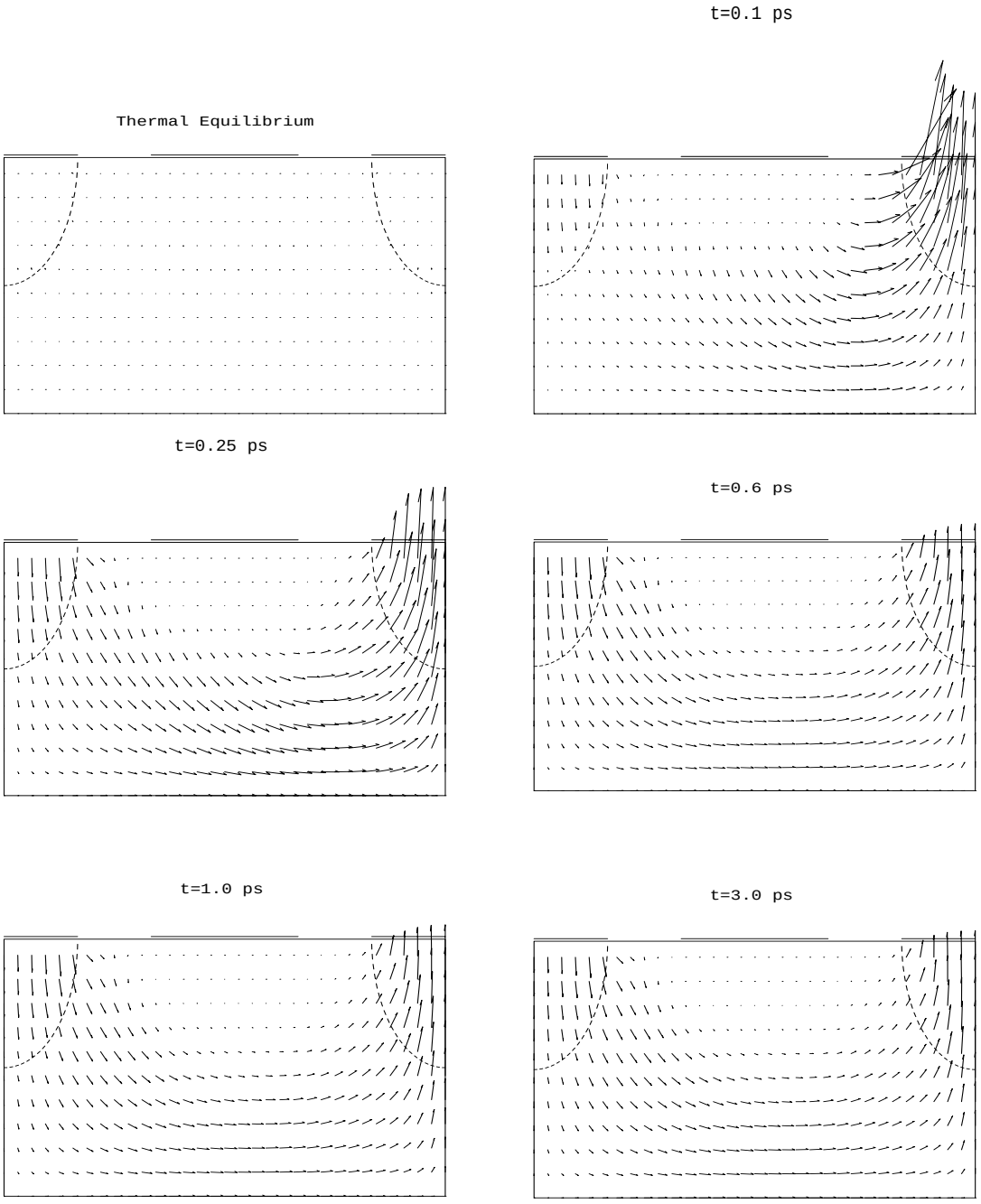

Figure 6.19: Evolution of the electron current for example 2.

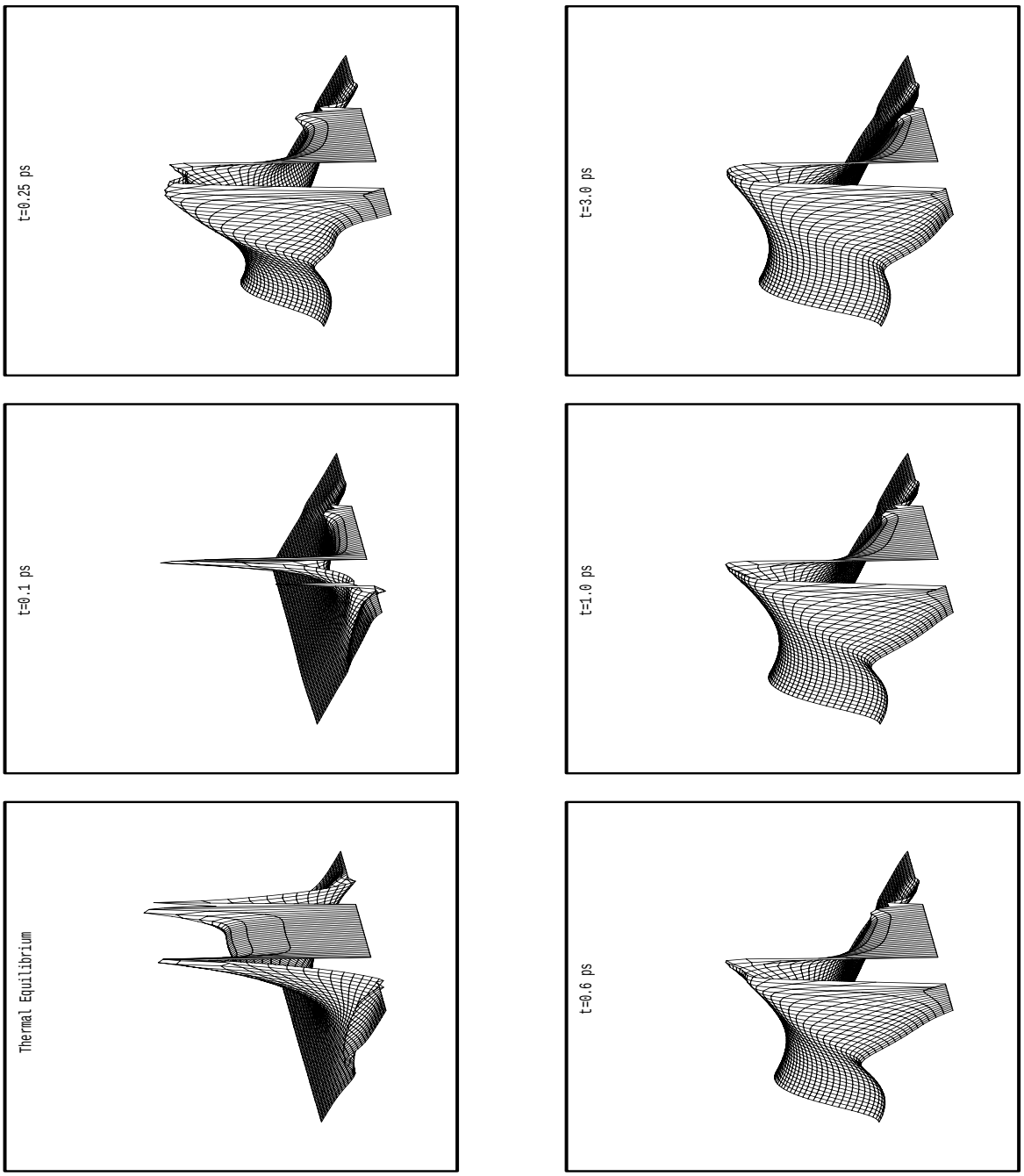

Figure 6.20: Evolution of the electron temperature for example 2.

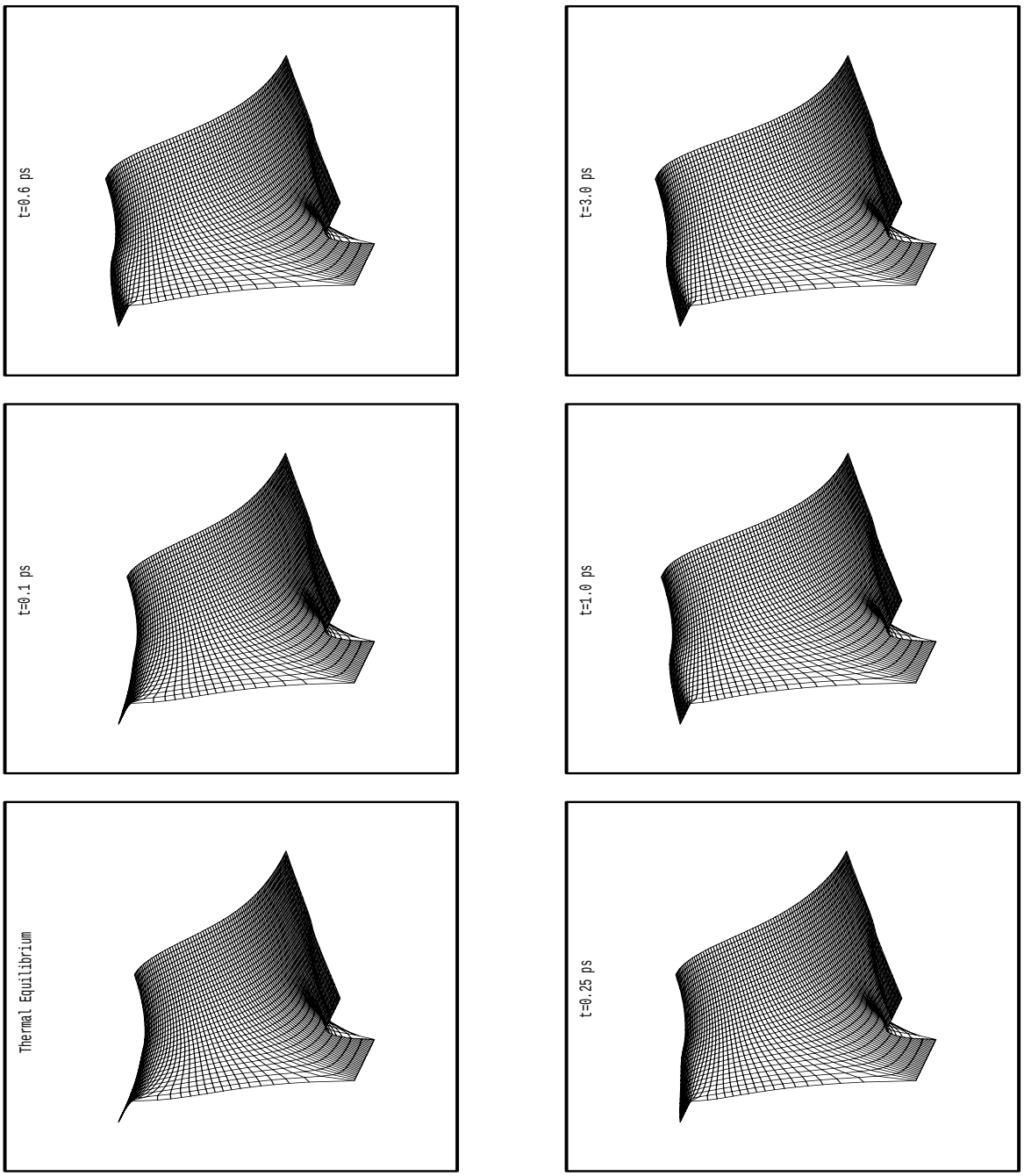

Figure 6.21: Evolution of the potential for example 2.

Chapter 7

Conclusion

7.1 Summary

Theoretical and practical aspects of the design and implementation of the streamline-diffusion (SD) finite element methods to the solutions of the semiconductor device models have been explored systematically in this thesis. The two major device models, i.e., the fundamental drift-diffusion (DD) model and the hydrodynamic (HD) model, which are widely used today, were considered. Emphasis, however, was placed on the HD model, which is computationally more challenging in the context of device simulations than the traditional DD model, but provides some important physical information missing in the DD model [68, 57, 76].

Under certain assumptions, the simplified HD (SHD) model, the mixed-formulation DD (DD2) model and the conventional DD (DD1) model have been deduced hierarchically from the full HD model with gradually reduced orders of complexity. These models were solved by our non-symmetric SD method in a uniform framework.

The non-symmetric SD method for the convection-diffusion systems was designed to avoid the extra complexity of symmetric formulations of the systems involved. We derived a non-trivial SD operator for the non-symmetric system. The designing work includes two concerns: one is to follow the correct directions of the streamlines and another is to provide suitable scaling. The proper choice of the operator is important - a careless choice of it leads to serious problems, as was shown in this work. With

an exploration of useful properties of the semiconductor device models, we derived the SD operator for these models. Linear stability analysis was carried out for the model problem. We have shown that our proposed numerical scheme is stable if the system can be symmetrized. Stability arguments and numerical experiments presented suggest that the method of lines with SD semi-discretization schemes may not be appropriate for transient problems. Such combinations were used previously by some researchers.

The SD method developed was applied to the models of semiconductor device transport equations. From the mathematical point of view, an "in-flow" boundary condition is needed for the HD model unlike the other models [80]. The weak treatment of this extra "in-flow" boundary condition was incorporated in the SD formulation for the HD model. This practical consideration alleviates the possible discrepancy introduced by the intuitive artificial boundary condition and enhances the stability of the numerical scheme.

Pertaining to Poisson equation for the potential, an efficient method consistent with the SD method is desired. It should provide an accurate electric field, i.e., an accurate derivative of the potential as well. For the HD model, for example, not much attention was previously paid in the method design regarding the consistency of schemes for the conservation laws and the potential equation. We proposed a consistent Poisson solver which provides a higher order convergence rate for the electric field. The order of accuracy of the electric field is the same as that of solutions for the system of conservation laws when employing finite element subspaces with the same degree of polynomials. Different from the commonly used mixed method that uses a staggered grid, this Poisson solver uses the same grid points for the potential and electric field, which are also used by the SD scheme for the system. Therefore the device simulation algorithm can be more easily coded.

The new Poisson solver absorbs the idea of the augmented and least-squares methods

[10, 52, 53], but it is superior to them. Its decoupled nature saves computation time as compared with the mixed method, the augmented method and the usual least-squares method. Error estimation was presented. The convergence result for such a method is better than the usual least-squares method [63] and the augmented method.

The ρ^+-ρ-ρ^+ diode and the MESFET device were simulated by using our numerical methods. Shocks were captured for the ρ^+-ρ-ρ^+ diode in one and two space dimensions. For the two-dimensional MESFET device, electron depletion near the gate was simulated. The leakage current of electrons was correctly reflected, although it is very small and can be neglected. The method successfully handles the case where the abrupt junctions are not aligned with grid lines. Experiments show that the performance of the method is very satisfactory and the computational results confirm the physical expectations.

Model comparisons were implemented. The difference in solutions between the HD and DD models was significant in simulation of the MESFET device. However, the solution difference between the SHD and HD models was negligible in this simulation. In the engineering field, the SHD model and other simplifications of the HD model appearing in the literature (such as the so-called energy balance (EB) model [7, 8]) have often been viewed as good approximations of the full HD model and have been comfortably used in replacement of the full HD model in many applications. However, as was demonstrated in our numerical experiments, if a strong field is applied or shock waves develop in the HD model, the solutions of the SHD model will no longer approximate those of the HD model well.

Comparison of steady state numerical solutions between DD1 and DD2 models confirms that the performance of our non-symmetric extension of the SD operator for the convection-diffusion system is almost as good as that of the optimal one given in [42] for the scalar convection-diffusion equation. In the context of numerical device simulations, the latter is associated with the well-known Scharfetter-Gummel (SG) discretization.

Therefore, our SD formulations are reasonable extensions of the SG formulation for general convection-diffusion systems in multi-space dimensions.

7.2 Future Research Directions

Although the numerical method that we use in this thesis is robust in simulation for a wide parameter range, it is not entirely trouble-free as is reported in Chapters 5 and 6. From our numerical experience, as well as others' in the literature [22, 13], we found that the solution for the electron current, the important part in the simulation, is not completely satisfactory near sharp layers in comparison with other solution components. Numerical tests in the thesis indicate that the current error is sensitive to perturbations - including perturbations in the strength of the artificial diffusion introduced by the scheme in order to achieve numerical stability and to suppress oscillation at sharp layers. However, even though it is sensitive to perturbations, the approximate electron current obtained does not exhibit non-physical behavior, i.e., there was no recirculation of the electron flow (cf. [13]). It is thus of great interest to design a new approach to obtain a more reliable approximation for the electron current in sensitive regions.

As far as the device simulations are concerned, our further research activities will involve introducing quantum corrections in the HD model. Some work has been done recently by Gardner *et al* (see [27, 28, 14]). It seems also relevant to tunneling devices like the heterojunction bipolar transistor (HBT). The application of the new method in Chapter 4 to the DD model for devices is of interest too.

Bibliography

[1] U. Ascher, *On Numerical Differential Algebraic Problems with Application to Semiconductor Device Simulation.* SIAM Numer. Anal., **Vol. 50**, **No. 3**, pp.517-538, (1989).

[2] U. Ascher, P.A. Markowich, P. Pietra and C. Schmeiser, *A Phase Plane Analysis of Transonic Solutions for the Hydrodynamic Semiconductor Model.* Math. Models and Methods Appl. Sci., **Vol. 1**, **No. 3**, pp.347-376, (1991).

[3] U. Ascher, P.A. Markowich, C. Schmeiser, H. Steinrück and R. Weiss, *Conditioning of the Steady State Semiconductor Device Problem.* SIAM J. Appl. Math., **Vol. 49**, **No. 1**, pp.165-185, (1989).

[4] R.E. Bank, D.J. Rose and W. Fichtner, *Numerical Methods for Semiconductor Device Simulation.* IEEE Trans. El. Dev., **Vol. 30**, **No. 9**, pp.1031-1041, (1983).

[5] R.E. Bank, W. Fichtner, D.J. Rose and R.K. Smith, *Computational Aspects of Semiconductor Device Simulation.* Numer. Anal. Manuscript, **85-3**, AT & T Bel Lab., (1985).

[6] K. Blotekjær, *Transport Equations for Electron in Two-valley Semiconductors.* IEEE Trans. El. Dev., **Vol. ED-17**. pp.38-47, (1970).

[7] A. Benvenuti, W.M. Coughran, Jr., M.R. Pinto and N.L. Schryer, *Hierarchical PDE Simulation of Nonequilibrium Transport Effects in Semiconductor Devices.* NUPAD IV, pp.155-160, (1992).

[8] A. Benvenuti, M.R. Pinto, W.M. Coughran, Jr., N.L. Schryer, C.U. Naldi and G. Ghione, *Evaluation of the Influence of Convective Energy in HBTs Using a Fully Hydrodynamic Model.* International Electron Device Meeting, pp.499-502, (1991).

[9] G.J. Le Beau, S.E. Ray, S.K. Aliabali and T.E. Tezduyar, *SUPG Finite Element Computation of Compressible Flows with the Entropy and Conservation Variables Formulations.* Comput. Methods Appl. Mech. Engrg., **Vol. 104**, pp.397-422, (1993).

[10] F. Brezzi and M. Fortin, *Mixed and Hybrid Finite Element Methods.* Springer-Verlag, New York, Berlin, Heidelberg, London, Paris, Tokyo, Hong Kong and Barcelona, (1991).

[11] F. Brezzi, L. Marini and P. Pietra, *Two-Dimensional Exponential Fitting and Applications to Semiconductor Device Equations.* SIAM J. Numer. Anal., **Vol. 6**, **No. 6**, pp.1342-1355, (1989).

[12] E. Carmo and A. Galeão, *Feedback Petrov-galerkin Methods for Convection-Dominated Problems.* Comput. Methods Appl. Mech. Engrg., **Vol. 88**, pp.1-16, (1991).

[13] Z. Chen, B. Cockburn, J.W. Jerome and C.W. Shu, *Mixed-RKDG Finite Element Methods for the 2-D Hydrodynamic Model for Semiconductor Device Simulation.* J. Comput. Phys., to appear, (1995).

[14] Z. Chen, B. Cockburn, C.L. Gardner and J.W. Jerome, *Quantum Hydrodynamic Simulation of Hysteresis in the Resonant Tunneling Diode.*, IMA Preprint Series #1227, University of Minnesota, (1994).

[15] R. Codina, *A Discontinuity-Capturing Crosswind Dissipation for the Finite Element Solution of the Convection-Diffusion Equation.* Comput. Methods Appl. Mech. Engrg., **Vol. 110**, pp.325-342, (1993).

[16] F. Chalot, T.J. Hughes and F. Shakib, *Symmetrization of Conservation Laws with Entropy for High-temperature Hypersonic Computations.* Comput. Sys. Engrg., **Vol. 1**, **No. 2-4**, pp.495-521, (1990).

[17] R.K. Cook and J. Frey, *Two-Dimensional Numerical Simulation of Energy Transport Effects in Si and GaAs MESFET's.* IEEE Trans. El. Dev., **Vol. ED-29**, **No. 6**, pp.970-977, (1982).

[18] P.G. Ciarlet, *The Finite Element Method for Elliptic Problems.* North Holland, Amsterdam, (1978).

[19] P. Degond and P.A. Markowich, *On a One-Dimensional Steady State Hydrodynamic Model for Semiconductors.* Appl. Math. Lett., **Vol. 3**, **No. 3**, pp.25-29, (1990).

[20] E.P. Doolan, J.J.H. Miller and W.H.A. Schilders, *Uniform Numerical Methods for Problems with Initial and Boundary Layers.* Boole Press, Dublin, (1980).

[21] E. Fatemi, C.L. Gardner, J.W. Jerome, S. Osher and D.L. Rose, *Simulation of a Steady-State Electron Shock Wave in a Submicron Semiconductor Device Using High-Order Upwind Methods.* Computational Electronics: Semiconductor Transport and Device Simulation, pp.27-32, Boston, Kluwer Academic Publishers, (1991).

[22] E. Fatemi, J.W. Jerome and S Osher, *Solution of the Hydrodynamic Device Model Using High-Order Non-Oscillatory Shock Capturing Algorithms.* IEEE Trans. Comput.-Aided Design, **Vol. 10**, **No. 2**, pp.232-244, (1991).

[23] L.P. Franca and T.J. Hughes, *Two Classes of Mixed Finite Element Methods.* Comput. Methods Appl. Mech. Engrg., **Vol. 69**, pp.89-129, (1988).

[24] I.M. Gamba, *Stationary Transonic Solutions of a One-Dimensional Hydrodynamic Model for Semiconductors.* Technical Report **No. 143**, Department of Mathematics, Purdue University, (1990).

[25] I.M. Gamba, *Boundary Layer Formation for Viscosity Approximations in Transonic Flow.* Technical Report **No. 149**, Department of Mathematics, Purdue University, (1991).

[26] C.L. Gardner, *Numerical Simulation of a Steady State Electron Shock Wave in a Submicrometer Semiconductor Device.* IEEE Trans. El. Dev., **Vol. 38**, **No. 2**, pp.392-398, (1991).

[27] C.L. Gardner, *The Quantum Hydrodynamic Model for the Semiconductor Devices.* SIAM J. Appl. Math., **Vol. 54**, pp.409-427, (1994).

[28] C.L. Gardner, *Resonant Tunneling in the Quantum Hydrodynamic Model.* VLSI Design, to appear, (1995).

[29] C.L. Gardner, J.W. Jerome and D.J. Rose, *Numerical Methods for the Hydrodynamic Device Model: Subsonic Flow.* IEEE Trans. Comput.-Aided Design, **Vol. 8**, pp.501-507, (1989).

[30] A. Gnudi, F. Odeh and M. Rudan, *An Efficient Discretization Scheme for the Energy Continuity Equation in Semiconductors.* Proceeding of SISDP, pp.387-390, (1988).

[31] B. Gustafsson and A. Sundström, *Incompletely Parabolic Problems in Fluid Dynamics.* SIAM J. Appl. Math., **Vol. 35**, **No.2**, pp.343-357, (1978).

[32] J-M. Grygiel and P.A. Tanguy, *Finite Element Solution for Advection-Dominated Thermal Flows.* Comput. Methods Appl. Mech. Engrg., **Vol. 93**, pp.277-289, (1991).

[33] A. Harten, *On the Symmetric Form of Systems of Conservation Laws with Entropy.* J. Comput. Phys., **Vol. 49**, pp.151-164, (1983).

[34] T.J. Hughes and A. Brooks, *Multidimensional Upwind Scheme with No Crosswind Diffusion.* FEM for Conservation Dominated Flows, T.J. Hughes *et al* eds., AMD, **Vol. 34**, ASME, New York, pp.19-35, (1979).

[35] T.J. Hughes, L.P. Franca and G.M. Hulbert, *A New Finite Element Formulation for Computational Fluid Dynamics: VIII. The Galerkin/Least-squares Method for Advective-diffusive Equations.* Comput. Methods Appl. Mech. Engrg., **Vol. 73**, pp.173-189, (1989).

[36] T.J. Hughes, L.P. Franca and M. Balestra, *A New Finite Element Formulation for Computational Fluid Dynamics: V. Circumventing the Babuška-Brezzi Condition: A stable Petrov-Galerkin Formulation of the Stokes Problem According Equal-Order Interpolations.* Comput. Methods Appl. Mech. Engrg., **Vol. 59**, pp.85-99, (1987).

[37] T.J. Hughes and L.P. Franca, *A New Finite Element Formulation for Computational Fluid Dynamics: VII. The Stokes Problem with Various Well-posed Boundary Conditions: Symmetric Formulations that Converge for all Velocity Spaces.* Comput. Methods Appl. Mech. Engrg., **Vol. 65**, pp.85-96, (1987).

[38] T.J. Hughes, L.P. Franca and M. Mallet, *A New Finite Element Formulation for Computational Fluid Dynamics: I. Symmetric Forms of the Compressible Euler and Navier-Stokes Equations and the Second Law of Thermodynamics.* Comput. Methods Appl. Mech. Engrg., **Vol. 54**, pp.223-234, (1986).

[39] T.J. Hughes, L.P. Franca and M. Mallet, *A New Finite Element Formulation for Computational Fluid Dynamics: VI. Convergence Analysis of the Generalized SUPG Formulation for Linear-Dependent Multi-Dimensional Advective-Diffusive Systems.* Comput. Methods Appl. Mech. Engrg., **Vol. 63**, pp.97-112, (1987).

[40] T.J. Hughes and M. Mallet, *A New Finite Element Formulation for Computational Fluid Dynamics: III. The Generalized Streamline Operator for Multidimentional Advective-Diffusive Systems.* Comput. Methods Appl. Mech. Engrg., **Vol. 58**, pp.305-328, (1986).

[41] T.J. Hughes and M. Mallet, *A New Finite Element Formulation for Computational Fluid Dynamics: IV. A Discontinuity-Capturing Operator for Multidimensional Advective-Diffusive Systems.* Comput. Methods Appl. Mech. Engrg., **Vol. 58**, pp.329-336, (1986).

[42] T.J. Hughes, M. Mallet and A. Mizukami, *A New Finite Element Formulation for Computational Fluid Dynamics: II. Beyond SUPG.* Comput. Methods. Appl. Mech. Engrg. **Vol.54**, pp.223-234, (1986).

[43] T.J. Hughes, T.E. Tezduyar, *Finite Element Methods for First-Order Hyperbolic system with Particular Emphasis on the Compressible Euler Equations.* Comput. Methods Appl. Mech. Engrg., **Vol.45**, pp.217-284, (1984).

[44] J. Jaffre, C. Johnson and A. Szepessy, *Convergence of the Discontinuous Galerkin Finite Element Method for Hyperbolic Conservation Laws.* Technical Report, **No. 1993-11/ISSN 0347-2809**, Department of Mathematics, Chalmers University of Technology, The University of Göteborg, (1993).

[45] X. Jiang, *A Streamline-upwinding/Petrov-Galerkin Method for the Hydrodynamic Semiconductor Device Model.* To appear in Math. Models and Methods in Appl. Sci., (1995).

[46] C. Johnson and U. Nävert, *An Analysis of Some Finite Element Methods for Advection-Diffusion Problems.* Analytical and Numerical Approaches to Asymptotic Problems in Analysis, O. Axelsson, L.S. Frank and A. Van der Sluis eds., North-Holland, Amsterdam, pp.99-116, (1981).

[47] C. Johnson, U. Nävert and J. Pitkäranta, *Finite Element Methods for Linear Hyperbolic Problems.* Comput.Methods Appl. Mech. Engrg., **Vol.45**, pp.285-312, (1984).

[48] C. Johnson and A. Szepessy, *On the Convergence of a Finite Element Method for a Nonlinear Hyperbolic Conservation Law.* Math. Comput., **Vol. 49**, **No. 180**, pp.427-444, (1987).

[49] C. Johnson, A. Szepessy and P. Hansbo, *On the Convergence of Shock Capturing Streamline Diffusion Finite Element Method for Hyperbolic Conservation Laws.* Math. Comput., **Vol. 54**, **No. 189**, pp.107-129, (1990).

[50] C. Johnson, A.H. Schatz and L.B. Wahlbin, *Crosswind Smear and Pointwise Errors in Streamline Diffusion Finite Element Methods.* Math. Comp., **Vol. 49**, **No. 179**, pp.25-38, (1987).

[51] J.W. Jerome and C.W. Shu, *Energy Models for One-Carrier Transport in Semiconductor Devices.* ICASE Report, **No. 91-78**, Institute for Computer Applications in Science and Engineering, NASA Langley Research Center, Hampton, Virginia, (1991).

[52] M. Křížek and P. Neittaanmäki, *Finite Element Approximation for a Div-Rot System with Mixed Boundary Conditions in Non-Smooth Plane Domains.* Aplikace Matematiky, **Vol. 29**, pp.272-285, (1984).

[53] M. Křížek and P. Neittaanmäki, *Finite Element Approximation of Variational Problems and Applications.* (1990).

[54] J.P. Kreskovsky, M. Meyyappan and H.L. Grubin, *The Moments of the Boltzmann Transport Equation as Applied to the Gallium Arsenide Permeable Base Transistor.* COMPEL, pp.99-105, (1987).

[55] Q. Lin, N. Goldsman and G-C. Tai, *Highly Stable and Routinely Convergent 2-Dimensional Hydrodynamic Device Simulation.* (1993), to appear in Solid State Electronics.

[56] Q. Lin, *How to Sharpen the Error of Finite Element Methods.* Preprint, Inst. of Systems Science, Academia Sinica, Beijing, (1994).

[57] T.J. Maloney and J. Frey, *Transient and Steady-State Electron Transistor in GaAs and InP.* J. Appl. Phys., **Vol. 48**, pp.781-787, (1977).

[58] P.A. Markowich, *The Stationary Semiconductor Device Equations.* Springer-Verlag, Wein, New York, (1986).

[59] P.A. Markowich and P. Pietra, *A Non-Isentropic Euler-Poisson Model for a Collisionless Plasma.* Preprint, (1991).

[60] P.A. Markowich, C.A. Ringhofer and C. Schmeiser, *Semiconductor Equations.* Springer-Verlag, Wien, New York, (1990).

[61] U. Nävert, *A finite Element Method for Convection-Diffusion Problems.* Thesis, Chalmers Univ. of Tech. and Univ. of Gothenburg, (1982).

[62] F. Odeh, M. Rudan and J. White, *Numerical Solution of the Hydrodynamic Model for a One-Dimensional Semiconductor Device.* COMPEL, **Vol. 6**, pp.151-170, (1987).

[63] A.I. Pehlivanov, G.F. Carey and R.D. Lazarov, *Least-Squares Mixed Finite Elements for Second Order Elliptic Problems.* SIAM J. Numer. Anal., **Vol. 31**, **No. 5**, pp.1368-1377, (1994).

[64] T.E. Peterson, *A Note on the Convergence of the Discontinuous Galerkin Method for a Scalar Hyperbolic Equation.* SIAM J. Numer. Anal., **Vol. 28**, **No. 1**, pp.133-140, (1991).

[65] S.J. Polak, C.D. Heijer, W.H.A. Schilders and P.A. Markowich, *Semiconductor Device Modelling from the Numerical Point of View.* Inter. J. Numer. Engrg., **Vol. 24**, pp.763-838, (1987).

[66] D.L. Pulfrey and N. G. Tarr, *Introduction to Microelectronic Devices.* Prentice Hall Series in Solid State Physical Electronics, N. Holonyak, Jr. Editor, Prentice Hall, Englewood Cliffs, New Jersey, (1989).

[67] K. Rahmat, J. White and D.A. Antoniadis, *Computation of Drain and Substrate Currents in Ultra-Short-Channel NMOSFET's Using the Hydrodynamic Model.* IEEE, IEDM, pp.115-119, (1991).

[68] J. Ruch, *Electron Dynamics in Short Channel Field Effect Transistors.* IEEE Trans. El. Dev., **Vol. ED-19**, pp.652-654, (1972).

[69] M. Rudan and F. Odeh, *Multi-dimensional Discretization Scheme for the Hydrodynamic Model of Semicondctor Devices.* COMPEL, **Vol. 5**, **No. 3**, pp.149-183, (1986).

[70] W.V. Van Roosbroeck, *Theory of Flow of Electrons and Holes in Germanium and Other Semiconductors.* Bell Syst. Tech. J., **Vol. 29**, pp.560-607, (1950).

[71] D.L. Scharfetter and H.K. Gummel, *Large-Signal Analysis of a Silicon Read Diode Oscillator.* IEEE Trans. El. Dev., **Vol. ED-16**, pp.64-77, (1969).

[72] S. Selberherr, *Analysis and Simulation of Semiconductor Devices.* Springer-Verlag, Wien, Nwe York, (1984).

[73] M. Sever, *Symmetric Forms of Energy-Momentum Transport Models.* preprint, (1991).

[74] M. Sever, *Delaunay Partitioning in Three Dimensions and Semiconductor Models.* COMPEL, **Vol. 5**, **No. 2**, pp.75-93, (1986).

[75] F. Shakib and T.J. Hughes, *A New Finite Element Formulation for Computational Fluid Dynamics: IX. Fourier Analysis of Space-Time Galerkin/Least-Squares Algorithms.* Comput. Methods Appl. Mech. Engrg., **Vol. 87**, pp.35-58, (1991).

[76] M.S. Shur, *Influence of Nonuniform field Distribution on Frequency Limits of GaAs Field Effect Transistors.* Electron Lett., **Vol. 12**, pp.615-616, (1976).

[77] F. Shakib, T.J. Hughes and Z. Johan, *A New Finite Element Formulation for Computational Fluid Dynamics: X. The Compressible Euler and Navier-Stokes Equations.* Comput. Methods Appl. Mech. Engrg., **Vol. 89**, pp.141-219, (1991).

[78] M. Sharma and G.F. Carey, *Semiconductor Device Modeling Using Flux Upwinding Finite Elements.* COMPEL, **Vol. 8**, **No. 4**, pp.219-224, (1989).

[79] S.M. Sze, *The Physics of Semiconductor Devices.* John & Sons, New York, (1981).

[80] Thomann, E. and Odeh, F., *On the Well-Posedness of the Two-Dimensional Hydrodynamic Model for Semiconductor Devices.* COMPEL, **Vol. 9**, **No. 1**, pp.45-57, (1990).

[81] C.H. Wu, *Numerical Analysis of the Time-Dependent Two and Three Dimensional Semiconductor Device Equations.* Ph.D. Thesis, Univ. of Dublin, (1990).

[82] K. Yosida, *Functional Analysis.* Sixth Edition, Springer-Verlag, Berlin, Heidelberg, New York, (1980).

[83] G. Zhou, *An Adaptive Streamline Diffusion Finite Element Method for Hyperbolic Systems in Gas Dynamics.* Thesis, Universität Heideberg, (1992).

Appendix A

A Property for the Hydrodynamic Model (2.1)

For simplicity, only a one-space-dimensional problem is considered here. Multi-space dimensional problems can be treated similarly with a little extra work. We rewrite the conservation laws (2.1) in the following vector form

$$U_t + AU_x + C(U) = (KU_x)_x, \tag{A.1}$$

where

$$U^t = (\rho, J, W)^t \tag{A.2}$$

and

$$K = \frac{2\kappa}{3} \begin{pmatrix} 0 & 0 & 0 \\ 0 & 0 & 0 \\ \frac{J^2}{\rho^2} - \frac{W}{\rho} & -\frac{J}{\rho} & 1 \end{pmatrix}. \tag{A.3}$$

The matrix A can be diagonalized by a non-singular matrix Y, such that

$$Y^{-1}AY = \Lambda = diag(v - c,\, v,\, v + c), \tag{A.4}$$

where

$$Y = \begin{pmatrix} 1 & 1 & 1 \\ v - c & v & v + c \\ H - cv & \frac{v^2}{2} & H + cv \end{pmatrix} \tag{A.5}$$

and

$$Y^{-1} = \begin{pmatrix} \frac{1}{2}(S + \frac{v}{c}) & -\frac{1}{2}(\frac{1}{c} + vb) & \frac{b}{2} \\ 1 - S & vb & -b \\ \frac{1}{2}(S - \frac{v}{c}) & \frac{1}{2}(\frac{1}{c} - vb) & \frac{b}{2} \end{pmatrix}. \tag{A.6}$$

In the above, $c^2 = \frac{5T}{3}$, $H = \frac{3c^2}{2} + \frac{v^2}{2}$, $S = \frac{v^2}{3c^2}$ and $b = \frac{2}{3c^2}$ (see [22]).

Proposition A.1 *There exists* $\Lambda_\beta = diag(\beta_1, \beta_2, \beta_3)$ *with* $\beta_i > 0$ $(i = 1, 2, 3)$ *such that* $\Lambda_\beta Y^{-1} K Y$ *is symmetric positive semi-definite.*

Proof: Denote the last row of K

$$\eta^t(U) = (\frac{J^2}{\rho^2} - \frac{W}{\rho}, -\frac{J}{\rho}, 1). \tag{A.7}$$

Note that

$$Y^{-1}K = \frac{2\kappa}{3} b \begin{pmatrix} \frac{1}{2} \\ -1 \\ \frac{1}{2} \end{pmatrix} \eta^t(U) \tag{A.8}$$

$$\eta^t Y = T(1, -\frac{3}{2}, 1) \tag{A.9}$$

It is easy to see that

$$\Lambda_\beta = \mathrm{diag}(4, 3, 4) \tag{A.10}$$

satisfies what we need. □

Appendix B

Stability of the SD-Trapezoidal Scheme

We consider the SD-trapezoidal scheme (3.76) in the form

$$(A_0\frac{U^{h(n+1)}-U^{h(n)}}{\Delta t}\ ,\ \Psi)+(A_0\frac{U^{h(n+1)}-U^{h(n)}}{\Delta t},P^h(\Psi))$$
$$+\quad \mathcal{B}(\frac{1}{2}(U^{h(n+1)}+U^{h(n)}),\Psi)=0, \tag{B.1}$$

for any $\Psi\in\mathcal{V}^h$.

As we pointed out in section 3.5.2, existence of the second term above restricts us in obtaining a stability result for the general case. A restriction on the diffusion matrix is needed to obtain the following stability result.

Theorem B.1 *If $K=\kappa I_l$ then the one-dimensional SD-trapezoidal scheme (B.1) is unconditionally stable.*

Proof: Let $U^{h(n)}=A_0^{-1/2}Z\Lambda_\beta^{-1/2}V^{h(n)}$, $\Psi=A_0^{-1/2}Z^{-t}\Lambda_\beta^{1/2}\Phi$, then (B.1) is transformed into

$$(\frac{V^{h(n+1)}-V^{h(n)}}{\Delta t}\ ,\ \Phi)+(\frac{V^{h(n+1)}-V^{h(n)}}{\Delta t}\ ,\ \Lambda\Lambda_\tau\Phi_x)$$
$$+\frac{1}{2}\{(\Lambda(V^{h(n+1)}+V^{h(n)})_x\ ,\ \Phi)$$
$$(\kappa(V^{h(n+1)}+V^{h(n)})_x\ ,\ \Phi_x)$$
$$+(\Lambda(V^{h(n+1)}+V^{h(n)})_x\ ,\ \Lambda\Lambda_\tau\psi_x)\}=0, \tag{B.2}$$

where, Λ_τ is given in (3.28). Taking $\Psi=\Lambda_\tau(V^{h(n+1)}-V^{h(n)})/\Delta t$ in (B.2), we have

$$\frac{1}{\Delta t^2}\|\Lambda_\tau^{1/2}(V^{h(n+1)}-V^{h(n)})\|^2$$

$$
\begin{aligned}
&+\frac{1}{2\Delta t}\{(\Lambda(V^{h^{(n+1)}}+V^{h^{(n)}})_x\,,\,\Lambda_\tau(V^{h^{(n+1)}}-V^{h^{(n)}}))\\
&+(\kappa(V^{h^{(n+1)}}+V^{h^{(n)}})_x\,,\,\Lambda_\tau(V^{h^{(n+1)}}-V^{h^{(n)}})_x)\\
&+(\|\Lambda_\tau\Lambda V_x^{h^{(n+1)}}\|^2-\|\Lambda_\tau\Lambda V_x^{h^{(n)}}\|^2)\}=0.
\end{aligned}
\tag{B.3}
$$

Taking $\Psi=(V^{h^{(n+1)}}+V^{h^{(n)}})/2$, we have

$$
\begin{aligned}
&\frac{1}{2\Delta t}(\|V^{h^{(n+1)}}\|^2-\|V^{h^{(n)}}\|^2)\\
&\quad+\frac{1}{2\Delta t}(V^{h^{(n+1)}}-V^{h^{(n)}}\,,\,\Lambda_\tau\Lambda(V^{h^{(n+1)}}+V^{h^{(n)}})_x)\\
&\quad+\frac{1}{4}\{(\kappa(V^{h^{(n+1)}}+V^{h^{(n)}})_x\,,\,(V^{h^{(n+1)}}+V^{h^{(n)}})_x)\\
&\quad+\|\Lambda_\tau^{1/2}\Lambda(V^{h^{(n+1)}}+V^{h^{(n)}})_x\|^2\}=0.
\end{aligned}
\tag{B.4}
$$

We define $|||\cdot|||$, an auxiliary norm, by

$$
|||V|||^2=\|V\|^2+\|\Lambda_\tau\Lambda V_x\|^2+\kappa(\Lambda_\tau V_x,V_x).
\tag{B.5}
$$

Then (B.3) + (B.4) yields

$$
\begin{aligned}
&\frac{1}{2\Delta t}(|||V^{h^{(n+1)}}|||^2-|||V^{h^{(n)}}|||^2)\\
&\quad+\frac{1}{\Delta t}(V^{h^{(n+1)}}-V^{h^{(n)}},\tilde{\tau}\Lambda(V^{h^{(n+1)}}+V^{h^{(n)}})_x)\\
&\quad+\frac{1}{\Delta t^2}\|\Lambda_\tau^{1/2}(V^{h^{(n+1)}}-V^{h^{(n)}})\|^2\\
&\quad+\frac{1}{4}\|\Lambda_\tau^{1/2}\Lambda(V^{h^{(n+1)}}+V^{h^{(n)}})_x\|^2\le 0.
\end{aligned}
\tag{B.6}
$$

Applying the inequality $a^2+b^2/4\ge ab$ to the last three terms above, we obtain

$$
|||V^{h^{(n+1)}}|||^2\le|||V^{h^{(n)}}|||^2\square
\tag{B.7}
$$

Fourier analysis applied to (B.1) for the one-dimensional linear scalar convection-diffusion problem was carried out in [40]. It was shown that (B.1) can be considered as a counterpart of the one-pass implicit predictor/multi-corrector algorithm for the linear-linear SD method.

Appendix C

1-D Test for a Set of Parameters

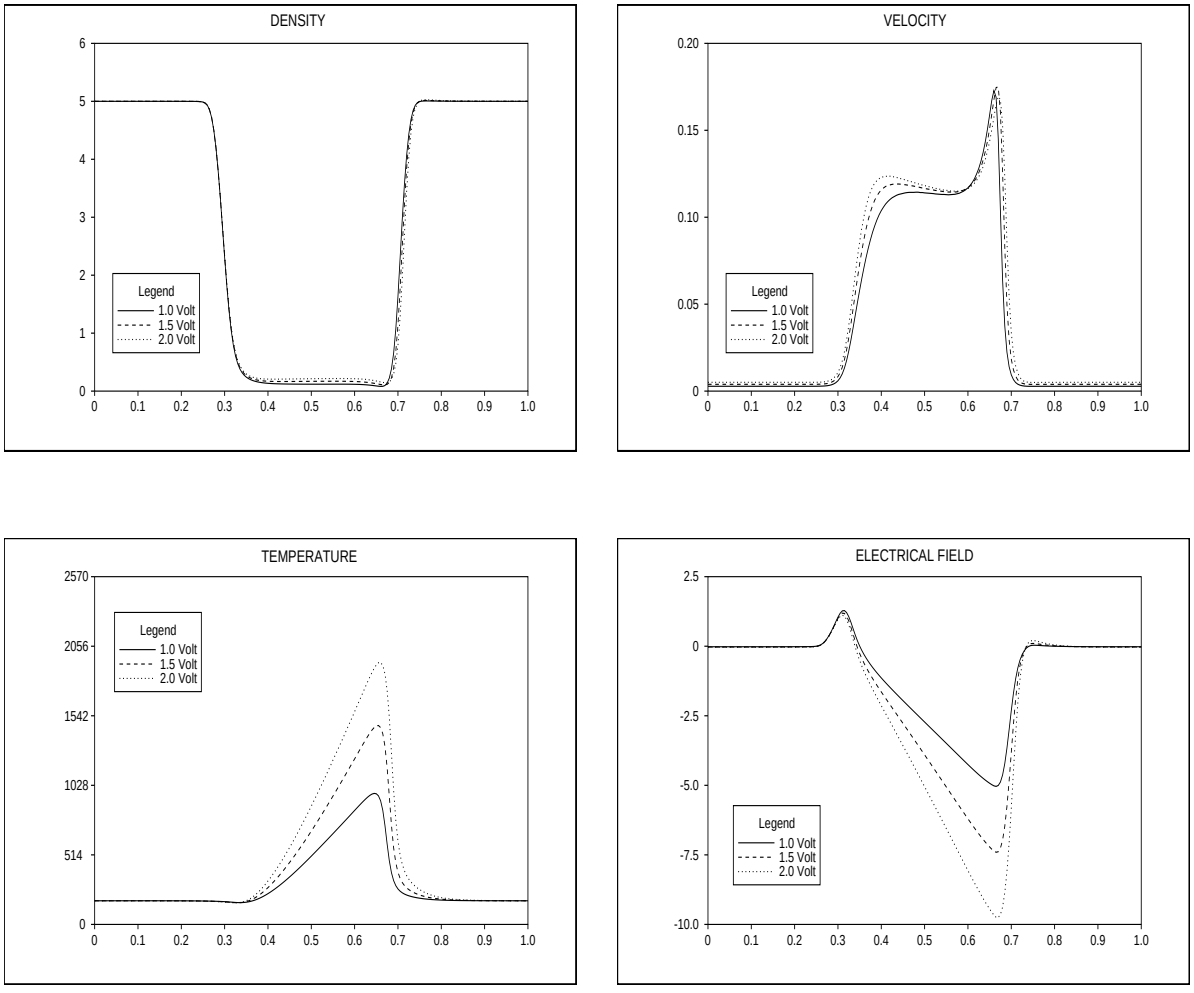

Figure C.1: HD model at 300K: using Fatemi *et al.*'s parameters $\mu_0 = 0.145$, $v_s = 0.1$ and $\kappa = \frac{3\mu_0 m T_0}{2e}$.